Advancements in Biomanufacturing: The Impact of Analytical Methods

Article Collection

WILEY

WILEY Analytical Science

Sponsored by:

bio-techne® | proteinsimple

bio-techne®

Publication Spotlight

Pfizer's icIEF Method Optimizes AAV Characterization for Gene Therapy Development

Pfizer recently published a peer-reviewed study entitled *Development of an icIEF Assay for Monitoring AAV Capsid Proteins and Application to Gene Therapy Products* in the journal of Molecular Therapy. The study described the development of an imaged cIEF (icIEF) platform method on the Maurice™ system for charge heterogeneity analysis of AAV capsid proteins, which in turn provided critical insights into post-translational modifications (PTMs) and associated decrease in potency as a stability indicating assay. Importantly, the study also drew comparisons between the results obtained from icIEF, RP-HPLC, and a multi-attribute method (MAM) using high-resolution LC-MS, demonstrating the suitability of GMP compliant icIEF method for routine product testing.

The study demonstrated multiple uses of Maurice icIEF for AAV product characterization, from differentiating between serotypes to deducing potential impacts on potency based on capsid stability. If you're interested in optimizing your AAV characterization, read the full paper for details, or visit our website to learn more about Maurice!

*PS: The study in the paper used RP-HPLC for AAV charge isoform fractionation, but we now offer that capability too with our brand-new MauriceFlex™ system!

Highlights of the study

- The development of an icIEF platform method for resolving AAV capsid proteins (VP1, VP2, and VP3) and other charges species linked to PTMs
- Fractionation and analysis of different charged species with RP-HPLC MS, and subsequent isoelectric point (pI) verification with icIEF
- The introduction of point-mutations in AAVs to induce and measure deamidation
- Forced degradation of AAVs and charge assessment to confirm that icIEF is stability-indicating, validating the results against RP-HPLC and MAM
- Correlation of AAV stability with transduction efficiency (relative potency)

> "While a quantitative peptide map or MAM, as in the data we presented, is a powerful tool to monitor capsid deamidation, a more rapid and suitably GMP-compliant method benefits routine product testing."
>
> - Xiaoping He *et al.*, 2023

Read Paper | https://www.ncbi.nlm.nih.gov/pmc/articles/PMC10070887

Meet Maurice | https://www.bio-techne.com/instruments/ice

Contents

Imprint

Senior Account Manager:
Joseph Tomaszewski

Editor:
Dr. Christene A. Smith

Introduction

This article collection delves into the intersection of advanced analytical methods, biomanufacturing, and biopharmaceuticals. The studies demonstrate how these techniques enhance our understanding of complex biological systems, improve therapeutic interventions, and drive innovation in the biomanufacturing process, holding immense potential for the future of healthcare.

This collection begins with a study on an enhanced icIEF immunoassay for analyzing adeno-associated viruses (AAV) capsid proteins, crucial for gene therapy. The method by Ramírez *et al*. offers higher sensitivity and specificity [1], enabling detailed protein characterization, stability monitoring, and serotype identification, especially useful in upstream process development.

Next, Krebs *et al*. explored the isoelectric points of SARS-CoV-2 proteins [2], using theoretical values and the Maurice capillary isoelectric focusing (cIEF) system for measurements. The study found that theoretical values align with experimental results, providing useful predictions about the isoelectric points of these proteins. The method proved robust across various experimental conditions.

Geurink *et al*. then investigates the use of capillary electrophoresis (CE) in vaccine analysis [3], demonstrating its applicability in characterizing and testing various viral vaccines. They developed and validated diverse CE methods for analyzing virus, protein, DNA, and excipients. These methods, which improved process and product understanding, were applied across the vaccine development process, enhancing safety, efficacy, and quality.

Lastly, Kumar *et al*. delved into the role of CE in the analytical characterization of biopharmaceutical products [4]. They highlighted its advantages, such as fast separation and high resolution, and its use in process development, characterization, quality control, and release testing. The study also discussed the emerging trend of combining CE with mass spectrometry for assessing the primary structure of therapeutic proteins and their impurities.

This collection underscores the significance of advanced CE-based analytical methods in understanding and developing biopharmaceuticals. The studies collectively highlight the power of these techniques in enhancing our knowledge of complex biological systems, improving the safety and efficacy of therapeutic interventions, and driving innovation in biomanufacturing processes. These advancements are

pivotal in the face of emerging health challenges and hold immense potential for the future of healthcare and medicine.

Through the methods and applications presented in this article collection, we hope to educate researchers on new technologies and techniques biomanufacturing analytics. To gain a deeper understanding of available options for improving your research, we encourage you to visit Bio-techne's website.

Dr. Christene A. Smith, PhD
Editor at Wiley

References

[1] Ramírez, F. *et al*. (2023). Development of a highly sensitive imaged cIEF immunoassay for studying AAV capsid protein charge heterogeneity. *Electrophoresis*. DOI: 10.1002/elps.202300039.

[2] Krebs, F. *et al*. (2021). Isoelectric point determination by imaged CIEF of commercially available SARS-CoV-2 proteins and the hACE2 receptor. *Electrophoresis*. DOI: 10.1002/elps.202100015.

[3] Geurink, L. *et al*. (2022). Sixteen capillary electrophoresis applications for viral vaccine analysis. *Electrophoresis*. DOI: 10.1002/elps.202100269.

[4] Kumar, R. *et al*. (2022). Applications of capillary electrophoresis for biopharmaceutical product characterization. *Electrophoresis*. DOI: 10.1002/elps.202100182.

Received: 22 February 2023 | Revised: 14 April 2023 | Accepted: 18 April 2023

DOI: 10.1002/elps.202300039

ELECTROPHORESIS

RESEARCH ARTICLE

Development of a highly sensitive imaged cIEF immunoassay for studying AAV capsid protein charge heterogeneity

Francisco Ramírez | **Jiaqi Wu** | **Charles Haitjema** | **Chris Heger**

ProteinSimple, a Bio-Techne Brand, San Jose, California, USA

Correspondence
Jiaqi Wu, ProteinSimple, a Bio-Techne Brand, San Jose, CA, USA.
Email: jiaqi.wu@bio-techne.com

Color online: See the article online to view Figure 3 in color.

Abstract

Post-translational modifications (PTMs) of adeno-associated virus (AAV) capsid proteins tune and regulate the AAV infective life cycle, which can impact the safety and efficacy of AAV gene therapy products. Many of these PTMs induce changes in protein charge heterogeneity, including deamidation, oxidation, glycation, and glycosylation. To characterize the charge heterogeneity of a protein, imaged capillary isoelectric focusing (icIEF) has become the gold standard method. We have previously reported an icIEF method with native fluorescence detection for denatured AAV capsid protein charge heterogeneity analysis. Although well suited for final products, the method does not have sufficient sensitivity for upstream, low-concentration AAV samples, and lacks the specificity for capsid protein detection in complex samples like cell culture supernatants and cell lysates. In contrast, the combination of icIEF, protein capture, and immunodetection affords significantly higher sensitivity and specificity, addressing the challenges of the icIEF method. By leveraging different primary antibodies, the icIEF immunoassay provides additional selectivity and affords a detailed characterization of individual AAV capsid proteins. In this study, we describe an icIEF immunoassay method for AAV analysis that is 90 times more sensitive than native fluorescence icIEF. This icIEF immunoassay provides AAV stability monitoring, where changes in individual capsid protein charge heterogeneity can be observed in response to heat stress. When applied to different AAV serotypes, this method also provides serotype identity with reproducible quantification of VP protein peak areas and apparent isoelectric point (p*I*). Overall, the described icIEF immunoassay is a sensitive, reproducible, quantitative, specific, and selective tool that can be used across the AAV biomanufacturing process,

Abbreviations: AAV, adeno-associated virus; icIEF, imaged capillary isoelectric focusing; p*I*, isoelectric point; PTMs, post-translational modifications.

especially in upstream process development where complex sample types are often encountered.

KEYWORDS
adeno-associated virus, capillary immunoassay, capsid proteins, identity, isoelectric focusing

1 | INTRODUCTION

Delivery of a genetic payload with a viral vector like adeno-associated viruses (AAVs) is becoming a widely used therapeutic approach for the treatment of rare genetic diseases [1]. AAVs are nonpathogenic viruses belonging to the *Parvovirinae* subfamily of *Parvoviridae*, comprising a protein capsid, formed from three capsid proteins, VP1, VP2, and VP3 into a 60-mer, and a 4.7 kb single-stranded DNA (ssDNA) genome [2]. Ten naturally occurring AAV serotypes determine tissue tropism, with nonnatural variants (e.g., AAV2/5) engineered to improve various functional or physiochemical attributes [3]. The serotypes differ at the amino acid level across the three capsid proteins and consequently have different cellular receptors [4].

Like all other biotherapeutics, AAV-based therapies are subject to regulatory guidelines, like those provided by the FDA [5]. Following these guidelines, the physiochemical properties of AAV therapeutics including identity and purity need to be characterized [5]. Extended characterization includes a wide variety of techniques and attributes testing, including post-translational modification (PTM) monitoring. Indeed, therapeutic antibodies are closely monitored for changes in glycosylation, deamidation, and glycation [6]. As many as 75 PTMs on the individual capsid proteins of AAVs have been identified in AAVs produced in HEK293 cells and several of these PTMs have been shown to tune and regulate aspects of AAV function [7, 8]. Many of these PTMs are process-related, therefore monitoring AAV products for these changes is important throughout product processing. Several PTMs found on the AAV capsid proteins induce charge changes to the modified amino acid, including asparagine deamidation, methionine oxidation, serine/threonine phosphorylation, and *O*-linked glycosylation [7–9].

Among the methods used to characterize the charge heterogeneity of proteins, imaged capillary isoelectric focusing (icIEF) is one of the most widely used technologies in the biopharmaceutical industry [10]. This method has been applied to diverse molecules, including therapeutic monoclonal antibodies, fusion proteins, and viruses [10]. Recently, a platform AAV capsid protein method based on icIEF with native fluorescence detection was published [11]. That method detects as little as 10^{10} VP/mL and is suitable for the analysis of late-stage or pure AAV products. The AAV capsid protein charge characterization method was applied to eight different serotypes and was shown that both the peak patterns and averaged isoelectric point (p*I*) values of the serotypes could be used for AAV identity [11]. Subsequently, a second denatured icIEF capsid protein method was put forth by He et al. [12]. Importantly, this icIEF method correlated with both reverse-phase high-performance liquid chromatography and multi-attribute monitoring for monitoring capsid protein deamidation. A major finding of the study was that the degree of capsid protein deamidation observed by icIEF correlated with loss of vector potency.

Although the published icIEF native fluorescence methods are fast and sensitive, they cannot be used in highly complex samples like bioreactor supernatants where the abundance of the AAV product is lower and the concentration of contaminating proteins is higher. Additionally, because icIEF separates proteins based on their charge, and owing to the high degree of similarity between the AAV capsid proteins, the charge heterogeneity p*I* of each viral protein cannot be characterized individually without pre-separation by their sizes, for example, 2D–PAGE. In this study, we describe an icIEF capillary immunoassay method using Simple Western™ that combines the resolving power of icIEF with the specificity, selectivity, and sensitivity of an immunoassay to support extended characterization of AAVs in upstream process steps. The method has significantly higher sensitivity compared to the reported icIEF methods, and crude AAV samples in complex matrices can be characterized directly without sample purification. Like the published icIEF native fluorescence method [11], the method described herein is also stability indicating, but with the added value of characterizing stress changes at the individual capsid protein level.

2 | MATERIALS AND METHODS

2.1 | Materials

AAV samples of different serotypes (2×10^{13} VP/mL) were purchased from Virovek (Hayward, CA, USA). HEK293T whole-cell lysate was from OriGene (LY500001).

Formamide (>99.5%, 47 671), dimethyl sulfoxide (DMSO, >99.7, D2650), and dithiothreitol (DTT, >99.0%, D0632) were purchased from SIGMA. Overall, 1% methylcellulose (101 876), p*I* standard ladder 1 (040-644), p*I* marker 8.4 (041-036), isoelectric focusing (IEF) anolyte (042-337), IEF catholyte (042-338), Antibody Diluent 2 (042-203), and anti-mouse HRP-conjugated secondary antibody (042-205) were products of ProteinSimple. Pharmalyte 3-10 (SIGMA, GE17-0456-01) and Pharmalyte 5-8 (SIGMA, GE17-0453-01) were purchased from Cytiva. Mouse monoclonal antibodies to AAV VP1 (61 056) and to VP1/2/3 (61 058) were obtained from PROGEN. All solutions were made using Millipore deionized water.

2.2 | Instruments

Analysis by icIEF immunoassay was performed with Peggy Sue™ (004-800, ProteinSimple) and analysis by icIEF native fluorescence was performed with Maurice™ (090-000, ProteinSimple).

2.3 | Sample preparation

AAVs (2×10^{13} VP/mL) were denatured in the presence of 50% DMSO and 12 mM DTT by heating the solution at 70°C for 10 min then cooling to room temperature for 5 min. Denatured AAVs were then mixed with the IEF master mixture at a 1:50 ratio to form a final IEF sample solution containing 50% formamide, 0.7% methylcellulose, 2% Pharmalyte 3-10, 2% Pharmalyte 5-8, 2 mM DTT, and 5% DMSO, with p*I* standard ladder 1 and p*I* marker 8.4. The final mixture was vortexed for 30 s and stored on ice until use. For stability testing, AAV samples were incubated at 37°C for 1, 4, 7, 11, and 14 days prior to denaturation and analysis.

2.4 | icIEF immunoassay analysis

Denatured AAVs, as described above, were focused on Peggy Sue (ProteinSimple, San Jose, CA, USA) for 1 min at 1.5 kV, then, at 3 kV for 12 min. At the end of focusing, protein zones inside the capillary were immobilized to the capillary wall for 200 s. Focused AAV samples were then probed with either anti-VP1/2/3 monoclonal antibody (mAb) (1:50 dilution in Antibody Diluent 2) or anti-VP1 mAb (1:25 dilution in Antibody Diluent 2) for 60 min. Bound primary antibodies were detected using a species-specific HRP-conjugated secondary antibody (anti-mouse IgG secondary antibody 042-205, ProteinSimple) followed by chemiluminescence detection and HDR imaging using the Compass for Simple Western software (Version 5.0.1).

To determine the limit of quantitation (LOQ), we adapted the method defined in ICH Q2 (R1) [5], which is based on the standard deviation and the slope of the detection response [5]. The method considers the response linearity and noise level in the baseline. In the experiment, a twofold serial dilution series of purified AAV9 was prepared from 4×10^{10} to 1.6×10^{8} VP/mL. A no-analyte sample was included as a control. To determine the LOQ in a matrix background, an identical serial dilution series was prepared in the presence of 20 µg/mL HEK293T whole-cell lysate (OriGene, PN LY500001). The resulting peak areas were plotted by concentration for each serial dilution series, and a linear regression analysis was performed to generate a calibration curve. The analysis was performed three times at each concentration point. Using the linear equation from the calibration curve, the curve's intercept point of the curve at zero analyte concentration was determined. The standard deviation (σ) of the intercept points from the three tests was calculated. The LOQ was determined by the following equation:

$$LOQ = 10\sigma/S$$

where S is the average value of the slopes of the three calibration curves. The above equation was used to calculate LOQs for the analyte in both the presence and absence of HEK293T whole-cell lysate.

2.5 | icIEF native fluorescence analysis

The analysis of AAV9 by icIEF native fluorescence was performed as described previously [10] using the Maurice instrument (ProteinSimple).

3 | RESULTS AND DISCUSSION

3.1 | AAV analysis by icIEF immunoassay and comparability to native fluorescence

To establish the icIEF immunoassay method for characterizing denatured AAV capsid proteins, we started with AAV9 due to its prevalence in clinical pipelines [13–15]. AAV9 samples were prepared according to Section 2 and analyzed by the icIEF immunoassay. For the detection of the denatured AAV9 capsid proteins, a monoclonal antibody was used that recognizes all three capsid proteins (VP1, VP2, and VP3). The results from this analysis showed 3 major peaks between p*I* 6 and 7, labeled as Peak 1, 2, and 3 (Figure 1, top panel). We compared the results of the icIEF immunoassay method to the published results of AAV9 analysis by the icIEF native fluorescence method [11]. The

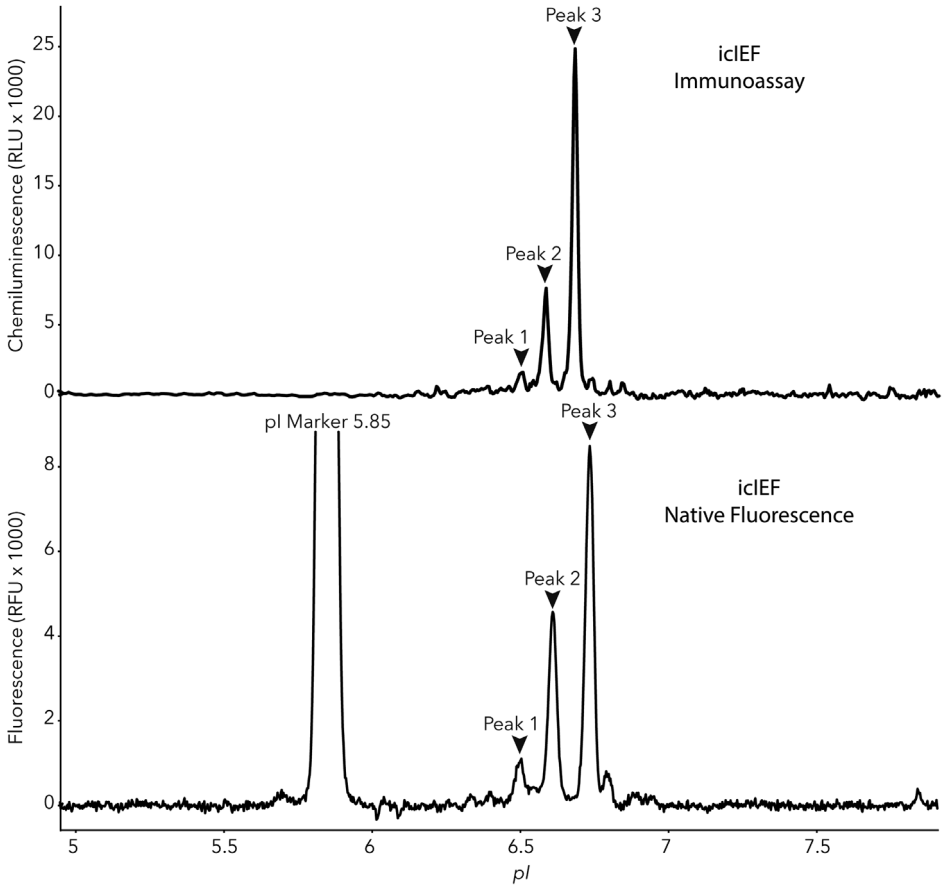

FIGURE 1 Comparison of AAV9 peak profiles between the imaged capillary isoelectric focusing (icIEF) immunoassay and icIEF native fluorescence methods. (Top panel) chemiluminescent detection of AAV9 (2.3×10^{10} VP/mL) using anti-VP1/2/3 monoclonal antibody (mAb) for detection. (Bottom panel) native fluorescence detection of AAV9 (9.3×10^{11} VP/mL) with 80 s exposure time.

TABLE 1 Peak area percentages of the three main peaks in AAV9 were measured by imaged capillary isoelectric focusing (icIEF) with immunoassay detection and with native fluorescence detection as shown in Figure 1.

	Peak 1 (%)	Peak 2 (%)	Peak 3 (%)
icIEF native fluorescence	8.4	32.6	59.0
icIEF immunoassay	10.5	22.7	66.9

two methods demonstrated similar resolution of protein separation, peak signature, overall p*I* range (Figure 1, bottom panel), and peak area percentage (Table 1). It should be noted that the icIEF immunoassay method used 30 times less AAV9 sample when compared to icIEF native fluorescence (2.3×10^{10} VP/mL vs. 9.3×10^{11} VP/mL).

3.2 | Analysis of AAVs in HEK293T whole-cell lysate

An advantage of combining icIEF with protein immobilization and subsequent immunodetection is the ability to detect target proteins in complex samples. AAVs are typically produced in HEK293T cells and are harvested from the cell supernatants and lysates [8, 16]. Thus, we tested the method's ability to characterize AAV capsid protein charges in a complex matrix, specifically HEK293T whole-cell lysate. To do so, a titration series of AAV9 was prepared in the absence or presence of HEK293T whole-cell lysate (20 µg/mL) and compared for dynamic range (Figure 2A). The results show that there is almost no effect on AAV quantification by the addition of the lysate (Figure 2B). HEK293T at 20 µg/mL has 300–30,000 times higher protein concentration than the AAV sample in this titration, and such complex samples are difficult to analyze by icIEF with native fluorescent detection. The tolerance to the sample matrix illustrates the use of this method to directly monitor AAV capsid protein modifications in upstream samples prior to sample cleanup or purification.

To determine the method's sensitivity, the LOQs for purified AAV9 and for AAV9 in a sample matrix of HEK293T whole-cell lysate were calculated, as described in Section 2. The LOQ was 1.5×10^8 VP/mL for purified AAV9 and 2.1×10^8 VP/mL for AAV9 in 20 µg/mL HEK293T

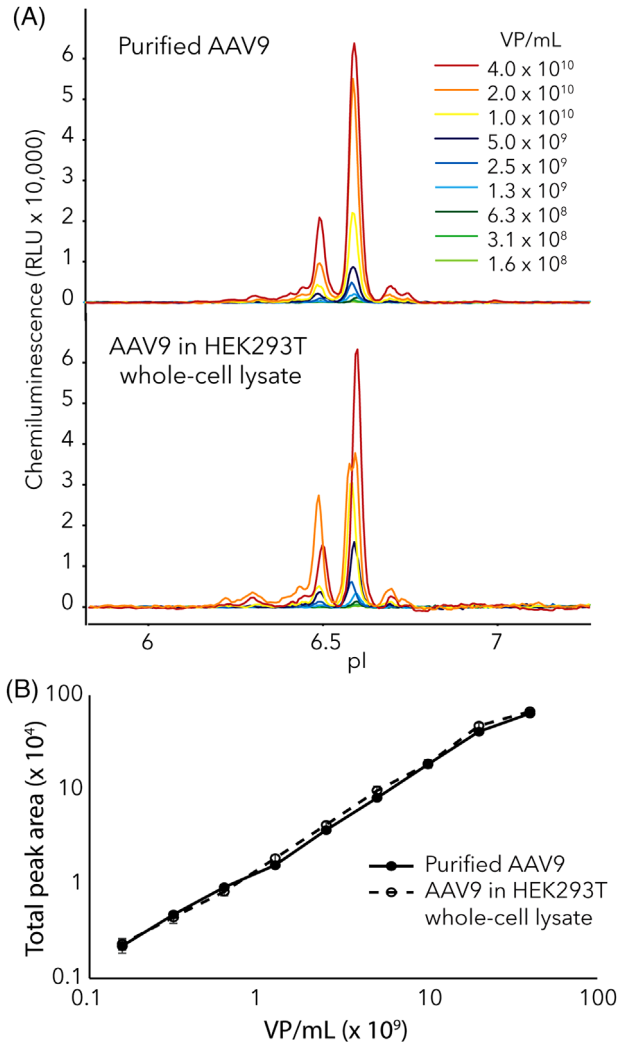

FIGURE 2 Method comparability in a complex matrix: (A) analysis of an AAV9 titration from 4.0×10^{10} to 1.6×10^{8} VP/mL (top panel) and analysis of the same concentration series in the presence of 20 µg/mL HEK293T lysate (bottom panel); (B) the dynamic range of the assay in the absence (solid line) or presence (dashed line) of 20 µg/mL HEK293T lysate.

whole-cell lysate. Thus, the LOQ for the icIEF immunoassay method described here is at least 90× more sensitive than the native fluorescence detection method for AAV9 analysis [11].

3.3 | Method reproducibility

We next sought to understand the method intraassay reproducibility. The overlaid electropherograms resulting from this analysis showed closely reproducible separation profiles of AAV9 (Figure 3). The standard deviation of each peak's apparent p*I* was ≤0.01 (Table 2A), and the relative standard deviation of each peak's area was less than 6% (Table 2B). In evaluating the overall reproducibility of measured p*I* value and peak area percentage, we used the concept of "averaged p*I*" value as previously described [11]. The averaged p*I* value is calculated by the sum of each peak's p*I* value weighed by the peak's percentage. This value represents the entire peak pattern and can be used in sample identification. The standard deviation of the averaged p*I* values of the six injections is 0.001 (Table 2C).

3.4 | Selective analysis of AAV capsid proteins

Due to their high sequence homology, the three AAV capsid proteins can only be partially separated by IEF, thus making it difficult to observe changes in the charge heterogeneity of each capsid protein [9]. Therefore, the method described here is valuable, as the charge profiles of the capsid proteins are more sensitive indicators of AAV stability than size or hydrophobicity [17, 18]. Modifications like deamidation and glycation cause very small changes in molecular weight and hydrophobicity; however, these modifications can alter vector function [9, 17, 18] and can be monitored with icIEF [12].

A key advantage of the icIEF immunoassay method described here is that each capsid protein can be characterized individually using different antibodies, which allows for a more complete understanding of the stability and changes of individual AAV capsid proteins. We probed AAV9 with both anti-VP1/2/3 and anti-VP1 antibodies separately as shown in Figure 4. The AAV9 capsid protein charge profile as detected with the anti-VP1 antibody (Figure 4, orange shading) highlights the acidic region of the complex profile detected with the anti-VP1/2/3 mAb. These data agree with both 2D–PAGE and the newer denatured icIEF paper [9, 12]. Using this capsid protein-specific detection approach, the method provides a rapid and specific identity assay that can be used to monitor the modifications of each capsid protein.

3.5 | AAV stability monitoring

Product stability is a critical quality attribute that is monitored during manufacturing and product release, and icIEF methods have been applied to understand the stability of various biotherapeutics [10, 11, 17, 18]. The described icIEF immunoassay was used to examine the degradation patterns of VP1 in AAV9 compared to the overall capsid proteins profile (VP1/2/3). AAV9 (2×10^{13} VP/mL) was stressed at 37°C (1, 3, 7, 11, and 14 days) before analysis using capsid protein-specific antibodies. The acidic shifting is apparent in both the overall charge profile (using anti-VP1/2/3) and the VP1 charge profile (Figure 5).

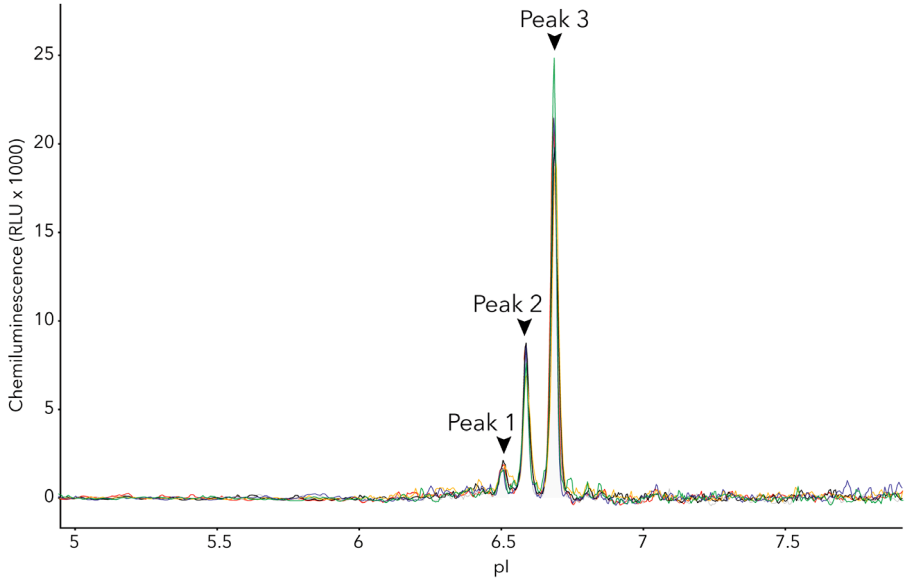

FIGURE 3 Intra-assay reproducibility of the denatured adeno-associated virus (AAV) capillary immunoassay. Overlay of six injections of the AAV9 sample (2.3×10^{10} VP/mL) in the same run batch, detected with the anti-VP1/2/3 primary antibody.

TABLE 2A Peak area percentages of the six injections as shown in Figure 3.

	Peak 1	Peak 2	Peak 3
Injection 1	6.4	25.2	68.4
Injection 2	6.9	26.6	66.5
Injection 3	6.8	25.4	67.8
Injection 4	6.0	27.7	66.3
Injection 5	6.6	27.0	66.4
Injection 6	7.1	27.0	66.0
RSD%	5.9	3.7	1.4

TABLE 2B Peak isoelectric point (p*I*) values of the six injections as shown in Figure 3.

	Peak 1	Peak 2	Peak 3
Injection 1	6.51	6.58	6.69
Injection 2	6.50	6.59	6.69
Injection 3	6.51	6.59	6.69
Injection 4	6.51	6.59	6.69
Injection 5	6.50	6.58	6.69
Injection 6	6.51	6.59	6.68
STD	**0.01**	**0.01**	**0.00**

Using the described "averaged p*I*" approach, we measured the shift from temperature stress. The averaged p*I* value decreases from 6.63 for the reference AAV9 sample to 6.54 for the sample stressed at 37°C for 14 days using the anti-VP1/2/3 detection (Table 3). This decrease of 0.09 pH units

TABLE 2C Averaged isoelectric point (p*I*) values of the six injections as shown in Figure 3.

	Averaged p*I* value
Injection 1	6.651
Injection 2	6.650
Injection 3	6.652
Injection 4	6.650
Injection 5	6.648
Injection 6	6.650
STD	**0.001**

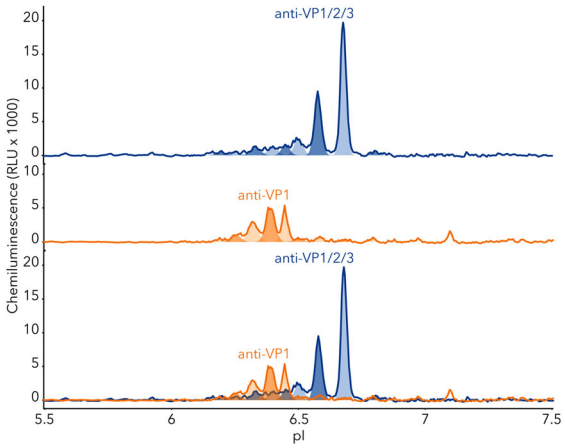

FIGURE 4 Identification of individual adeno-associated virus (AAV) capsid proteins in the denatured imaged capillary isoelectric focusing (icIEF) profile. AAV9 (2.3×10^{10} VP/mL) sample using anti-VP1/2/3 (blue) or anti-VP1 monoclonal antibody (mAb) (orange). VP1 peaks focus on the acidic side of the denatured AAV profile (middle panel). Overlay of two capillaries to illustrate peak identification of VP1 peaks in VP1/2/3 profile (bottom panel).

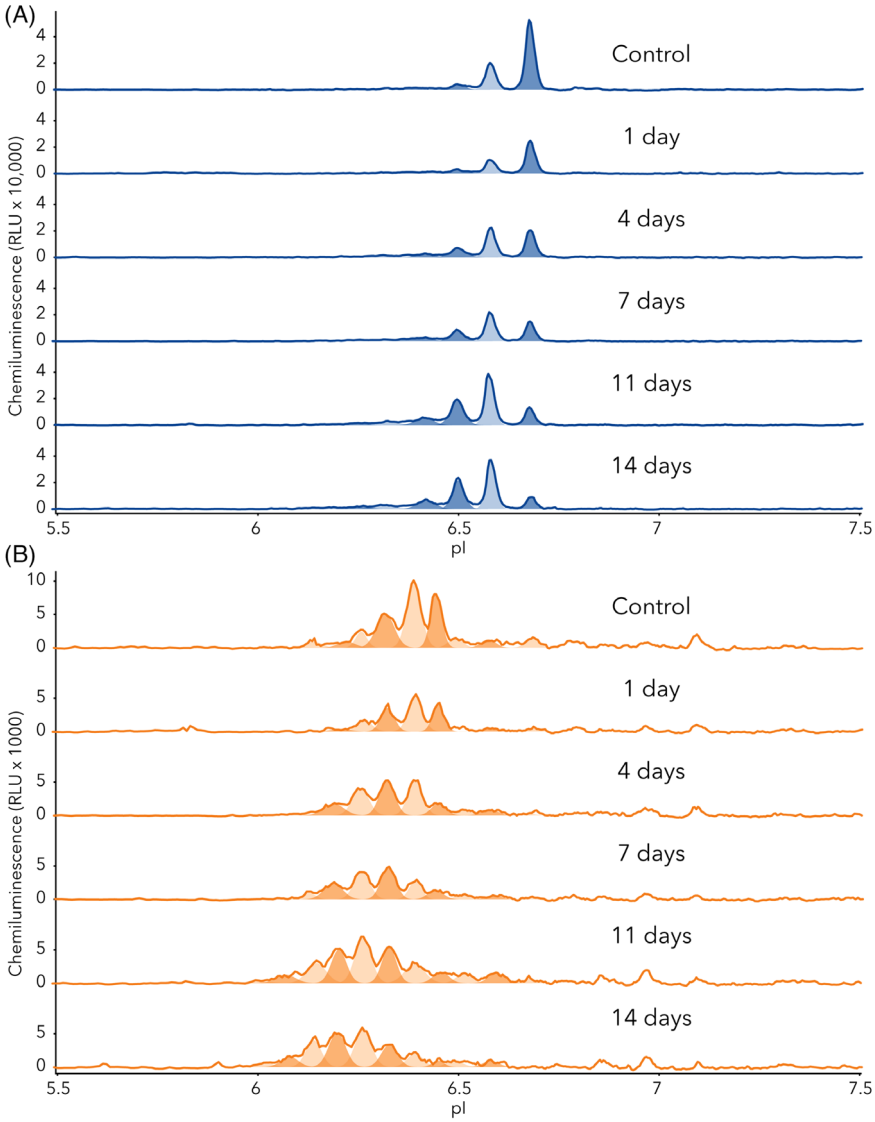

FIGURE 5 VP-specific stability monitoring. Heat-stressed AAV9 samples (1.8×10^{11} VP/mL) were analyzed with (A) anti-VP1/2/3 monoclonal antibody (mAb) to detect all three VPs or (B) in separate capillaries, with anti-VP1 mAb. Reference AAV9 was compared to AAV9 which was stressed at 37°C for 1, 4, 7, 11, and 14 days. Averaged isoelectric point (p*I*) values were calculated for each time point and are summarized in Table 3.

TABLE 3 Averaged isoelectric point (p*I*) values resulting from the stress test as shown in Figure 5.

	Averaged p*I* values	
Sample	**Anti-VP1/2/3**	**Anti-VP1**
Control	6.634	6.374
1 day	6.617	6.374
4 days	6.584	6.317
7 days	6.566	6.299
11 days	6.545	6.251
14 days	6.541	6.239

is above the resolution of the method in averaged p*I* value shown in Table 2C.

The VP1 charge profile exhibits more changes than the observed change in the overall AAV9 charge profile. Notably, more peaks in the acidic region arose after only 1 day at 37°C. Using the averaged p*I* value to quantitatively measure the degradation, we observed a decrease from 6.37 for the reference sample to 6.24 for the 14-day stressed AAV9 (Table 3). This decrease of 0.13 p*I* units is greater than the change in the overall charge profile of 0.09 p*I* units and suggests that VP1 is more sensitive to stress and may serve as a stronger stability indicator compared to the overall VP peak pattern. This is the first time that the charge profile changes of individual AAV viral proteins (VP1 and VP1/2/3) are characterized separately and simultaneously.

3.6 | Evaluation and identification of other AAV serotypes

AAVs are a diverse family of viruses, with 10 naturally occurring serotypes that infect different tissues. All AAV serotypes contain the three capsid proteins (VP1, VP2, and VP3) that assemble in a stochastic manner to form

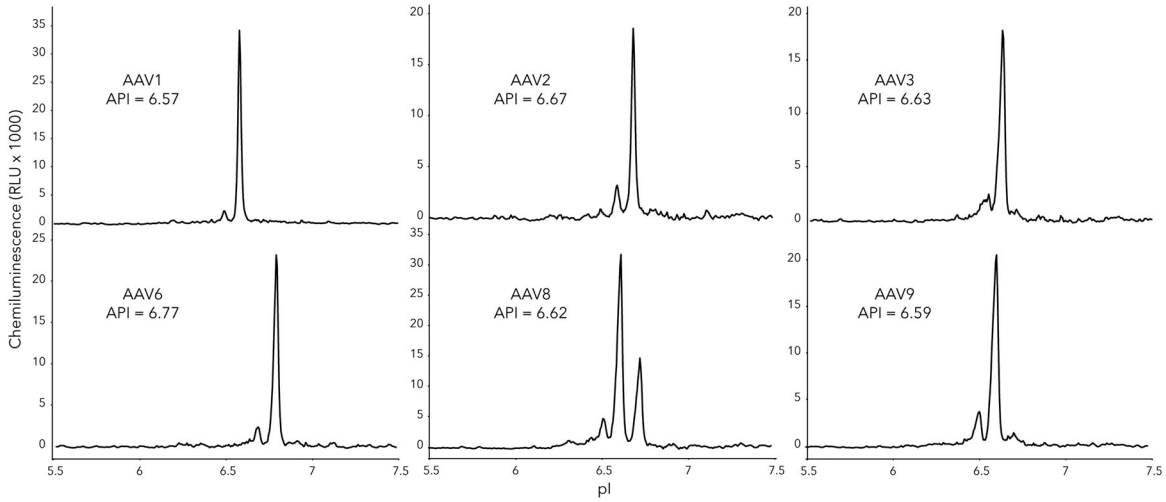

FIGURE 6 Charge profiles of six different adeno-associated virus (AAV) serotypes. AAV 1, 2, 3, 6, 8, and 9 (of 4.0×10^{10} VP/mL) were analyzed by the capillary isoelectric focusing (cIEF) immunoassay using the anti-VP1/2/3 antibody. Individual peak signatures and calculated average isoelectric point (p*I*) values (API) of the most abundant peak are shown for each serotype.

a 60-mer capsid that protects a ssDNA genome [2]. The capsid proteins range in homology from 99% identical (AAV1/AAV6) to around 50% for the least related serotypes [4]. These capsid proteins differ at the amino acid level but have minimal differences in molecular mass. However, we have previously shown that there are significant differences in the peak patterns of the various AAV serotypes when separated by icIEF [11]. We similarly verified the ability of this new method to differentiate various AAV serotypes, and thereby also serve as an identity assay. Six AAV serotypes (AAV1, AAV2, AAV3, AAV6, AAV8, and AAV9) were analyzed with the anti-VP1/VP2/VP3 antibody. Like our previous observations, the peak patterns of each AAV serotype and their averaged p*I* values are unique (Figure 6). Because the standard deviation (0.001) of the averaged p*I* measurement shown in Table 2C is smaller than the averaged p*I* differences of the AAVs of different serotypes (Figure 6), the method can be used as an identity assay. Interestingly, the API of AAV9 in Figure 6 is slightly less acidic than the API reported earlier (Tables 2C and 3), and this could be because the AAV9 analyzed and summarized in Figure 6 was from a different AAV9 lot. Therefore, we envision that this capillary IEF (cIEF) immunoassay may be used as an orthogonal method to provide batch-to-batch identity information as defined by regulatory agencies [5], where subtle changes in manufacturing are expected to change the capsid protein charge heterogeneity.

4 | CONCLUDING REMARKS

Here, we describe an icIEF immunoassay for the detailed study of AAV capsid protein charge heterogeneity. Unlike the icIEF method with direct detection [11, 12], this method uses ultrasensitive chemiluminescence, which demonstrated a 90× sensitivity improvement compared to direct detection. Furthermore, this icIEF immunoassay platform has high sample throughput, processing up to 96 samples in a fully automated overnight run, resulting in reproducible quantification of each peak area percentage and apparent p*I*. The high reproducibility of this method can be leveraged to identify different AAV serotypes by calculating their averaged p*I* values from peak area percentage and the p*I* of each peak. This method also provides stability monitoring at the capsid protein level, delineating the changes in VP1 from those of the other capsid proteins. With the development of new antibodies for specific serotypes, specific capsid proteins, and even other viral vectors, we anticipate that this versatile method will provide detailed insight into capsid protein heterogeneity that can be broadly applicable to not just diverse AAV serotypes, but other viral vectors like lentivirus as well.

As an immunoassay, the specificity of this method enables specific target protein analysis in complex sample types. With this specificity, the charge heterogeneity of AAV capsid proteins in complex matrices like HEK293T whole-cell lysates can be characterized. The method was shown to perform without influence from as much as 20 μg/mL HEK293T lysate, indicating the method can be used to study upstream samples for capsid protein charge heterogeneity and serve as an early indicator of product change from events like deamidation. Furthermore, purity assays using anti-HCP antibodies are compatible with the cIEF immunoassay [19], and the Peggy Sue instrument allows for up to 8 probing cycles with 8 different antibodies on the same sample. Therefore, purity analysis

using anti-HCP antibodies may be combined with charge heterogeneity analysis using antibodies targeting capsid proteins to provide multi-attribute viral vector analysis in a single platform, improving in-process development for biomanufacturing workflows.

By combining and automating the high-resolution protein separation of capillary electrophoresis with the specificity, selectivity, and sensitivity of, the icIEF immunoassay method can rapidly monitor AAV samples and their individual capsid proteins to inform process development in both upstream and downstream bioprocess workflows. Thus, we anticipate that this icIEF immunoassay will be a useful tool to monitor AAVs in different stages of manufacturing.

CONFLICT OF INTEREST STATEMENT

The capillary electrophoresis instruments used in the study are products of the authors' employer.

DATA AVAILABILITY STATEMENT

The data that support the findings will be available from the corresponding author upon reasonable request following an embargo from the date of publication to allow for commercialization of research findings.

ORCID

Jiaqi Wu https://orcid.org/0000-0002-0692-1033

REFERENCES

1. Clark KR. Recent advances in recombinant adeno-associated virus vector production. Kidney Int. 2002;61(Suppl 1):S9–15.
2. Wörner TP, Bennett A, Habka S, Snijder J, Friese O, Powers T, et al. Adeno-associated virus capsid assembly is divergent and stochastic. Nat Commun. 2021;12:1642.
3. Büning H, Srivastava A. Capsid modifications for targeting and improving the efficacy of AAV vectors. Mol Ther Methods Clin Dev. 2019;12:248–65.
4. Mietzsch M, Jose A, Chipman P, Bhattacharya N, Daneshparvar N, McKenna R, et al. Completion of the AAV structural atlas: serotype capsid structures reveals clade-specific features. Viruses. 2021;13(1):101.
5. Chemistry, Manufacturing, and Control (CMC) Information for Human Gene Therapy Investigation New Drug Applications (INDs) - Guidance for Industry. US Food and Drug Administration. Center for Biologics Evaluation and Research. 2020. https://www.fda.gov/regulatory-information/search-fda-guidance-documents/q2r1-validation-analytical-procedures-text-and-methodology-guidance-industry
6. Xu Y, Wang D, Mason B, Rossomando T, Li N, Liu D, et al. Structure, heterogeneity and developability assessment of therapeutic antibodies. mAbs. 2019;11(2):239–64.
7. Mary B, Maurya S, Arumugam S, Kumar V, Jayandharan GR. Post-translational modifications in capsid proteins of recombinant adeno-associated virus (AAV) 1-rh10 serotypes. FEBS J. 2019;286(24):4964–81.
8. Strasser L, Boi S, Guapo F, Donohue N, Barron N, Rainbow-Fletcher A, et al. Proteomic landscape of adeno-associated virus (AAV)-producing HEK293 cells. Int J Mol Sci. 2021;22(21):11499.
9. Giles AR, Sims JJ, Turner KB, Govindasamy L, Alvira MR, Lock M, et al. Deamidation of amino acids on the surface of adeno-associated virus capsids leads to charge heterogeneity and altered vector function. Mol Ther. 2018;26:2848–64.
10. Wu J, McElroy W, Pawliszyn J, Heger CD. Imaged capillary isoelectric focusing: applications in the pharmaceutical industry and recent innovations of the technology. TrAC Trends Anal Chem. 2022;150:116567.
11. Wu J, Heger C. Establishment of a platform imaged capillary isoelectric focusing (icIEF) characterization method for adeno-associated virus (AAV) capsid proteins. Green Anal Chem. 2022;3:100027.
12. He XZ, Powers TW, Huang S, Liu Z, Shi H, Orlet JD, et al. Development of an icIEF assay for monitoring AAV capsid proteins and application to gene therapy products. Mol Ther Methods Clin Dev. 2023;29:133–44.
13. Pattali R, Mou Y, Li XJ. AAV9 vector: a novel modality in gene therapy for spinal muscular atrophy. Gene Ther. 2019;26(7–8):287–95.
14. Foust KD, Nurre E, Montgomery CL, Hernandez A, Chan CM, Kaspar BK. Intravascular AAV9 preferentially targets neonatal neurons and adult astrocytes. Nat Biotechnol. 2009;27(1):59–65.
15. Dayton RD, Wang DB, Klein RL. The advent of AAV9 expands applications for brain and spinal cord gene delivery. Expert Opin Biol Ther. 2012;12(6):757–66.
16. Chahal PS, Schulze E, Tran R, Montes J, Kamen AA. Production of adeno-associated virus (AAV) serotypes by transient transfection of HEK293 cell suspension cultures for gene delivery. J Virol Methods. 2014;196:163–73.
17. Lin J, Lazar AC. Determination of charge heterogeneity and level of unconjugated antibody by imaged cIEF, In: Ducry L, editor. Antibody-drug conjugates. New York: Humana; 2013. p. 295–302.
18. Quan C, Alcala E, Petkovska I, Matthews D, Canova-Davis E, Taticek R, et al. A study in glycation of a therapeutic recombinant humanized monoclonal antibody: where it is, how it got there, and how it affects charge-based behavior. Anal Biochem. 2008;373(2):179–91.
19. Bioprocess contaminant detection using Simple Western. Application Note, ProteinSimple, a Bio-Techne brand. 2018. https://www.bio-techne.com/resources/literature/bioprocess-contaminant-detection-using-simple-western

bio-techne® / proteinsimple

ONE SYSTEM FOR

CE-SDS, cIEF & cIEF Fractionation

Get answers on protein size, charge, and even collect charge variants for further analysis with the Maurice™ and MauriceFlex™ systems.

- Understand your molecules quickly with results in 5-15 minutes
- Make informed decisions with high-quality data
- Collect charge fractions and analyze with any mass spectrometric method
- Easily transfer methods across labs
- Use industry-approved software for regulatory compliance

Learn More

Scan the QR Code or Visit:

bio-techne.com/mauriceflex

bio-techne® // Global Developer, Manufacturer, and Supplier of High-Quality Reagents, Analytical Instruments, and Precision Diagnostics.

INCLUDES R&D Systems™ Novus Biologicals™ Tocris Bioscience™ ProteinSimple™ ACD™ ExosomeDx™ Asuragen® Lunaphore™

Electrophoresis 2021, *42*, 687–692

Finja Krebs
Christin Scheller
Kristina Grove-Heike
Lena Pohl
Hermann Wätzig

Institute of Medicinal and Pharmaceutical Chemistry, Technische Universität Braunschweig, Braunschweig, Germany

Received January 15, 2021
Revised January 29, 2021
Accepted February 1, 2021

Short Communication

Isoelectric point determination by imaged CIEF of commercially available SARS-CoV-2 proteins and the hACE2 receptor

Abstract In order to contribute to the scientific research on the severe acute respiratory syndrome coronavirus 2 (SARS-CoV-2), we have investigated the isoelectric points (pI) of several related proteins, which are commercially available: the receptor-binding domain (RBD) with His- and Fc-tag, the S1 subunit with His-tag, the S1/S2 subunits with His-tag and the human angiotensin-converting enzyme 2 (hACE2) with His-tag. First, the theoretical pI values, based on the amino acid (AA) sequences of the proteins, were calculated using the ProtParam tool from the Bioinformatics Resource Portal ExPASy. The proteins were then measured with the Maurice imaged CIEF system (native fluorescence detection), testing various measurement conditions, such as different ampholytes or ampholyte mixtures. Due to isoforms, we get sections with several peaks and not just one peak for each protein. The determined pI range for the RBD/Fc is 8.24–9.32 (theoretical pI: 8.55), for the RBD/His it is 7.36–9.88 (8.91) and for the S1/His it is 7.30–8.37 (7.80). The pI range of the S1/S2/His is 4.41–5.87 (no theoretical pI, AA sequence unknown) and for hACE2/His, the determined global range is 5.19–6.11 (5.60) for all experimental conditions chosen. All theoretically derived values were found within these ranges, usually close to the center. Therefore, we consider theoretical values as useful to make predictions about the isoelectric points of SARS-CoV-2 proteins. The experimental conditions had only a minor influence on the pI ranges obtained and mainly influenced the peak shapes.

Keywords:
CIEF / COVID-19 / hACE2 / Isoelectric point / SARS-CoV-2 proteins
DOI 10.1002/elps.202100015

The Coronavirus Disease 2019 (COVID-19) pandemic is currently shaking up the whole world. Since the beginning of the outbreak, research has been conducted into medicines and vaccines against the virus in the field of pharmaceutical research. For research purposes, there are several significant proteins of the severe acute respiratory syndrome coronavirus 2 (SARS-CoV-2) on the market. Therefore, our intention was to contribute to the progress of research in this field with the means available to us. In this short communication, the results of the capillary isoelectric focusing (CIEF) measurements of different sections of the SARS-CoV-2 spike protein and the human angiotensin-converting enzyme 2 (hACE2) are presented.

SARS-CoV-2 uses the receptor-binding domain (RBD) of its surface glycoprotein (spike protein) to enter the human body via the hACE2 receptor [1]. The spike protein is comprised of two functional subunits: S1 and S2. While the S1 subunit binds to the hACE2 receptor, the S2 subunit is implicated in the merging of the viral and human cell membranes [2]. For more information on the physicochemical properties of SARS-CoV-2, please refer to the review of Scheller et al. [3].

In the CIEF, the isoelectric focusing takes place in a capillary, as a charge-based analysis via capillary electrophoresis. The CIEF method was implemented by Hjerten et al. in the 1980s and can be seen as an improved, new version of the conventional isoelectric focusing in slab gels [4,5]. The advantages of CIEF over IEF with slab gels are, for example, a smaller sample volume required, shorter analysis times, and higher sensitivity [6]. Using CIEF, a pH gradient is built up in the capillary. The ampholytic analytes migrate in this pH gradient and then remain in the pH zone that corresponds to their pI value [7]. It is also possible in CIEF to use immobilized pH gradients as applied in slab gels. This technique is still under development, but can bring many advantages [6, 8–10]. In this case, the imaged CIEF with carrier ampholytes was used, i.e., an on-line imaging detection system that does not require the mobilization of the analytes after focusing [11].

Since the isoelectric point of proteins is an important property, we sought to determine it using the Maurice (imaged) CIEF system from ProteinSimple, a Bio-Techne brand.

Correspondence: Prof. Dr. Hermann Wätzig, Institute of Medicinal and Pharmaceutical Chemistry, Technische Universität Braunschweig, Beethovenstraße 55, 38106 Braunschweig, Germany
Email: h.waetzig@tu-bs.de

Abbreviations: **hACE2**, human angiotensin-converting enzyme 2; **RBD**, receptor-binding domain; **SARS-CoV-2**, severe acute respiratory syndrome coronavirus 2

Table 1. Experimental conditions for the determination of the isoelectric points via Maurice CIEF of the SARS-CoV-2 proteins and the hACE2 receptor from R&D Systems; sample Load: 55 s, anolyte: 80 mM phosphoric acid in 0.1% methyl cellulose, catholyte: 100 mM NaOH in 0.1% methyl cellulose, V_{well}: 100 µL, 40% SimpleSol Protein Solubilizier (except for experiment **f** of hACE2/His), 0.35% methyl cellulose, 10 mM arginine (except for experiment **f** of hACE2/His); ρ = mass concentration of the respective protein in mg/mL

	RBD/Fc	RBD/His	S1/His	S1/S2/His	hACE2/His
Catalog number	#10499-CV	#10500-CV	#10522-CV	-	#933-ZV
$\rho_{initial}$ [mg/mL]	2.100	1.860	0.350	0.470	0.468
Buffer	PBS pH 7.4	PBS pH 7.4	PBS pH 7.4	PBS pH 7.4	12.5 mM Tris, NaCl, $ZnCl_2$ and glycerol
Theoretical pI	8.55	8.91	7.80	-	5.60
Separation	1 min 1500 V 7.5 min 3000 V	1 min 1500 V 7.5 min 3000 V	1 min 1500 V 8.5 min 3000 V	1 min 1500 V 11 min 3000 V	1 min 1500 V a-e: 20 min, f: 15 min 3000 V
Fluorescence exposure time	50 s	50 s	50 s	50 s	a: 5 s, b: 50 s, e: 30 s, f: 10 s
ρ_{final} [mg/mL]	0.036	0.035	0.040	0.080	a: 0.040 b: 0.016 e: 0.041 f: 0.098
Urea [mol/L]	-	-	-	-	e: 2 f: 7
Ampholyte	a/b: 3–10 (4%) c: 3–10 (1%), 8–10.5 (3%) d: 8–10.5 (4%)	a/b: 3–10 (4%) c: 3–10 (1%), 8–10.5 (3%)	a/b: 3–10 (4%) c: 3–10 (1%), 8–10.5 (3%) d: 8–10.5 (4%)	a: 3–10 (4%)	a/b/e: 3–10 (4%) f: 2.5–5 (3%), 5–8 (2%)
pI markers (1% each)	a: 3.38, 9.99 b/c/d: 7.05, 9.50	a: 3.38, 9.99 b/c: 7.05, 10.17	a: 3.38, 9.99 b/c/d: 7.05, 9.50	a: 3.38, 9.99	a: 3.38, 9.99 b/e/f: 4.05, 7.05

We used the SARS-CoV-2 proteins currently available on the market, namely the RBD with His- and Fc-tag, the S1 subunit with His-tag, and the S1/S2 subunits with His-tag.

As the virus binds to the hACE2 in the human body, this receptor was included in the study (all proteins were provided by R&D Systems, a Bio-Techne brand, Minneapolis, Minnesota, USA).

First, the theoretical pI values of the proteins were calculated using the ProtParam tool from the Bioinformatics Resource Portal ExPASy [12]. The basis for this was the given AA sequence of the corresponding protein, which can be found in the R&D Systems catalog [13] on the page of the respective protein (see catalog numbers in Table 1).

The SARS-CoV-2 RBD/Fc is derived from the surface glycoprotein (NCBI Reference Sequence: YP_0 097 24390.1) Arg319-Phe541, which is linked to human IgG1 (Pro100-Lys330) via the sequence IEGRMD. The pI value calculated using this sequence is 8.55. The His-tagged SARS-CoV-2 RBD, with a theoretical pI of 8.91, is also the surface glycoprotein Arg319-Phe541, but with a C-terminal 6-His-tag. The S1/His subunit is also the surface glycoprotein, but the sequence Val16-Pro681, with a C-terminal 6-His-tag. A pI of 7.80 can be calculated from this sequence. The S1/S2/His protein is not yet commercially available and therefore not included in the R&D Systems catalog. For this reason, no theoretical pI value can be calculated as the exact AA sequence is unknown. The hACE2/His receptor consists of the AA sequence of the hACE2 protein (UniProtKB/Swiss-Prot: Q9BYF1) Gln18-Ser740, with a C-terminal 10-His-tag. The pI value of this sequence calculated via ExPASy is 5.60.

Subsequently, it is investigated to what extent the theoretical pI values agree with the experimentally measured ones.

For the Maurice CIEF system, the Maurice CIEF cartridges and the Maurice CIEF method development kit (including all reagents used, such as the anolyte, catholyte, ampholytes, pI markers, SimpleSol, etc.) were used (provided by ProteinSimple, a Bio-Techne brand, San Jose, California, USA). With native fluorescence at an excitation wavelength of 280 nm, emitted light at 320–450 nm was used for detection [14].

The measurements were performed under the experimental conditions shown in Table 1.

The preparation of the samples is now explained using the sample from experiment **a** of the RBD/Fc as an example. 8.5 µL of protein, dissolved in PBS buffer ($\rho_{initial}$ = 2.100 mg/mL), was mixed with 35 µL of 1% methyl cellulose, 40 µL SimpleSol, 4 µL ampholyte 3–10, 2 µL of 500 mM arginine, 1 µL each of pI markers 3.38 and 9.99 and 8.5 µL DI water, resulting in a total volume of 100 µL. Samples were then vortexed and centrifuged to be pipetted into a 96-well plate.

In order to get a general overview of the pI value of the respective protein, the wide range ampholyte with markers at the edges of the range was first selected (**a**).

In a second step, pI markers whose pI values were as close as possible to those of the respective protein were chosen (**b**).

Next step was to improve the resolution of the peaks by using ampholyte mixtures. For this purpose, wide range ampholytes and narrow range ampholytes were mixed in a ratio

Electrophoresis 2021, *42*, 687–692

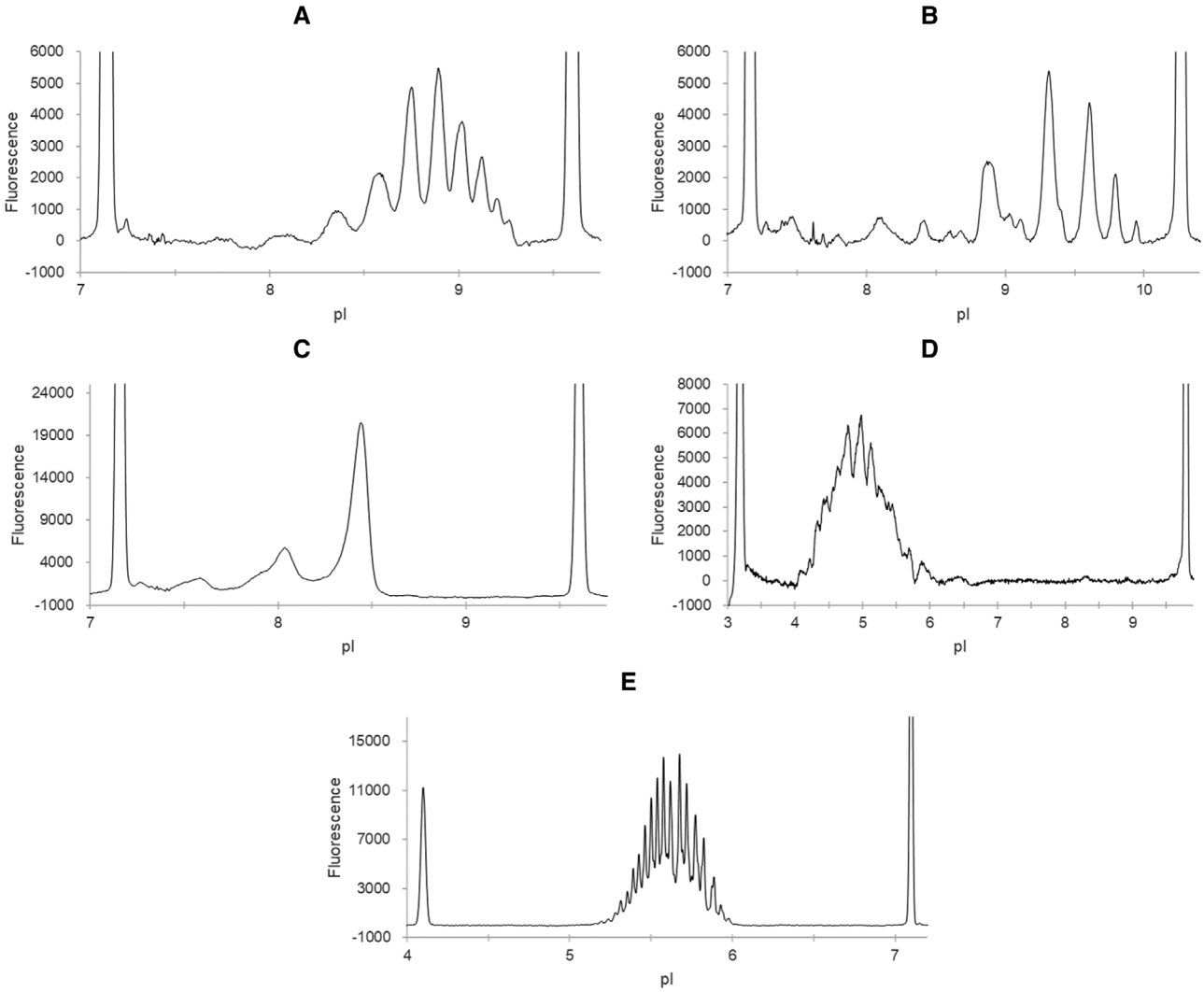

Figure 1. Electropherograms of the Maurice CIEF measurements. **A**: SARS-CoV-2 RBD/Fc experiment **b**; **B**: RBD/His experiment **b**; **C**: S1/His experiment **b**; **D**: S1/S2/His experiment **a**; **E**: hACE2/His experiment **f**. For better visualization, the y-axes were displayed only in the area of fluorescence of the sample peaks.

of 1:3 (**c**). The mixing ratio was chosen based on the work of Kahle et al. [15].

An additional approach was to only use narrow range ampholytes (**d**). Because the peak profile of the hACE2/His protein was not as reproducible, this protein was also measured with an addition of urea. For **e**, the two protein solubilizers SimpleSol and urea were used. Since the addition of SimpleSol and urea did not lead to a good peak shape either, SimpleSol was subsequently omitted and the concentration of urea was increased. In addition, several ampholyte mixtures were tested. Finally, a concentration of 7 M urea and a mixture of ampholytes 2.5–5 (3%) and 5–8 (2%) was used and thus well reproducible peaks were obtained (**f**).

Since the proteins are very expensive and only available in small quantities, further optimization attempts were not conducted. Furthermore, there were no repetitions of non-evaluable measurements, as the proteins will be used for future affinity capillary electrophoresis (ACE) experiments, in which the binding behavior of the SARS-CoV-2 proteins to the hACE2 receptor will be investigated.

Figure 1 shows the electropherograms of each measured protein in the particular experiment where the protein yielded the most reproducible peaks with the best peak shape.

The electropherograms show, that the proteins produce very different peak profiles. In case of the SARS-CoV-2 RBD/Fc (Figure 1A), the individual isoforms can be seen very clearly. SARS-CoV-2 RBD/His (Figure 1B), on the other hand, shows very small peaks in the approximate range of pI 7 to 8.5 and then some larger ones in the range of pI 8.5 to 10.

The S1/His subunit (Figure 1C) produces three peaks, whose areas increase with pI, so the one with the highest pI is the largest at about 8.4.

Table 2. Results of the Maurice CIEF measurements of SARS-CoV-2 proteins and the hACE2 receptor (experiments **a**-**f**). Given are the mean values of the isoelectric points determined from a certain number of repetitions (n) and the relative standard deviation (RSD) in %

a					**RBD/Fc (theoretical pI: 8.55)**					***n* = 5**
mean	8.359	8.572	8.782	8.924	9.052	9.153	9.250	9.316		
RSD [%]	0.219	0.222	0.064	0.093	0.142	0.088	0.085	0.061		
b										***n* = 8**
mean	8.254	8.478	8.649	8.794	8.915	9.021	9.103	9.164		
RSD [%]	0.157	0.158	0.029	0.032	0.048	0.044	0.051	0.049		
c										***n* = 6**
mean	8.390	8.633	8.757	8.886						
RSD [%]	0.054	0.134	0.036	0.061						
d										***n* = 6**
mean	8.235	8.429	8.629	8.877						
RSD [%]	0.050	0.159	0.007	0.069						
a					**RBD/His (theoretical pI: 8.91)**					***n* = 7**
mean	7.412	7.738	8.025	8.338	8.799	9.229	9.503	9.691	9.833	
RSD [%]	0.114	0.137	0.201	0.203	0.081	0.110	0.084	0.073	0.072	
b										***n* = 8**
mean	7.357	7.685	7.991	8.314	8.766	9.217	9.509	9.695	9.849	
RSD [%]	0.135	0.117	0.104	0.117	0.212	0.085	0.061	0.047	0.131	
c										***n* = 6**
mean	7.925	8.199	8.440	8.733	9.086	9.316	9.477	9.702	9.875	
RSD [%]	0.060	0.307	0.098	0.125	0.106	0.058	0.070	0.075	0.056	
a					**S1/His (theoretical pI: 7.80)**					***n* = 8**
mean	7.545	7.994	8.372							
RSD [%]	1.394	1.349	1.376							
b										***n* = 8**
mean	7.479	7.932	8.334							
RSD [%]	0.103	0.037	0.025							
c										***n* = 6**
mean	7.303	7.706	8.064							
RSD [%]	0.040	0.066	0.015							
d										***n* = 6**
mean	7.681	7.837	8.012	8.134						
RSD [%]	0.048	0.185	0.039	0.114						
a					**S1/S2/His**					***n* = 6**
mean	4.406	4.507	4.605	4.817	4.974	5.157	5.309	5.423	5.608	5.872
RSD [%]	0.154	0.059	0.040	0.106	0.165	0.059	0.252	0.176	0.481	0.109
a					**hACE2/His (theoretical pI: 5.60)**					***n* = 8**
mean	5.605	5.673	5.790	5.846	5.908	5.939	6.004	6.109		
RSD [%]	0.402	0.807	0.438	0.119	0.129	0.046	0.085	0.094		
b										***n* = 8**
mean	5.355	5.428	5.497	5.576	5.692					
RSD [%]	0.133	0.087	0.102	0.123	0.090					
e										***n* = 5**
mean	5.370	5.416	5.465	5.528	5.581	5.618	5.751			
RSD [%]	0.057	0.020	0.027	0.076	0.054	0.054	0.116			
f										***n* = 12**
mean	5.188	5.231	5.263	5.304	5.341	5.375	5.413	5.451	5.489	5.526
RSD [%]	0.086	0.022	0.076	0.053	0.057	0.053	0.048	0.044	0.048	0.049
mean	5.570	5.626	5.670	5.723	5.771	5.834	5.884	5.928		
RSD [%]	0.042	0.044	0.036	0.036	0.032	0.037	0.030	0.019		

Electrophoresis 2021, *42*, 687–692

With the S1/S2/His subunit (Figure 1D), it was challenging to get peaks at all. Using a very high concentration, a broad peak with some spikes is finally obtained.

After some optimization of the experimental conditions, the hACE2/His receptor (Figure 1E) shows a very reproducible peak profile, in which the different isoforms can be well recognized.

With the peak profiles of the individual proteins in mind, we now take a look at the determined isoelectric points of the proteins. Table 2 summarizes the results of the CIEF measurements of the five proteins.

With regard to the results, the RBD/Fc protein will be discussed first. The theoretically calculated pI value of this protein is 8.55. In all experiments (**a**-**d**) pI values in the range of 8.24 to 9.32 were obtained. The measured values are therefore in the range around the theoretically calculated pI, the distribution is probably due to isoforms.

Next, we come to the results of the SARS-CoV-2 RBD with His-tag. For the two measurements in ampholyte 3–10 (**a**, **b**) we have very similar pI values in the range between about 7.36 and 9.85. The pI values in measurement **c**, i.e., the measurement in the ampholyte mixture, lie between 7.93 and 9.88, which is probably due to the fact that the pI gradient in the ampholyte mixture at the edges of the narrow range ampholyte is not linear. The measurement with the narrow range ampholyte (**d**) could not be evaluated for this protein and was not repeated due to the small amount of material available. The theoretical pI of this protein is 8.91. In the measurements, this is in the range of the large peaks of the protein. Overall, the experimentally determined pI values can be found around the theoretically determined value in the range ± 1 pH unit for this protein.

Looking at the S1 subunit with His-tag, the pI range of the experiments **a** and **b** again hardly differs, so the pI values seem to behave nearly linear over the whole pI area. The determined range in these two experiments is about 7.48 to 8.37. The differences in comparison to the measurement in the ampholyte mixture (**c**) are probably due to the fact that the pI value of the protein is located at the border of the narrow range ampholyte (8–10.5) and pI values in this border area are probably somewhat distorted.

The pI values determined using the narrow range ampholyte in experiment **d** lie in the range from 7.68 to 8.13, i.e., the range is significantly smaller than in the previous measurements. The theoretically calculated pI of the S1 subunit with His-tag is 7.80 and thus approximately in the middle of the experimentally determined ranges.

When measuring the S1/S2 subunit with His-tag, the first problem was that no peaks could be found. The concentration of the protein was then continuously increased until peaks could finally be identified. These peaks, shown in the electropherogram in Figure 1D, could also be described as very broad and flat. Because of the high sample consumption due to the high concentration and the failed experiments before, only experiment **a** was performed. The experimentally determined pI values lie in a range from 4.41 to 5.87. Due to the unknown AA sequence, there is no theoretically calculated pI value and therefore it is not possible to assess whether the values are in the same range.

The last protein investigated is the His-tagged hACE2 receptor, whose theoretically calculated pI value is 5.60. The pI range determined with the wide range ampholyte and the markers 3.38 and 9.99 is 5.61 to 6.11 (experiment **a**), but the peaks looked as if the protein was aggregated.

Subsequently, a lower concentration was chosen for measurements **b**, **c**, and **d** to avoid aggregation, whereby only experiment **b** could be evaluated. The pI range determined there is 5.36 to 5.69 and is in the range determined in experiment **a**, but smaller. Since the peaks still looked as if the protein was aggregated, a measurement with urea and SimpleSol as protein solubilizers was conducted afterwards (**e**). The reproducibility of the peak profiles was slightly improved and the values (5.37–5.75) hardly differ from those of measurement **b**. In order to obtain a reproducible peak shape and no aggregation, an attempt was made to optimize the method. In the following, SimpleSol was omitted and the concentration of urea was increased. In addition, several ampholyte mixtures were tried. In experiment **f**, with 7 M urea and ampholytes 2.5–5 (3%) and 5–8 (2%), peaks with recognizable isoforms of the receptor were finally obtained, which were very reproducible. The pI values in this experiment are between 5.19 and 5.93 and therefore in the range of the previously performed experiments. Thus, the aggregation did not have a strong effect on the pI value determination. Due to the good reproducibility, this method could be well used for quality control of the receptor, since even the smallest impurities would presumably have an effect on the peak shape.

In summary, the theoretical pI values calculated on the basis of the AA sequence are in the same range as those determined experimentally. It is not possible to determine an exact value experimentally for these proteins, since all electropherograms show several peaks due to isoforms. However, these ranges always coincide with the calculated values.

Therefore, the model calculations for these proteins are useful to make predictions about the isoelectric points of the proteins, if they are needed and no time and/or equipment is available for own experiments regarding the pI value determination. The experimental conditions (ampholyte, pI markers, concentration) do not have a particularly large influence on the determined pI value and merely the number and shape of peaks vary. By optimizing the experimental conditions, aggregation can be prevented and the separation of the individual isoforms can be made possible. With further optimization, quality control methods using CIEF can be developed for these proteins.

The Maurice CIEF, including all reagents, and the proteins were provided by ProteinSimple, a Bio-Techne Brand. We would like to thank Susanne Doerks, Carsten Lueck, Udo Burger, and Chris Heger for their tremendous support.

Open access funding enabled and organized by Projekt DEAL.

The authors have declared no conflict of interest.

Data Availability Statement

The data that support the findings of this study are available from the corresponding author upon reasonable request.

References

[1] Walls, A. C., Park, Y.-J., Tortorici, M. A., Wall, A., McGuire, A. T., Veesler, D., *Cell* 2020, *181*, 281–292.e6.

[2] Matsuyama, S., Ujike, M., Morikawa, S., Tashiro, M., Taguchi, F., *Proc. Natl. Acad. Sci. USA* 2005, *102*, 12543–12547.

[3] Scheller, C., Krebs, F., Minkner, R., Astner, I., Gil-Moles, M., Wätzig, H., *Electrophoresis* 2020, *41*, 1137–1151.

[4] Hjerten, S., *J. Chromatogr. A* 1985, *346*, 265–270.

[5] Hjerten, S., Liao, J.-L., Yao, K., *J. Chromatogr. A* 1987, *387*, 127–138.

[6] Koshel, B. M., Wirth, M. J., *Proteomics* 2012, *12*, 2918–2926.

[7] Righetti, P. G., Drysdale, J. W., *J. Chromatogr. A* 1974, *98*, 271–321.

[8] Yang, C., Zhu, G., Zhang, L., Zhang, W., Zhang, Y., *Electrophoresis* 2004, *25*, 1729–1734.

[9] Wang, T., Ma, J., Wu, S., Sun, L., Yuan, H., Zhang, L., Liang, Z., Zhang, Y., *J. Chromatogr. B: Anal. Technol. Biomed. Life Sci.* 2011, *879*, 804–810.

[10] Liu, R., Pan, H., Zheng, Y., Hu, J., Cheddah, S., Wang, W., Wang, Y., Yan, C., *Electrophoresis* 2019, *40*, 1722–1730.

[11] Wu, J., Pawliszyn, J., *Anal. Chem.* 1992, *64*, 2934–2941.

[12] Swiss Institute of Bioinformations (SIB), *ExPASy: ProtParam Tool*, https://web.expasy.org/protparam/, last viewed January 2021.

[13] *R&D Systems*, https://www.rndsystems.com/, last viewed January 2021.

[14] ProteinSimple, *Maurice CIEF specification*, https://www.proteinsimple.com/maurice.html, last viewed January 2021.

[15] Kahle, J., Stein, M., Wätzig, H., *Electrophoresis* 2019, *40*, 2382–2389.

Electrophoresis 2022, *43*, 1068–1090

Lars Geurink[1,2]
Ewoud van Tricht[1]
Debbie van der Burg[1]
Gerard Scheppink[1]
Bojana Pajic[1]
Justin Dudink[1]
Cari Sänger–van de Griend[1,2,3]

[1]Janssen Vaccines and Prevention B.V., CN Leiden, The Netherlands
[2]Department of Medicinal Chemistry, Faculty of Pharmacy, Biomedical Centre, Uppsala University, Uppsala, Sweden
[3]Kantisto B.V., Baarn, The Netherlands

Received August 27, 2021
Revised October 14, 2021
Accepted October 25, 2021

Research Article

Sixteen capillary electrophoresis applications for viral vaccine analysis

A broad range of CE applications from our organization is reviewed to give a flavor of the use of CE within the field of vaccine analyses. Applicability of CE for viral vaccine characterization, and release and stability testing of seasonal influenza virosomal vaccines, universal subunit influenza vaccines, Sabin inactivated polio vaccines (sIPV), and adenovirus vector vaccines were demonstrated. Diverse CZE, CE-SDS, CGE, and cIEF methods were developed, validated, and applied for virus, protein, posttranslational modifications, DNA, and excipient concentration determinations, as well as for the integrity and composition verifications, and identity testing (e.g., CZE for intact virus particles, CE-SDS application for hemagglutinin quantification and influenza strain identification, chloride or bromide determination in process samples). Results were supported by other methods such as RP-HPLC, dynamic light scattering (DLS), and zeta potential measurements. Overall, 16 CE methods are presented that were developed and applied, comprising six adenovirus methods, five viral protein methods, and methods for antibodies determination of glycans, host cell-DNA, excipient chloride, and process impurity bromide. These methods were applied to support in-process control, release, stability, process- and product characterization and development, and critical reagent testing. Thirteen methods were validated. Intact virus particles were analyzed at concentrations as low as 0.8 pmol/L. Overall, CE took viral vaccine testing beyond what was previously possible, improved process and product understanding, and, in total, safety, efficacy, and quality.

Keywords:
Analytical quality by design / Application / CE / Validation / Virus vaccine
DOI 10.1002/elps.202100269

Additional supporting information may be found online in the Supporting Information section at the end of the article.

1 Introduction

Viral vaccines are key in the prevention of infectious diseases caused by viruses such as nCoV-2, Ebola virus, Respiratory syncytial virus (RSV), human immunodeficiency virus (HIV), influenza virus, Polio virus, and so on [1,2]. Vaccines must be proven safe, efficacious, and of constant quality, and must be authorized by health authorities before the vaccine can be administered [3]. Analytical methods are needed to prove safety, efficacy, and quality, by determining the product identity, product and process-related impurities, product content, and product potency [4]. First, vaccine products are characterized to determine the critical quality attributes (CQAs) of the vaccine that are linked to safety, efficacy, and quality. Second, the critical process parameters (CPPs) and the critical material attributes (CMAs) are determined, and proven acceptable

Correspondence: Lars Geurink, MSc., Janssen Vaccines and Prevention B.V., Archimedesweg 4–6, 2333 CN Leiden, The Netherlands.
Email: lgeurin1@its.jnj.com

Abbreviations: **Ad26**, adenovirus type 26; **AEX**, anion exchange; **AQbD**, analytical quality by design; **AUC**, analytical ultra-centrifugation; **BFS**, bare fused silica; **CH**, clarified harvest; **CMA**, critical material attribute; **CMP**, critical method parameter; **CPP**, critical process parameter; **CS**, control strategy; **DB**, domiphen bromide; **DLS**, dynamic light scattering; **DP**, drug product; **DS**, drug substance; **ELS**, electrophoretic light scattering; **FB**, formulation buffer; **HA**, hemagglutinin; **HIV**, human immunodeficiency virus; **(i)cIEF**, (imaging) capillary isoelectric focusing; **IPC**, in-process control testing; **LH**, lysed harvest; **NIBSC**, National Institute for Biological Standards and Control; **PAR**, proven acceptable range; **PNGase F**, N-glycosidase F; **PTM**, posttranslational modification; **qPCR**, quantitative polymerase chain reaction; **RP-HPLC**, reversed-phase high-performance liquid chromatography; **RSV**, respiratory syncytial virus; **SDS**, sodium dodecyl sulfate; **SE**, sedimentation equilibrium; **sIPV**, Sabin inactivated polio vaccine; **SRID**, single radial immunodiffusion; **SV**, sedimentation velocity; **UF/DF**, ultra- and diafiltration; **UV**, ultraviolet

Color online: See article online to view Figs. 1–15 in color.

ranges (PARs) and design space are set [2,5–8]. Subsequently, a control strategy (CS) is defined. Analytical testing is vital to support this process for determining and linking CQAs, CPPs, CMAs, and PARs, and defining a CS.

Due to the nature of CE, that is, efficient, sensitive, and fast separation in small volumes, the technique is intrinsically suitable for analytical analysis for many different CQAs, e.g., virus content and integrity [9–32], viral protein content, composition, integrity, and identity [33–44], protein [45], chloride [46], bromide [47,48] excipients, etc. However, only a few publications are in the context of pharmaceutical analysis of viral vaccines.

The objective of this paper is to demonstrate the applicability of CE for viral vaccine analysis by presenting studies done within Janssen Vaccines. Application of CE was studied for viral vaccine characterization, and release and stability testing of seasonal influenza virosomal vaccines, universal subunit influenza vaccines, Sabin inactivated polio vaccines (sIPV), and adenovirus vector vaccines.

2 Materials and methods

If not indicated otherwise, samples were produced at Janssen Vaccines and Prevention (Leiden, the Netherlands). Antibody 1 (Ab1) and antibody 2 (Ab2) were from ImmunoPrecise antibodies Ltd. (Victoria, Canada). NIBSC B/Brisbane/60/2008 was from NIBSC (Hertfordshire, UK). Ad5.ATCC was from American Type Culture Collection (Manassas, USA).

All CE experiments were performed on an Agilent 7100 capillary *Electrophoresis* system (Waldbronn, Germany) with either ChemStation (Agilent) or Waters Empower 3 (Milford, USA) software, if not indicated otherwise.

2.1 CE-SDS analysis

A 50 μm ID bare-fused silica (BFS) capillary, total length of 33.0 cm and detection window at 24.5 cm from Agilent was used. The capillary was conditioned with 0.1 M NaOH at 4 bar for 10 min and 0.1 M HCl at 4 bar for 3 min, Milli-Q water at 4 bar for 2 min, and filled with gel buffer at 4 bar for 10 min from the IgG purity and heterogeneity assay kit from Sciex (Nieuwerkerk aan den IJssel, The Netherlands) [49]. All samples were injected at 100 mbar for 100 s. Separations were performed with a pressure of 2 bar on both capillary ends and an applied voltage of –20 kV. Signals were recorded at 214 nm.

2.1.1 CE-SDS for critical reagent antibody purity

Samples were treated according to the purity and heterogeneity assay kit [49]. Separation was achieved with an applied voltage of –16.5 kV, and a cassette temperature of 25°C.

2.1.2 CE-SDS for seasonal influenza protein

Samples were reduced and denatured with 0.5% (v:v) sodium dodecyl sulfate (SDS, Invitrogen Bleiswijk, The Netherlands) and 62.5 mM 2-mercapthoethanol (2-ME, Sigma Aldrich Zwijndrecht, The Netherlands), set to 100°C, for 10 min. Deglycosylation was performed by adding 4 μL of phosphate buffer pH 7.4, 4 μL of N-glycosidase F (PNGase F, Roche Woerden, The Netherlands), and 4 μL of Triton X-100 (Sigma Aldrich) to 20 μL of the reduced sample, and incubation at 37°C for 1 h. Before analysis, 2 μL of 10% (w/v) SDS was added to the deglycosylated sample. The samples were injected on either the short end, 8.5 cm effective length, or long end, 24.5 cm effective length (100 mbar for 100 s). Separation was achieved with a cassette temperature of 32.5°C, and 85% v:v gel buffer (kit gel buffer diluted with Milli-Q water). See van Tricht et al. for more details [33].

2.1.3 CE-SDS for universal influenza protein

Samples were reduced and denatured with 0.45% w/v SDS and 4.5% v/v 2-ME and incubated at 70°C for 10 min and subsequently deglycosylated using 0.66% v/v Triton X-100, 6.6% of a mixture of deglycosylation enzymes consisting of PNGase F, O-glycosidase (New England Biolabs Evry, France), and neuraminidase from *Arthrobacter ureafaciens* (Sigma–Aldrich), and incubated at 37°C for 1 h. Before analysis, 0.32% w/v SDS and 1.6% v/v 10 kDa internal standard (Sciex) were added. Samples were injected (100 mbar for 100 s) at the short-end of the capillary, 8.5 cm effective length. The capillary temperature was kept at 20°C. See Geurink, et al. for more details [34].

2.1.4 CE-SDS for Sabin inactivated polio protein

Samples were reduced and denatured with 2% w/v SDS and 7% v/v 2-ME and incubated at 100°C for 20 min. Samples were injected (100 mbar for 100 s) at the long end of the capillary, 24.5 cm effective length. The separation conditions were 20°C capillary temperature, and 80% v:v gel buffer. See Geurink et al. for more details [34].

2.2 icIEF for universal influenza protein

Imaging capillary isoelectric focusing (icIEF) analyses were performed on a Maurice C. instrument (ProteinSimple San Jose, USA). Sialic acids were removed by the addition of 1.3% v/v sialidase from *Arthrobacter ureafaciens* (Sigma–Aldrich) to the sample and incubation for 2 h at 37°C. Subsequently, the samples were buffer exchanged and concentrated on a 10 kDa Amicon spin filter (MilliPore Merck Amsterdam-Zuidoost, the Netherlands). The icIEF separation master mix for one sample was composed of 2 μL Pharmalyte pI 3–10 (GE Healthcare Chicaco, USA), 6 μL Servalyt pI 4–9 (Biophoret-

ics Spars, USA), 70 μL 1% methylcellulose (ProteinSimple), 34 μL Milli-Q water, 2 μL Maurice C. pI marker 3.38 (ProteinSimple), 2 μL Maurice C. pI marker 7.05 (ProteinSimple), 5 μL 1.5 M urea solution (Sigma–Aldrich), and 11 μL Anodic spacer 200 mM iminodiacetic acid (Sigma–Aldrich). Equilibration and rinsing were performed using default Maurice C conditions. Twenty-five microliters of sample was mixed onboard with 100 μL of master mix and run at 1 min 1500 V and 6 min 3000 V. Native protein fluorescent signals were used for peak integration and apparent pI determination.

2.3 CZE for adenovirus analysis

A PVA coated capillary with extended light path, 50 μm ID, 33.0 cm total length, and 8.5 cm effective length (Agilent) was rinsed with 10 mM ortho-phosphoric acid (Merck Millipore) and filled with a BGE (pH 7.7) composed of a 125 mM Tris(hydroxymethyl)aminomethane (Merk Millipore), and 338 mM tricine (Sigma Aldrich), and 0.2% polysorbate-20 (Merck Millipore), both at 2.5 bar for 1 min. Samples were injected at 50 mbar for 5 s at the short end of the capillary (8.5 cm effective length) and separated with an applied voltage of –25 kV (12 s ramping) at 15°C cassette temperature. UV-absorbance at 214 nm was recorded. See for more details van Tricht et al. [20]. The adenovirus type 26 (Ad26) concentration was determined based on the corrected peaks area and a one-point calibration from a well-characterized in-house Ad26 reference material.

2.4 HC DNA analysis

DNA was purified from the samples using the DNA extractor WAKO kit (Fujifilm Neuss, Germany) [50]. To 500 μL of sample, 20 μL of sodium N-lauroyl sarcosinate solution, and 500 μL sodium iodide with glycogen were added and incubated for 15 min at 40°C. The sample was centrifugated at 10.000 g for 15 min. The supernatant was removed and the pellet was reconstituted in formulation buffer (FB).

2.4.1 Capillary gas electrophoresis

Analysis was performed according to the Sciex dsDNA 1000 kit [51]. A Sciex 8000 plus system was used with a Sciex DNA Capillary (100 μm ID, 40.2 cm total length, 30 cm effective length). The capillary was conditioned with dsDNA gel at 20 psi for 10 min, water dip for 0 min, and applied voltage at –5.0 kV for 10 min (with a 5 min ramp). Before each sample injection, the capillary was conditioned with the Sciex DSFNDA 1000 Gel Buffer with LIFluor™ EnhanCE dye at 20 psi for 10 min. The Thermo Fisher Scientific 200 bp (Breda, The Netherlands) was added as an internal standard to the sample and the sample was injected at –8 kV for 20 s. Separation was performed with an applied voltage of –7.8 kV, at 20°C, for 30 min. The fluorescent signal was recorded with excitation wavelength of 488 nm and emission wavelength of 520 nm.

2.4.2 Slab-gel electrophoresis

Slab-gel electrophoresis was performed according to the Bio-Rad Chemidoc user guide [52]. Lonza (Geleen, The Netherlands) 6x loading buffer was added to the samples 1:5 (v:v) and loaded on a Lonza Flash Gel cassette 2.2% agarose loading gel. Separation was performed on a Bio-Rad (Lunteren, The Netherlands) ChemiDac gel *Electrophoresis* instrument at 250 V for 6 min. Pictures were made with the Bio-Rad camera and processed with the Bio-Rad Image Lab software.

2.5 DLS and ELS

The determinations of the size and zeta potential of adenovirus particles were performed with a Malvern Panalytical Ltd. (Malvern, UK) Zetasizer Nano ZS. Measurements were carried out at 25°C with a disposable Folded Capillary cell (DTS 1070, Malvern Panalytical Ltd.) containing 800 μL sample. The size determination was measured by dynamic light scattering (DLS) with a 632.8 nm laser at a measuring angle of 173°. The laser power was set on automatic attenuation. For each size determination, a total of three measurements were performed, the measurement duration was set on automatic. The zeta potential was measured by electrophoretic light scattering (ELS). The zeta potential was determined by measuring the electrophoretic mobility with electrophoretic light scattering and converting this value into the zeta potential using the Smoluchowski equation. A total of three measurements consisting of 20 runs each were performed. The laser attenuation and the voltage selection were set on automatic. Data acquisition and processing were done by the Zetasizer software.

2.6 Domiphen concentration with RP-HPLC-CAD

Reversed-phase high-performance liquid chromatography (RP-HPLC) analyses were carried out on a Waters Alliance 2695 HPLC with a Waters XBridgeTM Shield RP18 column (4.6×100 mm, 3.5 μm). with mobile phases A: 10 mM ammonium acetate (Sigma Aldrich), pH 3, and B: acetonitrile (Sigma Aldrich). One hundred microliters sample was injected and elution was carried out at a flow rate of 1.0 mL/min starting with 5% B for 2.2 min, followed by a linear gradient of 1.8 min to 95% B and 95% B for 2 min. Column re-equilibration comprised a linear gradient of 95% to 5% B in 1 min followed by 5% B for 2 min. The column temperature was 60°C. Analytes were monitored with a UV detector at 262 nm. Data acquisition and processing were done by Empower 3 software. The concentration was determined based on the peak area and a calibration curve prepared with weighted in domiphen standards.

2.7 CZE for bromide analysis

An Agilent BFS capillary, with an extended light path, 50 μm ID, and a 48.5 cm total length (40 cm effective length), was used. The capillary was flushed at 1 bar with 0.1 M sodium hydroxide for 10 min and Milli-Q water for 2 min and equilibrated until 20°C before analysis. Before each injection, the capillary was flushed at 1 bar with Milli-Q water for 1 min, 60% v:v acetonitrile in Milli-Q water for 2 min, and the BGE for 3 min (100 mM methane-sulfonic acid (Sigma–Aldrich), 74 mM triethanolamine (Sigma–Aldrich), 60% v:v acetonitrile (Sigma–Aldrich). Samples were diluted five times in MS-water (Biosolve Valkenswaard, The Netherlands) and injected at 100 mbar for 5 s. Separation was performed with an applied voltage of –15 kV at 20°C (ramped to –15 kV in 30 s). UV-absorbance at 200 nm was recorded. The bromide concentration was determined based on the corrected peak area and a three-point calibration curve of potassium bromide (Sigma Aldrich) in MS-grade water standards.

2.8 CZE for Chloride analysis

Analysis was performed according to the CZE method for adenovirus analysis (see Section 3.2) with an analysis time of 1 min. The chloride concentration was determined based on the corrected negative peak area and a three-level calibration curve prepared from sodium chloride (Merck) in Milli-Q standards.

2.9 RP-HPLC for Ad26 protein analysis

A Waters Acquity H-class UPLC system with PDA detector, quaternary solvent manager, and autosampler with a Waters Acquity UPLC protein BEH C4 column, 2.1 mm diameter, 150 mm length, 300 Å pore size, and 1.7 μm particle diameter were used. New columns were conditioned with 3 injections of cytochrome c (Sigma–Aldrich). Samples were injected and proteins separated through a gradient from 20% - 60% v:v acetonitrile in 17 min, with a continuous TFA (Biosolve) concentration of 0.175% w/v. UV-absorbance at 280 nm was recorded and peaks were integrated to determine retention times and %peak areas. Peaks were identified with fraction collection and peptide mapping procedure with trypsin digestion and LC-MS^E analysis. See for more details van Tricht et al. [53].

3 Results and discussion

In general, we have found CE suitable for a wide range of applications within vaccine analysis. Here, we describe sixteen CE methods that were developed, of which thirteen were validated, see Table 1 for the list of applications and validation results, and see supporting information for validation result tables and the statistical procedures. The applications include the analysis of critical reagent antibody purity, seasonal virosomal influenza vaccine, universal subunit influenza vaccine, Sabin inactivated polio vaccine (sIPV), and adenovirus vector vaccines. For the adenovirus vector vaccine applications, applications during different steps of the process, i.e., seed production, cell lysis, clarification, anion exchange (AEX)-filtration, ultra- and diafiltration (UF/DF), and drug substance (DS) and drug product (DP), are described.

3.1 Critical reagents antibody purity

For many vaccine products, product identity and potency are determined as part of product release testing. Often, antibodies are being used in assays for the determination of potency and identity. Antibodies are highly selective due to their structure and posttranslational modifications (PTMs). Antibodies are hard to produce at consistent quality and are prone to degradation [54], which consequently impacts the selectivity for the antigen. Therefore, antibodies are seen as critical reagents [55] and the quality of the antibody needs to be determined and controlled before use in a potency or identity test.

CE-SDS and cIEF are techniques that can be used to determine antibody molecular size and isoform patterns and were extensively used for antibody analysis previously (e.g., [56,57]). CE-SDS is a specific form of CGE where proteins are denatured with SDS and separation is based on size. CE-SDS can be used to determine the size variants of an antibody and is sensitive to for example fragmentation. cIEF can be used to determine charge variants and is sensitive to oxidation and loss of charged PTMs like sialic acids.

Although many publications discuss the use of CE-SDS and cIEF for therapeutic antibodies, we have used these techniques for the analysis of antibodies that are critical reagents for release testing technologies such as Western Blot (WB) identity testing and ELISA potency testing. As an example, the quality of HIV antibodies used for these tests was determined with CE-SDS. Multiple and broad light chain (LC) and heavy chain (HC) peaks were observed for Ab1 and Ab2, see Figure 1. This suggested heterogeneous Ab materials. This was not observed for Ab3. In parallel, antibody specificity was tested with WB and ELISA. Both Ab1 and Ab2 resulted in nonspecific bands with WB and background signals with ELISA in the presence of cell lysates and other HIV vaccine antigens. Ab3 resulted in one band at the expected location for WB and no significant background signal for ELISA in the presence of cell lysates and other HIV vaccine antigens. Therefore, the heterogeneous antibody materials could not be used for release testing, and Ab3 was selected for further WB and ELISA method development. The results of CE-SDS and cIEF analysis were used to improve antibody selection and control antibody quality as these kit-based applications proved to be quick and easy to apply, see Table 1 application 1.

Table 1. List of CE applications for viral vaccine analysis

Application #	Product	CE mode	Type of target	Target	Method status	Type of assay	Method application	Method performance characteristics
1	Critical method reagent	CE-SDS	Protein (antibody)	Primary antibody	Developed	Purity	Critical method reagent integrity	
2	Seasonal influenza	CE-SDS	Protein (viral)	Hemagglutinin subunit 1	Validated	Content	Product and process development and characterization	Repeatability 8%–10% RSD, accuracy 93%– 109% compared to SRID, linearity $r^2 = 0.99$, range 7–76 μg/mL HA [33]
3	Seasonal influenza	CE-SDS	Protein (viral)	Influenza Matrix protein, Nuclear protein, Hemagglutinin subunit 2	Developed	Content	Product and process development and characterization	Repeatability 1.9%–7.9% RSD, linearity $r^2 = 0.96$–0.99, LOQ: 7 μg HA/mL [33]
4	Universal subunit influenza vaccine	CE-SDS	Protein (viral)	Hemagglutinin-stem based antigen [67–70]	Validated	Purity	Product and process development and characterization, stability indicating	Repeatability 0.8% RSD, Accuracy 99%–101%, Linearity $r^2 = 1.00$, range 0.50–3.13 mg/mL [34]
5	Universal subunit influenza vaccine	CE-SDS	PTM	Hemagglutinin-stem based antigen glycans [67–70]	Developed	Purity (quantitative)	Product and process development and characterization	
6	Universal subunit influenza vaccine	cIEF	Protein (viral)	Hemagglutinin-stem based antigen [67–70]	Validated	Purity (quantitative)	Product and process development and characterization, stability indicating	Repeatability p/ 0.0%–0.7% RSD, repeatability % peak area 0.5%–0.7% RSD, LOQ < 0.1 mg mini-HA/mL, Supporting Information Table S1?
7	Sabin inactivated polio vaccine	CE-SDS	Protein (viral)	Polio virus protein 1–4	Validated	Identity	Product characterization	Repeatability area 8%–16% RSD, intermediate precision migration time 0.4%–0.8% RSD , linearity $r^2 = 0.98$, LOD 10 μg sIPV/mL [34]
8	Adenovirus vector vaccine	CZE	Virus	Adenovirus	Validated	Content	Release (Seed)	Repeatability 1.4%–4.2% RSD, intermediate precision 5.1%–9.3% RSD, accuracy 91%–103%, linearity 0.98–1.06 90% C.I. on the slope, range 2.5×10^{10}–1.4×10^{11} VP/mL, Supporting Information Table 2
9	Adenovirus vector vaccine	CZE	Virus	Adenovirus	Validated	Content	In process control	Repeatability 0.7%–5.4% RSD, intermediate precision 1.8%–7.4% RSD, reproducibility 2.8%–5.4% RSD, accuracy 99%–110%, linearity 0.97–1.09 90% C.I. of the slope, range 6.7×10^{10}–3.0×10^{12} VP/mL, Supporting Information Table 3

(*Continued*)

BACK TO CONTENTS

Table 1. (Continued)

Application #	Product	CE mode	Type of target	Target	Method status	Type of assay	Method application	Method performance characteristics
10	Adenovirus vector vaccine	CZE	Virus	Adenovirus	Validated	Content	Release and stability (DS/DP) , stability indicating	Repeatability 0.9%–3.3% RSD intermediate precision 1.7%–5.1% RSD, accuracy 100%–104%, linearity 0.99–1.00 90% C.I. of the slope, range 2.5×10^{10}–1.9×10^{11} VP/mL, Supporting Information Table 4
11	Adenovirus vector vaccine	CZE	Virus	Adenovirus	Validated	Content	Product and process development and characterization, stability indicating	Intermediate precision $<$ 10% RSD Reproducibility $<$ 6% RSD, accuracy 90%–110%, linearity 0.99–1.03 90% CI of the slope Range 2.0×10^{10}–2.5×10^{12} VP/mL, [19]
12	Adenovirus vector vaccine	CZE	Virus	Adenovirus	Validated	Content	Process development (cell lysis)	Repeatability 0.7%–9.2% RSD, intermediate precision 0.8%–12% RSD, accuracy 94%–101%, linearity 0.99–1.01 90% CI of the slope, range $2.5 \times 10^{10} - 1.4 \times 10^{11}$ VP/mL, Supporting Information Table 5
13	Adenovirus vector vaccine	CGE	Nucleotides	Host cell DNA	Validated	Purity (quantitative)	Process development support	Repeatable 0.0%–2.4% RSD, Accuracy 98%–102% of mean value of $\leq$200 bp, Supporting Information Table 9
14	Adenovirus vector vaccine	CZE	Impurity	Br^-	Validated	Content	Process development support and validation	Repeatability 4.5%–10.5% RSD, intermediate precision 1.6%–21% RSD, accuracy 99%–107%, linearity 0.95–1.03 90% CI of the slope, range 5–100 μM, LOQ 0.2 μg/mL, Supporting Information Table 8
15	Product independent	CZE	Excipient	Cl^-	Validated	Content	Process development support and validation	Repeatability 1.8%–4.6% RSD, intermediate precision 2.2%–5.3% RSD, accuracy 90%–104%, linearity: 0.93–1.01 90% CI of the slope, range 38–113 mM, Supporting Information Table 7
16	Adenovirus vector vaccine	CZE	Virus	Adenovirus	Validated	Content	Low dose vaccine development support	Repeatability 2.3%–6.3% RSD, intermediate precision 2.3%–7.8% RSD, accuracy 95%–108%, linearity r^2 1.00, 1.00–1.06 90% CI of the slope, range 5×10^9–3.7×10^{11} VP/mL, Supporting Information Table 6

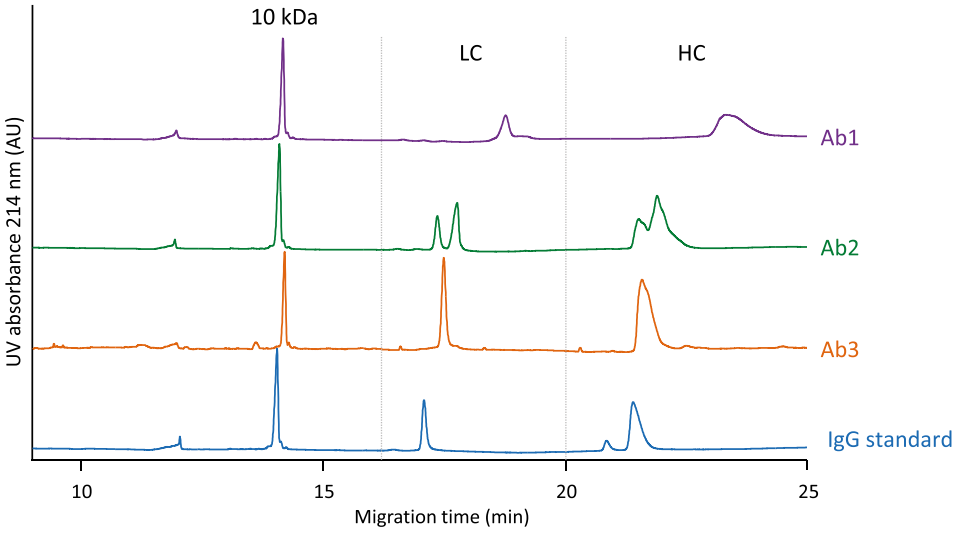

Figure 1. Critical antibody method reagent integrity testing of three HIV antibodies (Ab1, Ab2, and Ab3) with CE-SDS. The 10 kDa control standard is used as an internal standard and the light chains (LC) and heavy chains (HC) migration time ranges are depicted with dotted lines. For other conditions, see text.

3.2 Seasonal virosomal influenza vaccine

In addition to antibody analysis, the CE-SDS application developed for antibodies could be used for viral proteins as well [33,34,58–61]. For influenza vaccines, hemagglutinin (HA) is the most targeted influenza protein due to its immunogenic properties [62,63]. Due to the antigenic drift of HA, a new influenza vaccine with three different HA proteins needs to be developed each year. Usually, SDS-PAGE, single radial immunodiffusion (SRID) assays, and RP-HPLC methods were developed for identification and quantification. SDS-PAGE could not distinguish between different viral strains, could not quantify HA, and has low throughput. In addition, antibody selection for SRID is time consuming. RP-HPLC was not able to determine the HA concentration in complex matrices such as cell lysate and lacked precision and accuracy. For these reasons, a CE-SDS application was developed and validated (see Table 1 application 2) to quantify HA and identify the influenza strains. Potentially, the presence of other important proteins, such as neuraminidase (NA) [64,65], and matrix protein (M) [66], could be quantified as well [33], see Table 1 application 3. The method was further developed as short-end injection was tested to reduce analysis time and increase sample analysis throughput. The separation time decreased about threefold without significant loss of method performance, see Figure 2.

3.3 Universal subunit influenza vaccine "mini-HA"

3.3.1 Mini-HA size purity

A universal influence vaccine is being developed to avoid yearly redevelopment or the risk of potential off-target vaccines. The universal influenza vaccine, "mini-HA," is an HA-stem-based antigen called mini-HA and induces a broad-spectrum antibody response to cover many different influenza HA variations [67–70]. For the development and the production of a group 1 mini-HA, a quantitative protein purity method was needed to determine peptide backbone integrity. With the four-step approach described previously [34] and based on the Sciex CE-SDS application, we were able to develop and validate a CE-SDS method for group 1 mini-HA purity determination ([34], Table 1 application 4).

3.3.2 Mini-HA PTM heterogeneity

The mini-HA protein is a homotrimer protein linked by disulfide bridges and has several *N*-linked and one *O*-linked glycosylation sites per monomer, with potentially multiple sialic acids attached per glycan. Glycans could have a significant effect on safety and efficacy due to their effect on the folding and shielding of functional epitopes [71,72].

Glycans are known to affect the CE-SDS separation [73,74] and CE-SDS was used for glycoprotein analysis previously [38]. Therefore, the optimized CE-SDS method to determine the mini-HA protein by its primary structure required an optimal sample preparation protocol to reduce and deglycosylate the protein. Reduced and nonreduced samples were tested with combinations of different glycosidases. Different combinations of glycosidases resulted in different peak patterns, see Figure 3.

Analysis of only denatured mini-HA (Figure 3B) caused a broad peak around 35 min which represented glycosylated trimeric mini-HA. The peak was only partly captured as the analysis run time was 35 min. Mini-HA reduction (Figure 3C) resulted in a broad hump composed of several peaks of glycosylated monomers at around 23 min. PNGase F treatment (Figure 3D) removed the N-glycans and resulted in 4 peaks in the time window of 25–30 min, and 2 peaks in the time window 15–20 min under non-reduced conditions. The 4 peaks around 25–30 min were likely trimeric mini-HA with 0, 1, 2, or 3 O-glycans attached. The 2 peaks around 15–20 min

Electrophoresis 2022, *43*, 1068–1090

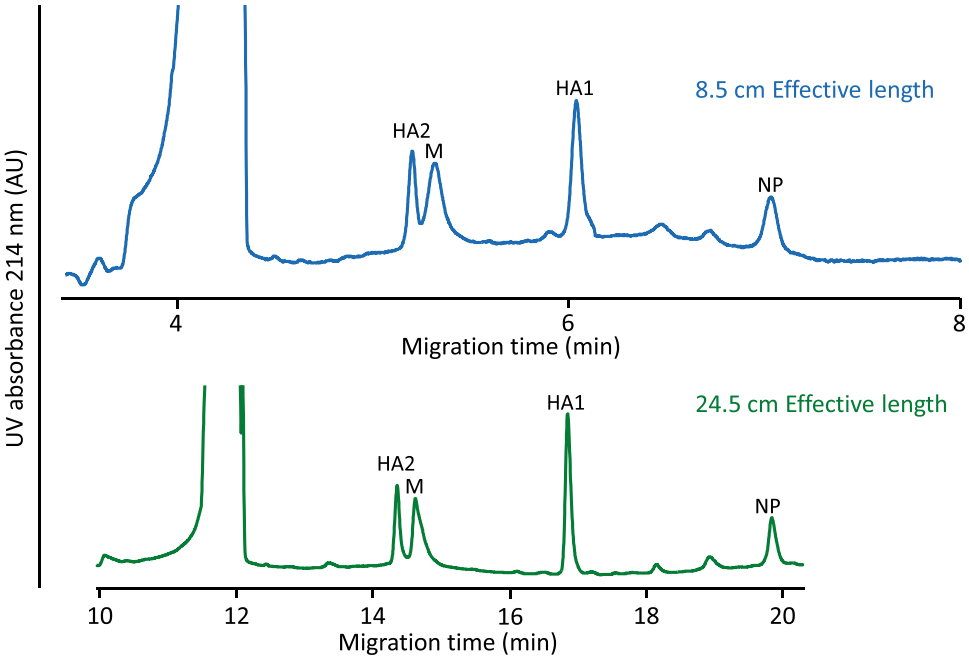

Figure 2. Electropherogram results of influenza reference standard NIBSC B/Brisbane/60/2008 analyzed with CGE with an effective length of 24.5 cm or 8.5 cm, and peaks Hemagglutinin subunit 1 (HA1), hemagglutinin subunit 2 (HA2), matrix protein (M), and nuclear protein (NP). For other conditions, see text.

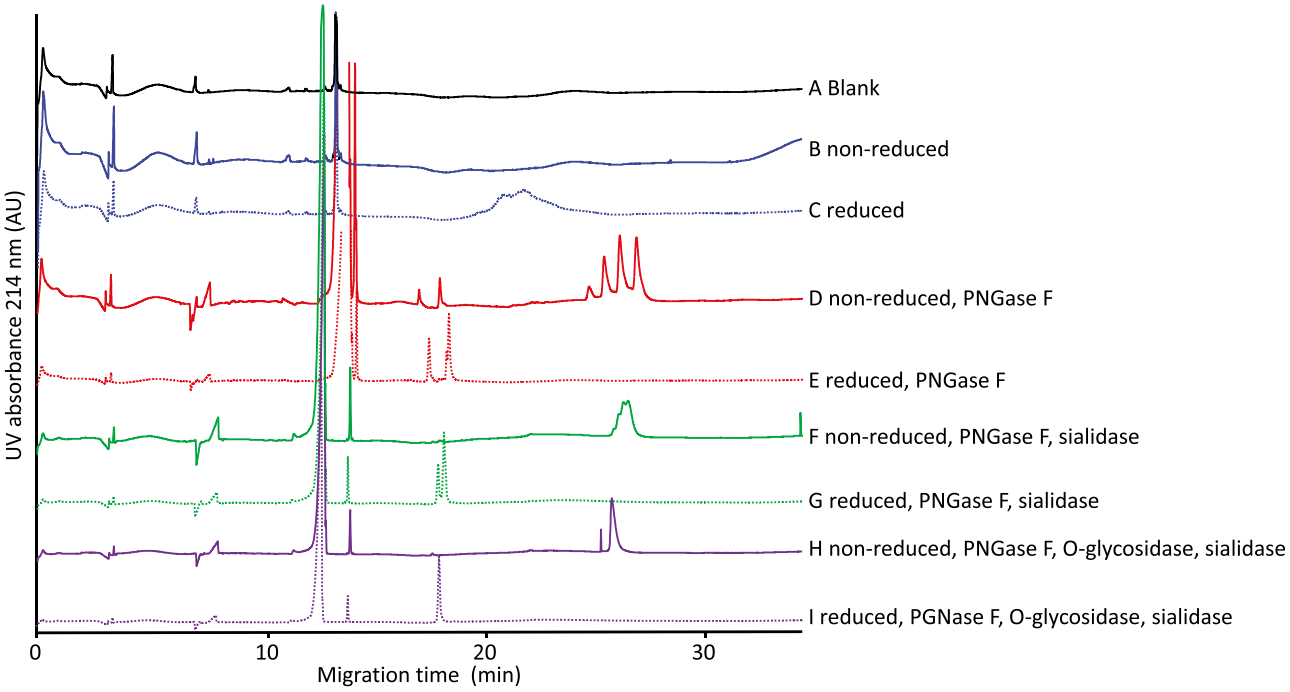

Figure 3. Effects of reduction and different deglycosylation protocols on the CE-SDS separation of a purified mini-HA sample, resulting in a glycan distribution overview of the protein, For experimental conditions, see text.

were also observed when the protein was reduced before PNGase F treatment (Figure 3E) and were likely monomer mini-HA with either 0 or 1 O-glycan attached. Sialidase treatment removed the sialic acids. Hence, a combination of PNGase F and Sialidase was expected to provide one peak. Nevertheless, multiple peaks were observed after PNGase F and Sialidase treatment under non-reduced (Figure 3F) or reduced (Figure 3G) conditions, which was thought to be the effect of the heterogeneity of the remaining O-glycans after removal of sialic acid. After Sialidase treatment, later migration times were observed which could be explained by the removed sialic acids decreasing the number of negative charges of the glycoprotein. After PNGase F, Sialidase, and O-glycosidase treatment, all glycans were removed and one peak for the gly-

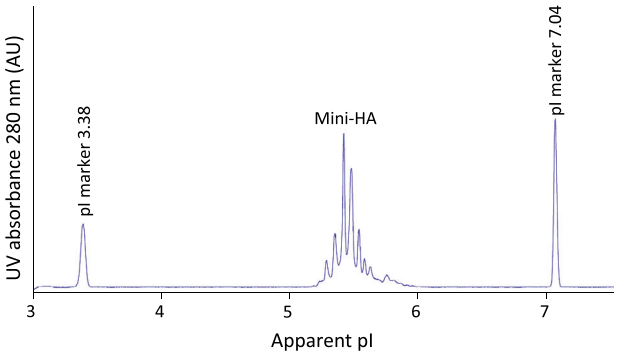

Figure 4. Typical electropherogram of a purified mini-HA sample with icIEF. For experimental conditions, see text.

can free primary protein structure was observed, which was trimeric for the non-reduced (Figure 3H), and monomeric for the reduced (Figure 3I) sample.

The different sample treatments revealed that the heterogeneity of the sample was caused by different features of the glycans attached. Different sample treatments resulted in different peak profiles characterizing the protein PTMs (e.g., disulfide integrity, glycan profiling, sialic acid loading). Studying glycans in this way does not yield in-depth characterization of the location and building blocks, as could possibly be determined by peptide mapping LC-MS [75,76], and the glycan derivatization assays like the CE-LIF application [77], and UPLC-LIF application [78]. Nonetheless, CE-SDS peak profiling provided an overview of the overall distribution of glycans on the mini-HA protein with different sample preparation and could be a quick high-throughput check for protein PTM quality, see Table 1 application 5.

3.3.3 Mini-HA Charge purity

A cIEF method was designed to determine the purity of mini-HA based on charge, in addition to the size-based CE-SDS method. The charge of proteins is affected by various factors such as amino acid composition, pH, and PTMs. Protein charge can be analyzed by several techniques such as cIEF [79], icIEF [80], CZE, and IEC. All of these techniques have the potential to separate the different charge species, the optimal technique might vary per protein. Both CZE and IEC methods have a lot of critical method parameters (CMPs) to be developed, e.g., capillaries, columns, buffers, etc., complicating method development. cIEF is more complex and has longer run times compared to icIEF due to the need of mobilization after focusing. The icIEF CMPs, such as the type and concentration of ampholytes, spacers, and sample diluent additives (e.g., urea, guanidine, etc.), could easily be optimized. Therefore, the icIEF application was selected, developed, and validated, see Table 1 application 6 and Figure 4. It should be noted that an apparent p*I* was determined and not a true pI for the same reason as for all other IEF methods (effect of sample treatment and separation conditions on the folding and PTMs and thus the net charge of the protein), and the ampholyte gradient being pseudo-linear [81,82].

3.3.4 Mini-HA Stability

Both the CE-SDS and the icIEF methods for mini-HA purity determination were used to study mini-HA degradation. Several stressed conditions (i.e., thermal stress (70°C and 95°C), basic stress, and chemical oxidative stress) were applied for 24 h and thereafter the samples were analyzed with the CE-SDS and icIEF methods and compared to the 24 h at RT control sample. The CE-SDS method was used to determine size changes, such as hydrolysis. The icIEF method was expected to be sensitive for PTMs changing the pI of the desialized mini-HA (e.g., disulfide-scrambling, deamidation, oxidation, isomerization, hydrolysis).

The main mini-HA peak area decreased, and the % peak area with migration times earlier than the main peak increased for all stressed samples determined with CE-SDS, see Table 2 and Figure 5A. The %peak area with migration times later than the main peak was increased after 24 h at 95°C and after 24 h in basic conditions, see Table 2. Peaks migrating earlier than the main peak were likely degraded mini-HA (e.g., hydrolyzed mini-HA), and the later migrating peaks were suggested to be larger mini-HA aggregates. However, analytical artifacts, such as the effect of stress conditions on the sample preparation efficiency, could not be excluded.

Very distinct pI ranges and profiles were determined with cIEF for each stressed condition, see Table 3 and Figure 5B. Incubation for 24 h at 70°C resulted in a narrow pI range and was thought to be caused by disulfide reduction, reducing trimers and possible dimers into monomers. Incubation for 24 h at 95°C resulted in an apparent pI shift to lower pH similar to basic conditions. The pI shift could be explained by deamidation, isomerization, and hydrolysis, which are related to pH and temperature stress. Oxidation increased the apparent pI compared to the control sample. The peaks were not identified at the time since peak identification in icIEF is challenging and applications like icIEF-MS [83,84] were not at hand.

It is important to note that the icIEF peak % areas were not used for degradation pathway analysis, since the apparent pIs of the peaks were significantly different and could not be correlated between conditions.

Due to the precision and the stability-indicating power of both methods, the methods were used to identify possible routes of degradation supporting an early product CQA analysis and future product quality and comparability assessments.

3.4 Sabin inactivated polio vaccine

Another example of using CE-SDS for viral protein analysis was for the development of a Sabin inactivated trivalent polio vaccine (sIPV). The identity of each serotype was to be

Table 2. Effects of several stressed conditions on a purified mini-HA sample analyzed with CE-SDS on the main peak corrected area recovery compared to the 24 h RT sample and the percentage of the main peak, low molecular weight (LMW), and high molecular weight (HMW) species

Condition	Deglycosilated mini-HA monomer [% recovery]	Deglycosilated mini-HA monomer [% Area]	LMW [% Area]	HMW [% Area]
24 h RT	100%	96.7%	2.6%	0.7%
24 h 70°C	51%	89.1%	10.9%	0.0%
24 h 95°C	5%	10.0%	86.1%	3.9%
24 h pH Basic	46%	21.3%	70.4%	8.3%
24 h pH Oxidized	73%	96.8%	2.0%	1.3%

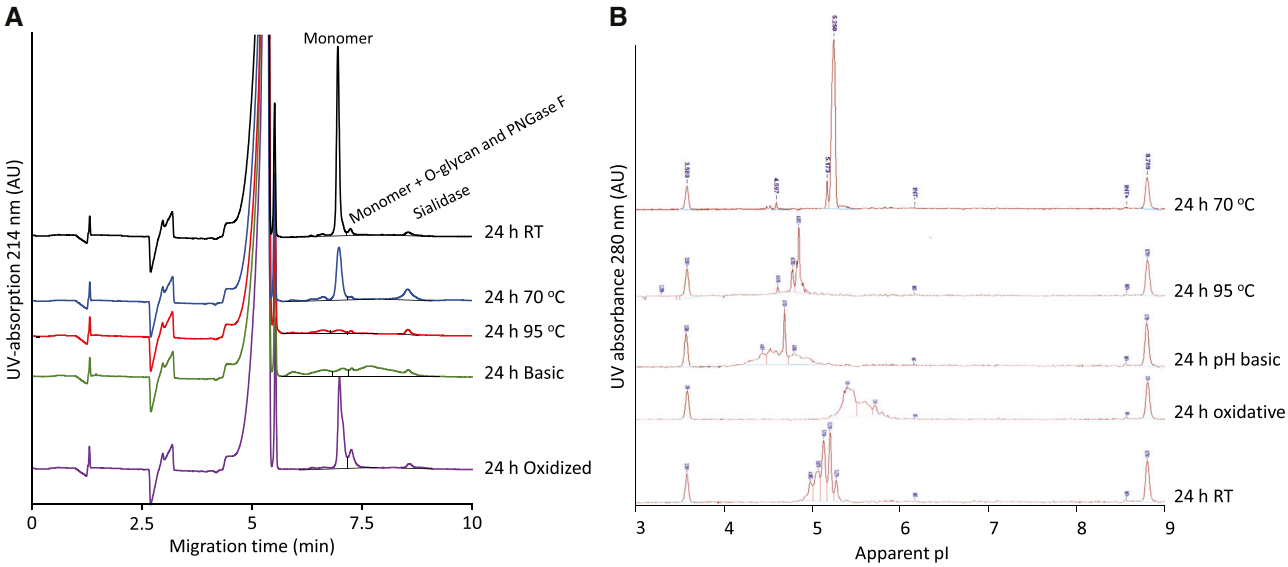

Figure 5. Effects of several stressed conditions on a purified mini-HA sample analyzed with (A) CE-SDS and (B) icIEF. For experimental conditions, see text.

Table 3. Effects of several stressed conditions on a purified mini-HA sample, analyzed with icIEF

Condition	Main peak apparent pI [pH]	Apparent pI range [pH]
24 h RT	5.13	4.99–5.28
24 h 70°C	5.25	5.17–5.25
24 h 95°C	4.85	4.62–4.85
24 h pH basic	4.81	4.45–4.81
24 h pH oxidative	5.39	5.39–5.71

confirmed by analytical testing. Immunochemical methodologies, like antibody-mediated viral neutralization assays, SRID assays, or D-antigen determination with ELISA, are commonly used for virus type identification [85–88]. All these methodologies use antibodies for specific detection of the virus subtype. Antibodies are very specific, but are also costly to develop, to produce, and to control the quality of. A four-step approach was used to optimize a CE-SDS method to identify poliovirus types based on protein profiles as an alternative non-antibody method. Due to this four-step approach, an sIPV identity method was developed in 4 days, see Table 1 application 7 and [34].

3.5 Adenovirus vector vaccine

The previously discussed vaccines are examples of attenuated, inactivated, or subunit vaccines. Another type of vaccines are the viral vector vaccines, where a safe virus is used as a carrier for a pathogenic gene in order to elicit a specific antigen immune response. Adenoviruses are a type of viruses used as viral vector vaccines, currently for example to combat COVID-19 [89] and Ebola [90]. Adenoviruses are non-enveloped common cold viruses with a diameter of about 90 nm. Double-stranded DNA is encapsidated by proteins and about 13 different types of proteins are present in the virion [91]. The individual proteins can be separated by UPLC [53]. The adenovirus vector vaccines are produced in bioreactors with cultured human

cells by adenovirus vector seed inoculation (e.g., HEK293, Per.C6®) [19,92–103]. Purification of the adenovirus can be performed via cell lysis, clarification of the adenovirus particles from the cell debris and host cell DNA (HC DNA), AEX-filtration, and UF/DF [19,92,95,104–109]. After purification, the adenovirus vaccines are formulated and packaged before storage, distribution, and clinical usage [110–116]. See Supporting Information Section 2 for a detailed process overview. Different CQAs and CPPs are important in the CS of each of these steps. Several examples are provided for the use of CE to determine these CQAs per process step.

3.5.1 Seed production

For bioreactor inoculation, a precise and accurate seed adenovirus concentration was needed. Previously, an adenovirus particle content CZE method for in-process control testing (IPC) of drug substance production was developed and validated [19,20], see Table 1 application 11. The development took experience from other large biomolecule and viral analysis CZE methods into account [9,13,15–18,21–27,30,117,118]. However, in the literature mostly BFS capillaries in combination with borate buffers and SDS were used. This is not appropriate for adenovirus particles, as SDS denatures and disintegrates the adenovirus particle, and the adenovirus particle adsorbs to BFS. Therefore, a neutrally polyvinyl alcohol (PVA) coated capillary in combination with a Tris-tricine buffer and polysorbate-20 BGE were used for adenovirus analysis with CZE. Downstream process samples can be analyzed without sample pretreatment, but for crude samples from the upstream process, DNA-related interference peaks and spikes were observed. With the addition of a cell lysis and a DNase sample pretreatment [19], the interference with the adenovirus concentration determination was reduced and this method was validated for seed release testing, see Table 1 application 8. See van Tricht, et al. for method details [19].

3.5.2 Cell lysis

The adenovirus purification process was designed with a detergent lysis step after adenovirus production to release the virus from the host cells and limit the host cell DNA and host cell protein (HCP) release. However, the detergent used was put on Annex XIV by the EU REACH-Committee as the degradation product was deemed environmentally hazardous and will, therefore, need to be replaced. Alternative lysing agents were studied for their effect on adenovirus yield, and HCP and HC DNA release. The number of analytical methods that can cope with complex matrices such as cell lysates without extensive sample prep is limited. However, the CZE method showed to be precise and accurate for a complex sample matrix such as clarified harvest (CH) ([19, 20], Table 1 application 12). Therefore, CZE was used to determine the Ad26 concentration, and to study the impact of the detergent on other peaks in the electropherogram that are related to HC DNA, HCP, cell components, or aggregates.

In general, the peak profiles, i.e., separation and peak shapes obtained after lysis with different detergents, were comparable, see Figure 6. No new peaks were observed that could be associated with excessive HC DNA, HCP, cell components, and aggregates. This suggested that each of these detergents performed equivalently. Subsequently, the CZE method was used during hold time studies to select the most optimal lysis agent and lysis conditions.

3.5.3 Clarification

Cell lysis is followed by HC DNA clarification. HC DNA content and size are safety CQAs due to potential infectiveness and oncogenic properties [119–122]. Therefore, regulatory authorities expect a CS to limit the HC DNA presence in vaccine products to 10 ng/dose for continuous cell lines and a median size of $\leq$200 bp [123–125]. The CS consisted of i) removal of DNA via detergent aided DNA precipitation with domiphen bromide (DB) [19,20,95] and ii) testing of HC DNA content and fragment size distribution throughout the vaccine production process.

Host cell DNA analysis

An HC DNA fragment size determination method was needed with an LOD of 10 ng/dose. First, four different DNA extraction methods were evaluated. The Wako DNA Extractor® kit [50] in combination with an RNase treatment was determined to be the best extraction method due to high DNA recoveries, high throughput, and short extraction time, and was deemed easiest to transfer to other testing sites. Second, for DNA fragment separation and detection, the Sciex eCAP DNA 1000 application was evaluated, see Table 1 application 13. Three pronounced bands were observed below 200 bp for the clarified harvest and AEX-filtrate with the slab-gel *Electrophoresis* (Figure 7A) and corresponded with the determined peak patterns with the Sciex eCAP DNA 1000 application (Figure 7B). The large band at >1000 bp with slab-gel *Electrophoresis* is Ad26 intact DNA, and out of scope for this method. Noteworthy, for the Sciex eCAP DNA 1000 application the samples were diluted to have the same adenovirus concentration, which is not performed for the slab-gel electrophoresis. The reason for this is that a too high Ad26 DNA concentration disturbed the electrophoresis. This effect could have been the reason for the observed spikes at >25 min in this electropherogram. A similar decrease in <200 bp fragments was observed with the slab-gel electrophoresis and the Sciex eCAP DNA 1000 application and were deemed interchangeable for this purpose.

Nonetheless, The eCAP DNA 1000 application took 3–4 h to prepare and analysis times were 35 min per sample, whereas the slab-gel application, with the usage of Flash Gels,

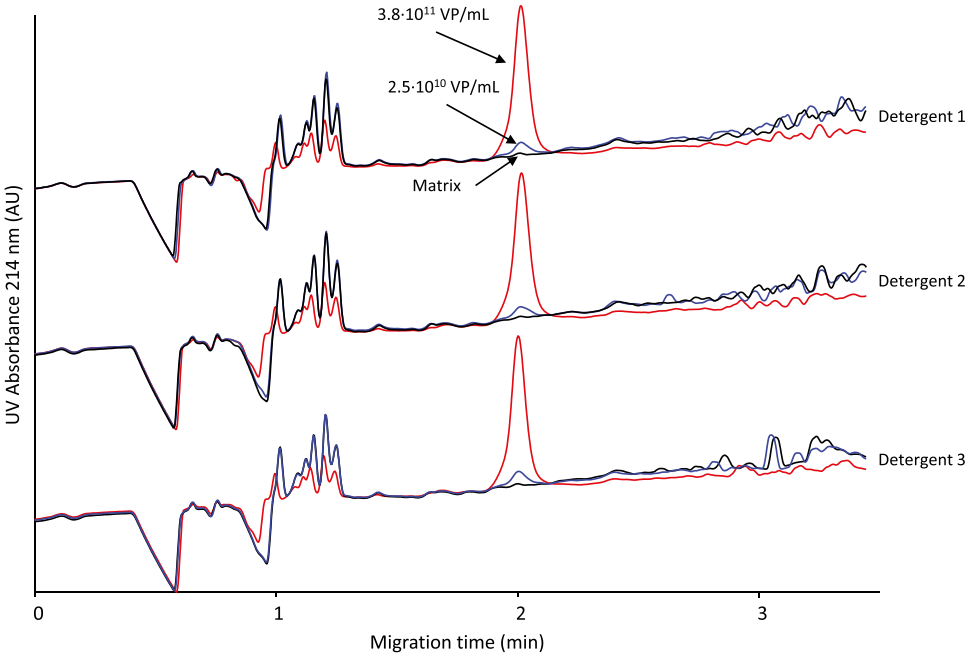

Figure 6. Effects of three different cell lysis detergents at 0, 2.5 × 10^{10}, and 3.8 × 10^{11} VP/mL on the Ad26 concentration determination and impurities with CZE. The 3.8 × 10^{11} VP/mL sample was diluted in FB to fit the CZE method range. The matrix was obtained from the supernatant after centrifugation at 20.000 rcf and 4°C for 1 h. For other conditions, see text.

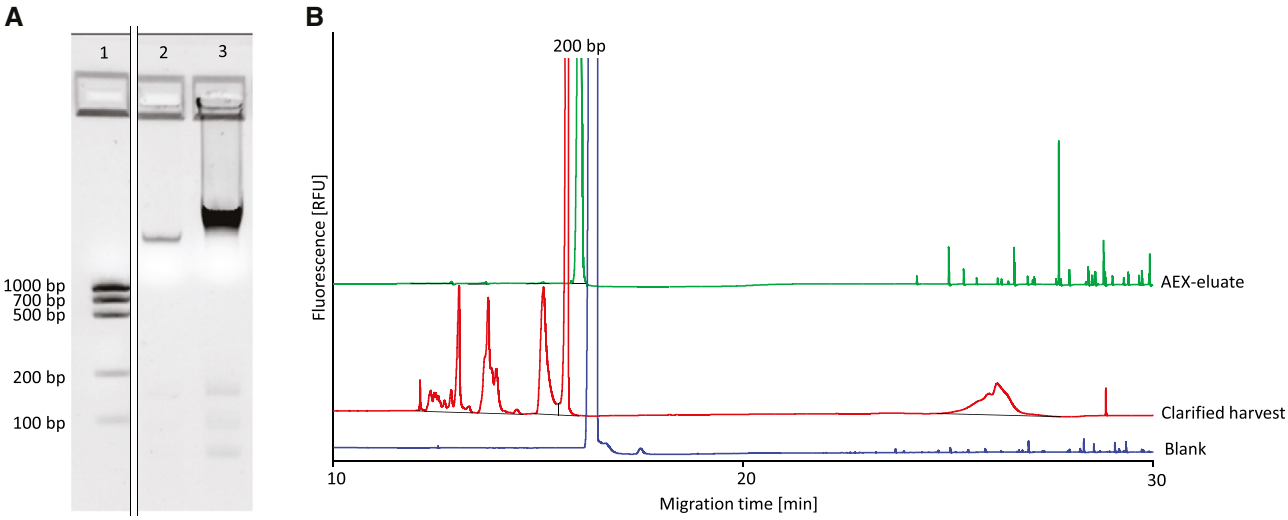

Figure 7. Example in-process samples analyzed with (A) slab-gel electrophoresis in lane 1 the DNA QuantLadder 100–1000 bp, lane 2 clarified harvest and lane 3 AEX-eluate, and (B) CGE eCAP 1000 application of blank (Blue), the clarified harvest (red), and the AEX-eluate (green). The DNA ladder, and two samples were ran on the same slab-gel and irrelevant lanes were removed by picture splicing indicating with a separator line in the figure. For experimental conditions, see text.

could be prepared in 10 min and 11 samples were analyzed simultaneously in 5 min. In addition, the slab-gel application was perceived to be less labor intensive, and to require less training.

Domiphen-adenovirus interaction

Domiphen is a cationic detergent that is added during clarification to precipitate the negatively charged HC DNA. The domiphen concentration is a CPP [95] and a sub-optimal concentration leads to ineffective DNA clearance, AEX-filter blockage, or low adenovirus yields. Other CPPs that have an impact on the domiphen-HC DNA interaction are the clarification incubation time and temperature, adenovirus concentration, ionic strength, and pH. Domiphen does not only interact with DNA, but also with other negatively charged components like the adenovirus particle. This has a potential impact on the affinity of the adenovirus particles for the AEX filter and on the CZE analysis for adenovirus concentration determination. To set PARs for the clarification, the effect of the domiphen concentration on the adenovirus particle was studied.

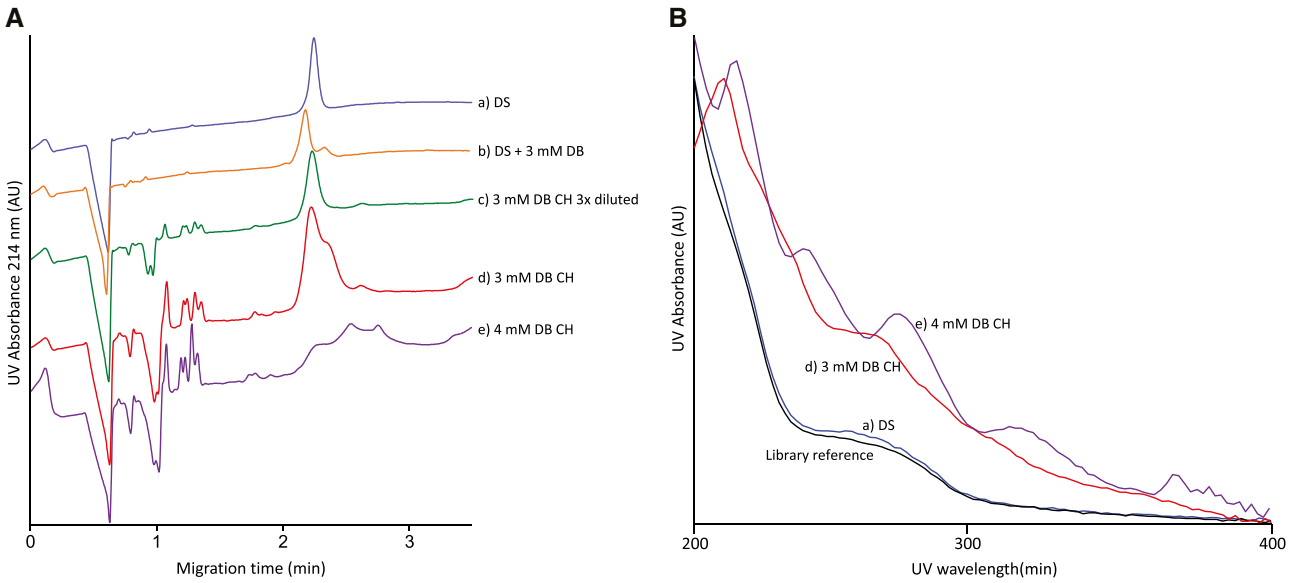

Figure 8. Effect of different concentrations of Ad26. In (A) CZE electropherograms with (a) DS, (b) DS with 3 mM DB added, (c) a 3 mM clarified harvest (CH) diluted with DS FB, (d) a 3 mM CH, and (e) a 4 mM CH, and (B) the respective Ad26 peak spectra of the library reference (black), (a) DS sample, and (d) 3 mM DB CH and (e) 4 mM DB CH. For experimental conditions, see text.

Clarification was originally performed at 3 mM DB (Figure 8A d)), and an additional later migrating adenovirus peak shoulder was observed in CH compared to a DS sample (Figure 8A a)) with CZE. Spiking of the 3 mM DB into the DS sample (Figure 8A b)) had a similar effect. The later migration time of the shoulder indicate lower electrophoretic mobility, so a lower charge/size ratio. This means that the Ad26 particle was larger, or less charged, or a combination of the two. Both a larger particle and a lower surface charge can be the result of an interaction of domiphen with adenovirus. DLS analysis confirmed that the hydrodynamic radius of Ad26 increased from 90–100 nm to 100 - 110 nm after DB addition to DS. The Ad26 peak ultra-violet (UV) spectrum also changed and indicated more scattering and thus larger particles (Figure 8B).

During further Ad26 AEX-filtration purification no yield loss was observed at 3 mM DB and no domiphen could be determined in the AEX-filtration sample with RP-HPLC with charged aerosol detection. Dilution of the CH sample with FB of the DS (Figure 8A c)) resulted in a narrow single peak. Both results indicate that the domiphen-adenovirus interaction is reversible, and that adenovirus is cleared from domiphen during AEX processing.

The Ad26 particle yield significantly decreased when clarification was done with 4 mM DB (Figure 8A e)) instead of 3 mM DB (Figure 8A d)). With CZE, the CH with 4 mM DB resulted in a broad pattern (2–3 min) with several peaks, indicating a very heterogeneous pool of adenovirus particles. With DLS, hydrodynamic radii of 500–1000 nm were observed in the CH samples containing 4 mM DB, compared to 90–100 for DS samples. Therefore, it is likely that clarification with 4 mM DB resulted in Ad26 particle aggregates which were lost in the process, possibly due to precipitation or a decreased affinity for the AEX-filter. The adenovirus pattern UV spectra were comparable to the 3 mM DB CH, suggesting scattering and thus larger particles.

Interestingly, re-injection of clarified samples after 24 h resulted in decreased Ad26 concentrations and the decrease was more pronounced with longer hold times and higher DB clarification concentrations. Clarification duration studies indicated that the Ad26 yield decreased rapidly with time and timely process continuation was essential. The use of CZE reduced analysis times and process hold times from approximately three days to less than 2 h, because of the combined effect of faster analysis and higher precision. Consequently, a fast, accurate, precise, and robust at-line assay for IPC testing was validated [20], and implemented at different sites, see Table 1 application 9. The observed shoulder with high DB concentration did not impact the method performance. Subsequently, the CZE method was used to set PARs for a robust and consistent adenovirus purification process, and the target DB concentration for clarification was set to a maximum value.

Bromide content

HC DNA Clearance with domiphen is performed by adding domiphen bromide to the bulk solution. As bromide is known to be an anticonvulsant and sedative, an acceptance limit of not more than 4 µg/dose for the adenovirus vaccine product was determined. During the purification process, bromide is cleared to well below this limit. A CZE method based on the CZE method from Stålberg et al. [47] was developed to determine the bromide concentration during the purification process to prove bromide clearance. Bromide and chloride are among the fastest migration anions that result

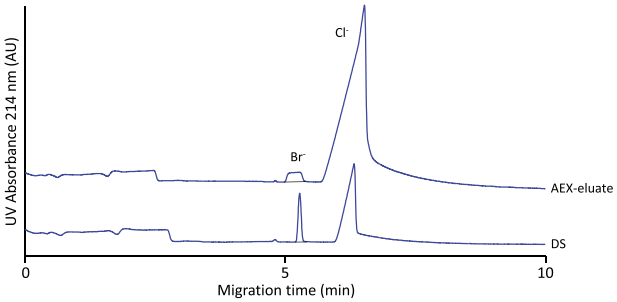

Figure 9. Bromide (8 μg/mL) spiked into AEX-eluate and DS samples and analyzed with CZE. For experimental conditions, see text.

in a method free of interference of matrix components. The method also makes use of the absorbance of bromide at low UV-wavelengths in order to avoid the need for indirect detection methods.

Although chloride has low UV-absorbance, high sample chloride concentrations could cause loss of separation between the bromide and chloride peak due to electromigration dispersion. Both the addition of iodide as leading electrolyte and milli-Q water sample dilution were tested to improve the peak efficiency and decrease electromigration dispersion by influencing the transient isotachophoresis mechanism. Dilution with milli-Q water improved the separation sufficiently, see Figure 9. Still, a squared bromide peak was observed for the sample with high chloride concentration, but despite the peak shape, the method was fit for purpose and was validated, see Table 1 application 14.

3.5.4 AEX-filtration and ultra- and diafiltration

After clarification, HCPs are removed during AEX-filtration and UF/DF is performed to reduce the concentration of remaining matrix components, and to formulate the adenovirus particles in a stable environment, resulting in so-called drug substance (DS).

Host cell Protein AEX-filter blockages

During the AEX-filtration process, the amount of material loaded on the AEX-filter is a CPP as overloading could result in yield loss or filter blockage, while underloading could result in yield loss due to adsorption.

In the example given in Figure 10A, (the front of) a new peak at 3.5 min was observed with CZE in cell lysed (LH 2) and clarified (CH 2) samples compared to the lysed harvest (LH 1) and clarified samples (CH 1) from a reference batch. The new peak did not interfere with the Ad26 determination, however, the appearance of this peak correlated with high AEX-filtration pressures. An absorbance maximum in the UV-spectrum at 280 nm suggested that the peak contained protein, see Figure 10B. Subsequently and as a result of this observation in the CZE determination, at-line analysis was performed allowing for fast root-cause investigation and resolution of the issue.

Chloride content

During AEX-filtration, high concentrations of NaCl are used for adenovirus elution from the AEX-filter. In addition, NaCl is present in the vaccine product as a tonicity agent and is therefore considered a CQA. A NaCl concentration outside the intended range leads to unnecessary pain at the injection site and is associated with adenovirus instability [110–116]. For these reasons, the chloride concentrations were determined in the FB raw material, throughout the UF/DF, and in the final DS, for process characterization and process validation purposes. For process validation, a concentration determination with accuracy 95–105% and intermediate precision $\leq$ 5% RSD was needed.

Several techniques could be considered to determine the chloride concentration. However, in the CZE method for Ad26 particle analysis, chloride is observed as an electromigration dispersed (triangular) indirect-UV peak in the migration time window 0.5–1.0 min. Therefore, we verified if the Ad26 CZE method could also be used for chloride quantification. This proved to be the case and the method was validated for Ad26 process validation as well as bed-site mixing studies of $AlOH_3$ adjuvanted mini-HA, see Table 1 application 15 and Figure 11.

3.5.5 Drug substance and drug product

After UF/DF, drug substance is obtained and drug product can be produced. Both DS and DP are subjected to extensive testing for clinical release and stability testing. Important CQAs for release testing are the adenovirus identity, the product-related impurities such as empty and incomplete adenovirus particles, and the adenovirus concentration. For stability testing, it is important to determine the adenovirus concentration loss and to identify the route of degradation.

Strain identity

Adenovirus vaccines are common cold viruses and subtypes were selected to avoid pre-existing immunity toward the viral vector [126,127]. Different adenovirus subtypes can be produced in the same manufacturing facility or analyzed in the same lab. The different adenovirus subtypes have different physicochemical properties, e.g., pI, and amino acid composition [91]. A method that can discriminate selectively between different strains is a requirement. With the Ad26 CZE method, all tested different adenovirus subtypes were separated. Therefore, the method can be used for viral vector identity confirmation, see Figure 12. As CZE separation is based on charge/size ratio, the migration correlates to the number of negative charges on the adenovirus particle. The adenovirus particle surface charge determines the NaCl

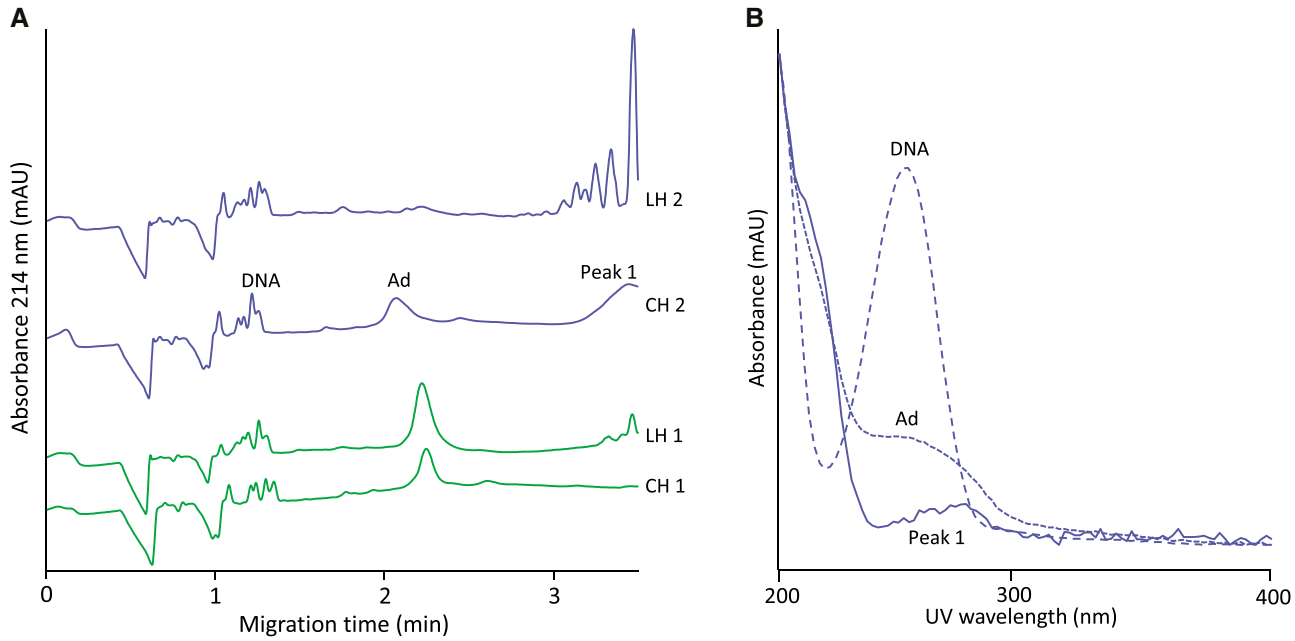

Figure 10. The front of a new peak observed in (A) electropherograms of lysed harvest (LH 2) and clarified harvest (CH 2) samples from a batch with AEX-filter blockage (blue), compared to lysed harvest (LH 1) and clarified harvest (CH 1) samples from a batch without AEX-filter blockage (green), analyzed with CZE, and (B) UV-spectra of annotated CH2 peaks. For experimental conditions, see text.

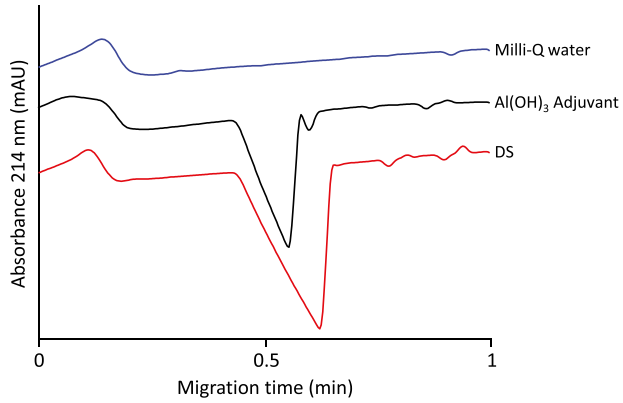

Figure 11. Chloride analysis of Milli-Q water, 50 mM NaCl added to aluminum hydroxide mini-HA ($Al(OH)_3$) adjuvant and purified Ad26 DS with CZE. Experimental conditions, see text.

concentration required during AEX-filtration, hence the CZE migration time is indicative of the NaCl concentration required for elution during AEX-filtration. For example, Ad35 migrated at 1.5 min and required a higher NaCl AEX-elution concentration than Ad26, which migrated at 2.1 min.

Adenovirus incomplete

During adenovirus production in the bioreactor, incomplete or empty particles are formed [128–131]. The concentrations of completes and incompletes can be determined by sedimentation velocity analytical ultra-centrifugation (SV-AUC) [132]. However, this method is elaborative, has low throughput, and is expensive. Therefore, we tested whether we could determine the incomplete impurity percentage with the Ad26 particle CZE method. Incomplete and complete fractions were obtained with sedimentation equilibrium analytical ultracentrifugation (SE-AUC) in cesium chloride (CsCl) [128]. Viral particle concentrations were determined with CZE and fractions of incomplete and complete were mixed ranging from 0 to 100% incompletes.

Complete particles and incomplete virus particles were not separated, see Figure 13A. So, independent of having encapsidated DNA or not, the mobility of the virus particle is the same since the charge and the hydrodynamic size remain the same. UV-spectra and the optical density ratio at 260 nm and at 280 nm were significantly different from 0% incompletes at 50% incompletes, see Figure 13B. This is above the expected %-incompletes in DS and DP samples. Therefore, the relative number of incomplete particles could not be determined with the CZE method.

Content release testing

Adenovirus vector-based vaccines are dosed based on the vector particle concentration to avoid lack of efficacy or causing adverse effects [121,133]. OD260 [134,135] or quantitative polymerase chain reaction (qPCR) [136–139] have been used for adenovirus concentration determination. Van Tricht et al. reported an intermediate precision for qPCR of 15.9% RSD (or 8.1% RSD for 3 runs with 3 replicates per run) and CZE of 6.9% RSD [20]. Since CZE was more precise, the Ad26 CZE method was initially validated in the range of 5.0×10^{10}–1.5×10^{11} VP/mL for DS and DP release testing,

Electrophoresis 2022, *43*, 1068–1090

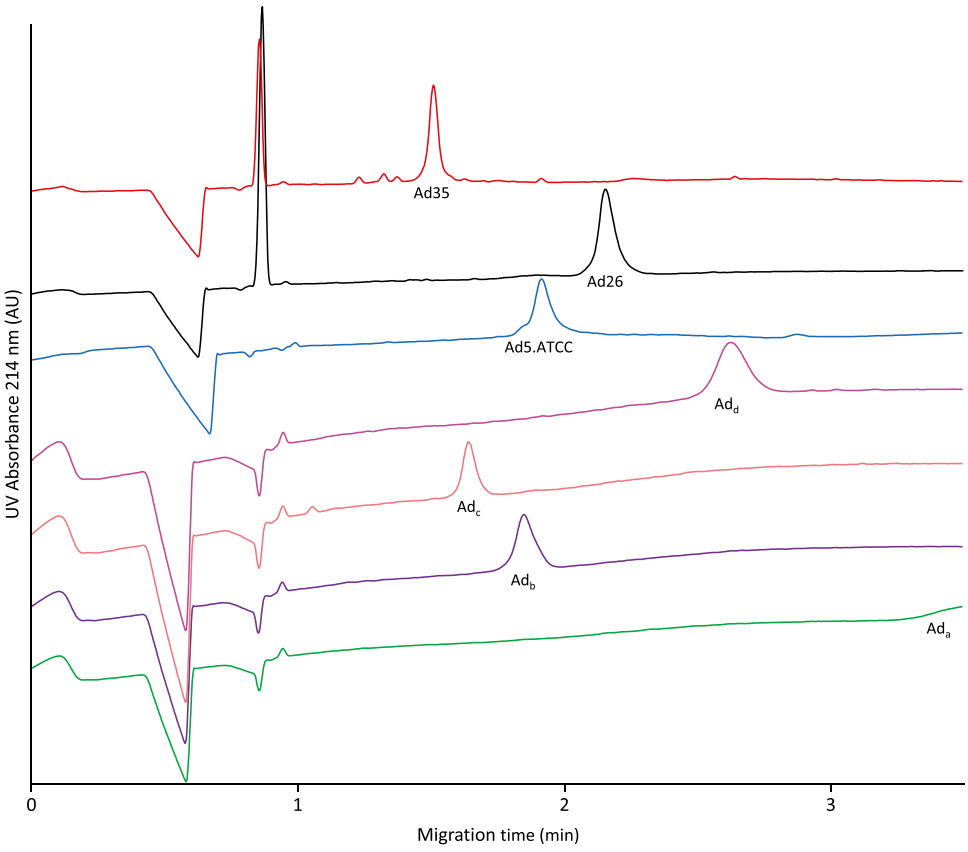

Figure 12. Electropherograms of different adenovirus subtypes analyzed with CZE, including human adenovirus 5 international reference standard Ad5.ATCC®[151]. For experimental conditions, see text.

see Table 1 application 10. In order to explore quantification of low-dose vaccines, additional sensitivity was needed.

A large-volume injection can be concentrated on-capillary based on a transient-ITP principle with chloride in the sample as leading electrolyte and tricine in the BGE as terminating electrolyte. In the Ad26 CZE method an injection of 1.4% of the capillary length was used. The transient-ITP principle provided the opportunity to increase the hydrodynamically injected sample volume to a maximum of approximately 50% of the capillary length. An LOD of 5×10^8 VP/mL (0.8 pmol/L) and an LOQ of 1.5×10^9 VP/ml (2.5 pmol/L) were readily achieved for DS and DP materials. A robust method was developed and validated for low-dose vaccines, with an injection volume of 25 s × –100 mbar (approximately 14% of the capillary), see Table 1 application 16.

Stability testing

Product degradation causes loss of infectious adenovirus particles and formation of degradants, which could potentially impact both efficacy and safety of the product. Development of a stable vaccine DP could prevent product degradation and is best supported by studying product stability and the routes of degradation.

The DS and DP release testing method was also validated for stability testing, see Table 1 application 10. The stability-indicating power of the Ad26 CZE method was validated by stressing a control sample at 50°C for 45 min (48% recovery compared to control), 50°C for 120 min (29% recovery compared to control), and 0.05% H_2O_2 for 24 h at RT (0% recovery compared to control). The method was used to study the effects of the formulation compositions and container types under different types of stress on the Ad26 particle stability. The FBs varied in buffer and salt types and concentrations with or without the presence of a preservative. The different vaccine FBs had no impact on the CZE method performance. Plastic and glass type containers were used, and the DP formulations were stored at 25°C during 7 or 90 days.

FB2 with the preservative (FB2+) resulted in the highest recoveries after 7 days at 25°C in both the glass and plastic containers, see Figure 14A. Formulations with the preservative resulted in higher recoveries than formulations without the preservative. Lower recoveries were observed for plastic compared to glass containers. In another study, incubation at 25°C for 90 days resulted in the loss of Ad26 in all formulations, see Figure 14B. Interestingly, for either formulations decreases in migration times that are linked to oxidation were observed after 90 days. FB2 was designed to prevent oxidation and showed the least migration time decrease. Hence, the CZE content method was successfully used to find optimal and stable DP conditions (FB2+) and provided additional information regarding Ad26 particle changes during stress testing.

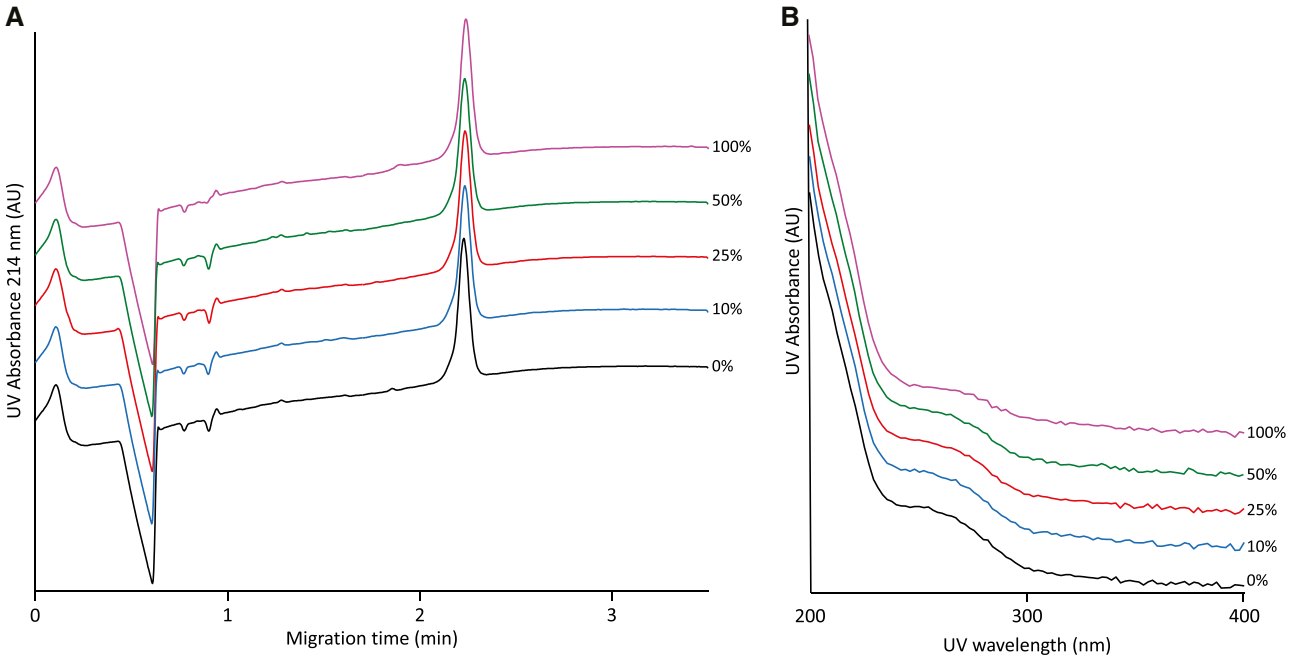

Figure 13. Effects of different fractions of incompletes at constant 214 nm UV absorbance analyzed with CZE, (A) electropherograms, and (B) UV-spectra of the Ad26 peak at 2.2 min. For experimental conditions, see text.

Concentration determination and adenovirus particle migration changes can be used to study the different routes of degradation, e.g., modification, aggregation, disintegration, and adsorption. Forced degradation studies were conducted to understand how Ad26 particles degraded and identify CQAs. Thermal stress (incubation at 50°C for 120 min or at 70°C for 45 min) and oxidation stress (incubation with 0.08% v:v H_2O_2 for 24 h or 0.40% v:v H_2O_2 for 17 h) were applied in this study example. The samples were analyzed with CZE [19], RP-HPLC [53], DLS, and ELS.

The CZE, RP-UHPLC, DLS, and ELS results for both oxidation conditions were similar, see Figure 15. The protein profiles for the oxidation conditions were different from the control sample, see Figure 15B. In RP-UHPLC, Protein II, the capsid protein hexon [91], shifted from 13.3 min in the control sample to 12.8 min after oxidative stress. The earlier retention time was most likely caused by a lower hydrophobicity due to adenoviral protein oxidation. The average hydrodynamic diameter was about 100 nm, comparable to the control sample, as expected from an intact non-aggregated

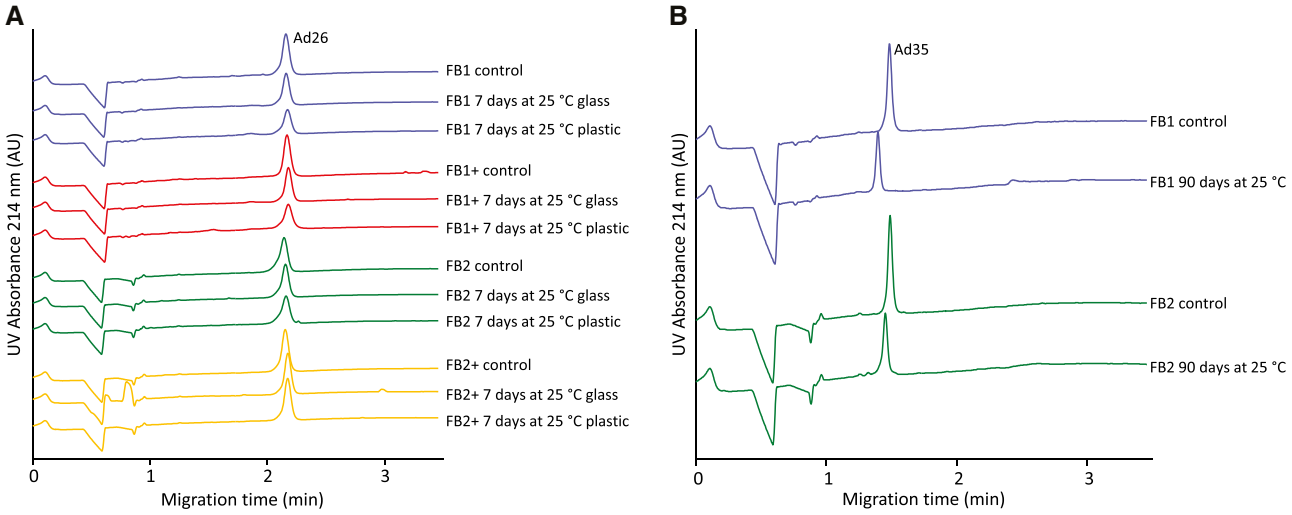

Figure 14. The effect of different FBs, some with preservative (+), analyzed with CZE after incubation in different containers (i.e., glass and plastic) at 25°C for, (A) 7 days, and (B) 90 days. For experimental conditions, see text.

Electrophoresis 2022, *43*, 1068–1090

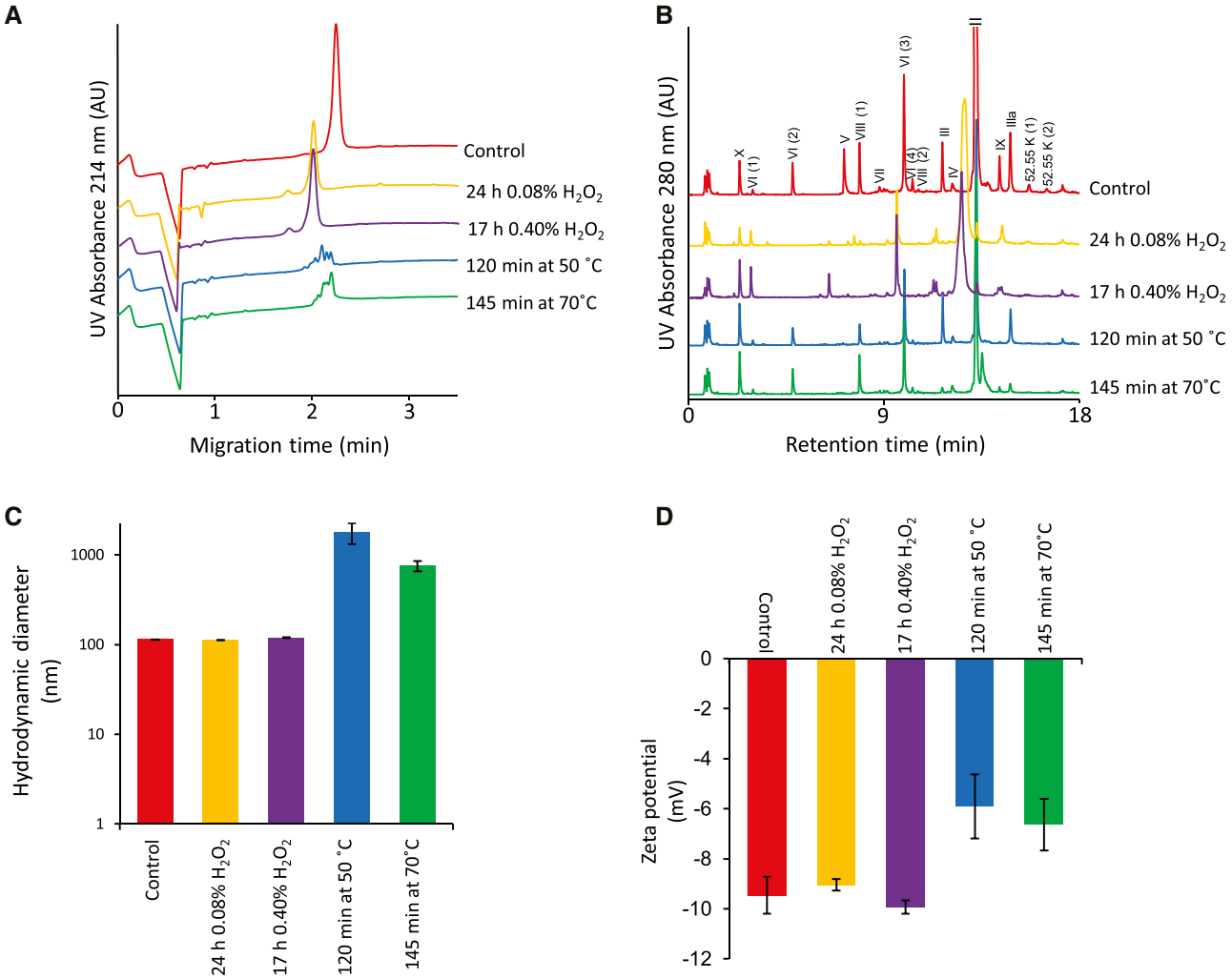

Figure 15. The effect of thermal stress 50°C 120 min (blue), and 70°C 45 min (green) and oxidation stress 0.08% w:v H_2O_2 for 24 h (yellow), and 0.40% w:v H_2O_2 for 24 h (purple) and a control sample (red), analyzed with (A) CZE, (B) RP-HPLC, (C) DLS, and (D) ELS. Experimental conditions, see text.

Ad26 particle, see Figure 15C. Nonetheless, higher polydispersity numbers (not presented) were found for oxidation stressed samples compared to the control, which suggested higher heterogeneity of particles diameters. In CZE, Ad26 peak at 2.2 min (control) was not detected in the oxidized samples, instead peaks at 2.0 min and 1.8 min were found, see Figure 15A. An earlier migration time indicates a smaller and/or more negatively charged particle. The peak at 2.0 min was identified as Ad26 and the peak at 1.8 min was suggested to be protein, based on the UV spectra (not presented). Ad26 particle destabilization and disintegration due to hydrophobicity decrease of hexon could result in free protein in the sample and higher particle diameter heterogeneity. The zeta potentials of the oxidized samples were similar to the control sample, suggesting that the average surface charge of the particles in the sample did not change, see Figure 15D. The hexon protein is much smaller than the Ad26 particle and could thus result in a higher electrophoretic mobility.

Differences were observed between the electropherograms (Figure 15A), hydrodynamic diameter (Figure 15C), and the zeta potential (Figure 15D) for the thermally stressed samples compared to the control sample, but not for the retention times for most of the Ad26 proteins (Figure 15B). In the electropherograms the main Ad26 peak was absent, and an earlier migrating cluster of peaks identified as aggregates (with UV spectrum, not presented) was observed. A higher hydrodynamic diameter was observed for the thermally stressed samples, also suggesting aggregation. The zeta potential was less negative for the thermally stressed samples compared to the control sample. This means that the average surface charge was less negative. A change in zeta potential could be caused by protein denaturation, followed by particle disintegration or aggregation. Aggregation cannot be detected with RP-HPLC due to the denaturing conditions applied to the sample before separation. Interestingly, the aggregates migration times were earlier and the total

corrected peak area was lower than for the adenovirus particles in the control samples. A later migration time was expected for aggregates of intact Ad26, due to the increase of size and the shielding of charge. The decrease in the area suggested components were not detected, which could be caused by precipitation, migration later than 3.5 min, or (unlikely) net positively charged aggregates migrating in the opposite direction. Disintegration of the Ad26 particle and aggregation of adenoviral protein with DNA could cause a heterogeneous pool of aggregates of different sizes and charges.

In total, the CZE results supported the interpretation of drug product stability and forced degradation studies, and determined CQAs, e.g., free in solution protein, on capsid protein, adenovirus melting, and aggregation temperature.

4 Concluding remarks

Although great results were obtained in using CE for vaccine analysis, similar challenges were encountered during the different application developments. A few are mentioned here.

Large biomolecules, such as proteins and viruses, are often heterogeneous due to PTMs or degradants. Large biomolecules are expected to result in more efficient peaks than small molecules due to the lower diffusion coefficients. However, broad adenovirus peaks were observed caused by the complexity and, therefore, heterogeneity of the adenovirus particle compared to for example a single protein virus-like particle [140,141]. In one example, glycans prevented the biomolecule from migrating through the gel buffer. Another frequent observation was aggregates/particulate matter in the form of spikes. Aggregates were possibly induced in the sample or in the capillary because of changing local environment due to, e.g., stacking or migration into the BGE. Sample treatment reduced the heterogeneity by removing PTMs, but could potentially cause a decreased stability of the analyte. Appropriate BGE selection can avoid degradation and aggregation of the sample and improve migration through the BGE.

Generally, ultra-pure or well-characterized standards are hardly available for viruses and vaccines. Because of the analyte heterogeneity in combination with the nanoliter sample volumes and the μL BGE volumes used in CE, peak identification by fraction collection in CE is challenging. BGEs, such as those used for the mentioned applications, are not compatible with other techniques such as MS and neither are complete viruses [16]. Nonetheless, great efforts are being made to develop applications with for example CE-SDS-MS and (i)cIEF-MS [142–147]. We used a combination of approaches for peak identification including the analysis of a selection of purified standards and blanks, physical removal of the component of interest, adding component-specific ligands (i.e., affinity capillary *Electrophoresis*), targeted component degradation, the use of highly specific detection (e.g., UV-spectra, intrinsic fluorescence or by staining, and others), and injection of characterized fractions collected with orthogonal techniques (e.g., ion-exchange chromatography, size exclusion chromatography, and others).

The use of high-grade chemicals and solution preparation best practices is important to improve assay ruggedness and robustness. Low-grade chemicals could potentially cause unwanted effects on the sample, such as degradation, aggregation, or adsorption, and have an impact on the BGE properties, such as ionic strength, viscosity, pH, etc., affecting the *Electrophoresis* separation. A new lot of any critical material needs to be verified before use, hence before the old lot runs out. Solution preparation best practices for capillary electrophoresis start with weighing in chemicals, instead of determining volumes or adjusting the pH or ionic strength manually. In addition, it is good practice to filter and/or sonicate solutions when chemicals are dissolved, or particles are to be expected. Reversed pipetting techniques could be beneficial in avoiding air bubble introduction during liquid transfer. The effects on pipetting accuracy of solution temperature, solution viscosity, and pipette tip adsorption should not be overlooked. If possible, ultra-sonication is a good practice to reduce air bubbles and undissolved particles.

Adsorption of biomolecules [148–150] and matrix effects [27] are well-known issues for the analysis of biomolecules, although often overlooked during method development. For CE applications, the analyte is only in contact with the capillary, not with any other parts of the instrument, limiting the type of surfaces to be dealt with. Adsorption was overcome during the adenovirus CZE method development by designing a BGE with low mobility, high ionic strength, high buffering capacity, and addition of a neutral surfactant in order to be robust for all process intermediates, within process variation and anticipated experimental process conditions, considering ionic strengths, pHs, viscosities, detergents, and DNA/protein content [19].

Sample preparation and stability are critical for biopharmaceutical applications, as the analytes are prone to degradation and aggregations, resulting in analytical artifacts. In addition, a solution that fits one biomolecule can be totally wrong for another one. Sample preparation and BGE and capillary selection for CE are often simplified by choosing an off-the-shelf standard application. However, the lack of fundamental method understanding of or knowledge about the composition of, for example, critical reagents, leads to robustness problems and sub-optimal assay conditions. Therefore, CMP effects need to be studied, and optimal methods to be designed, as demonstrated in [34].

For full control of methods, methods were designed and developed in-house. In general, there is a lot of uncertainty regarding the sample properties and the method parameter effects at the start of development. For some applications (not presented here), this uncertainty and complexity meant that a method could not be developed within the short time frame given. Having better knowledge of, e.g., physicochemical properties and sample stability, corroborates method development. Knowledge sharing among the CE community is key to overcome the method development threshold.

In our experience, designing a method from scratch, using the analytical quality by design (AQbD) principles, often resulted in a better method understanding and control,

and consequently led to a more robust and fit-for-purpose assay compared to off-the-shelf applications. In addition, fundamental technology understanding also provided the opportunity to use the method beyond the initial method scope, like the antibody CE-SDS application used for viral vaccine protein analysis such as (i) seasonal influenza HA quantification, (ii) universal mini-HA primary structure purity determination, (iii) polio protein identification, usage of the mini-HA primary structure CE-SDS method for (iv) glycan analysis, the Ad26 IPC CZE method that could be used for (v) all process intermediates, (vi) stability studies, (vii) product characterization, (viii) identification of additional protein in the context of AEX-filter blockage, (ix) domiphen adenovirus particle interaction studies, (x) low adenovirus concentration products, and the adenovirus content CZE method that could be used for (xi) chloride quantification.

In the end, however, the analytical test is as good as its user. Therefore, not only robust method design, but also operator training is of utmost importance. In our experience with method transfers, the normally expected and anticipated trainings are often analytical test procedure trainings only. Consequently, operators were not able to oversee and understand the consequences of habitual behaviors (e.g., local habits, and habits based on other technologies such as HPLC). Habitual behaviors were often overlooked during trainings and lead to method issues and difficult troubleshooting, especially in non-travel pandemic situations. We emphasize the importance of a holistic view on training and to include teaching the fundamentals of CE, the specific CE instrument, and the software, including the best practices for each. The test procedure is then the last step in the training. This approach, in combination with a sufficient number of trial runs, allows for building up experience and yields a decrease in the number of and time spend on troubleshooting. Eventually, it sets the basis for the operators to perform troubleshooting independently.

In total, the time we took to invest in understanding CE technology and develop applications resulted in a wide range of CE applications supporting viral vaccine analysis. CE took viral vaccine testing beyond what was previously possible and improved process and product understanding and, overall, the control of viral vaccine production with respect to safety, efficacy, and quality. Consequently, CE has become an indispensable asset to our analytical toolbox.

The authors thank Dr Martijn Schenning for the critical review of the manuscript, Martijn Kruger for data management, and Prof. Dr Hermann Wätzig for encouraging us to write this work.

The authors have declared no conflict of interest.

Data availability statement

The data that supports the findings of this study are available in the supplementary material of this article.

5 References

[1] World Health Organization (WHO), *WHO Library Cataloguing-in-Publication Data*, ID: 978 92 4 150498 0, WHO, Geneva 2013.

[2] European Medicines Agency (EMA), *ICH guideline Q8 (R2) on pharmaceutical development: Step 5*, ID: EMA/CHMP/ICH/167068/2004, EMA, London 2017.

[3] U.S. Food and Drug Administration (USFDA), *Process Validation: General Principles and Practices*, ID: FDA-2008-D-0559, USFDA, Silver Spring, MD 2011.

[4] European Medicines Agency (EMA), *ICH note for guidance on validation of analytical procedures: text and methodology*, ID: CPMP/ICH/381/95, EMA, London 1995.

[5] Parenteral Drug Association (PDA), *PDA Technical Report No. 60–3 (TR 60–3) Process Validation: A Lifecycle Approach, Annex 2: Biopharmaceutical Drug Substances Manufacturing*, PDA, Bethesda, MD 2021 (ISBN: 9781945584244).

[6] European Medicines Agency (EMA), *Guideline on process validation for finished products - information and data to be provided in regulatory submissions*, ID:EMA/CHMP/CVMP/QWP/BWP/70278/2012-Rev1,Corr.1, EMA, London 2016.

[7] Yu, L. X., Amidon, G., Khan, M. A., Hoag, S. W., Polli, J., Raju, G. K., Woodcock, J., *AAPS J.* 2014, *16*, 771–783.

[8] Hakemeyer, C., McKnight, N., st. John, R., Meier, S., Trexler-Schmidt, M., Kelley, B., Zettl, F., Puskeiler, R., Kleinjans, A., Lim, F., Wurth, C., *Biologicals* 2016, *44*, 306–318.

[9] Kenndler, E., Blaas, D., *TrAC Trends Anal. Chem.* 2001, *20*, 543–551.

[10] Kolivoška, V., Weiss, V. U., Kremser, L., Gaš, B., Blaas, D., Kenndler, E., *Electrophoresis* 2007, *28*, 4734–4740.

[11] Kremser, L., Konecsni, T., Blaas, D., Kenndler, E., *Anal. Chem.* 2004, *76*, 4175–4181.

[12] Kremser, L., Okun, V. M., Nicodemou, A., Blaas, D., Kenndler, E., *Anal. Chem.* 2004, *76*, 882–887.

[13] Kremser, L., Petsch, M., Blaas, D., Kenndler, E., *Anal. Chem.* 2004, *76*, 7360–7365.

[14] Kremser, L., Petsch, M., Blaas, D., Kenndler, E., *Electrophoresis* 2006, *27*, 2630–2637.

[15] Okun, V. M., Blaas, D., Kenndler, E., *Anal. Chem.* 1999, *71*, 4480–4485.

[16] Okun, V. M., Ronacher, B., Blaas, D., Kenndler, E., *Anal. Chem.* 1999, *71*, 2028–2032.

[17] Grossman, P. D., Soane, D. S., *Anal. Chem.* 1990, *62*, 1592–1596.

[18] Hjertén, S., Elenbring, K., Kilár, F., Liao, J.-L., Chen, A. J. C., Siebert, C. J., Zhu, M.-D., *J. Chromatogr. A* 1987, *403*, 47–61.

[19] van Tricht, E., Geurink, L., Backus, H., Germano, M., Somsen, G. W., Sänger–van de Griend, C. E., *Talanta* 2017, *166*, 8–14.

[20] van Tricht, E., Geurink, L., Galindo Garre, F., Schenning, M., Backus, H., Germano, M., Somsen, G. W., Sänger–van de Griend, C. E., *Electrophoresis* 2019, *40*, 2277–2284.

[21] Mann, B., Traina, J. A., Soderblom, C., Murakami, P. K., Lehmberg, E., Lee, D., Irving, J., Nestaas, E., Pungor, E., *J. Chromatogr. A* 2000, *895*, 329–337.

[22] Halewyck, H., Oita, I., Thys, B., Dejaegher, B., Heyden, Y. V., Rombaut, B., *Electrophoresis* 2010, *31*, 3281–3287.

[23] Oita, I., Halewyck, H., Pieters, S., Dejaegher, B., Thys, B., Rombaut, B., Heyden, Y. V., *J. Pharm. Biomed. Anal.* 2009, *50*, 655–663.

[24] Oita, I., Halewyck, H., Pieters, S., Dejaegher, B., Thys, B., Rombaut, B., Heyden, Y. V., *J. Pharm. Biomed. Anal.* 2011, *55*, 135–145.

[25] Oita, I., Halewyck, H., Pieters, S., Thys, B., Heyden, Y. V., Rombaut, B., *J. Virol. Methods* 2012, *185*, 7–17.

[26] Oita, I., Halewyck, H., Thys, B., Rombaut, B., Heyden, Y. V., *J. Pharm. Biomed. Anal.* 2012, *71*, 79–88.

[27] Oita, I., Halewyck, H., Thys, B., Rombaut, B., Heyden, Y. V., *Anal. Chim. Acta* 2012, *747*, 42–50.

[28] Kolesar, J. M., Allen, P. G., Doran, C. M., *J. Chromatogr. B: Biomed. Sci. Appl.* 1997, *697*, 189–194.

[29] Kolesar, J. M., Miller, J. A., Dhurandhar, N. V., Atkinson, R. L., *J. Chromatogr. B: Biomed. Sci. Appl.* 2000, *744*, 1–8.

[30] Schnabel, U., Groiss, F., Blaas, D., Kenndler, E., *Anal. Chem.* 1996, *68*, 4300–4303.

[31] Takátsy, A., Kilár, A., Kilár, F., Hjertén, S., *J. Sep. Sci.* 2006, *29*, 2802–2809.

[32] Végvári, A., Hjertén, S., *Electrophoresis* 2003, *24*, 3815–3820.

[33] van Tricht, E., Geurink, L., Pajic, B., Nijenhuis, J., Backus, H., Germano, M., Somsen, G.W., Sänger–van de Griend, C.E., *Talanta* 2015, *144*, 1030–1035.

[34] Geurink, L., van Tricht, E., Dudink, J., Pajic, B., Sänger–van de Griend, C. E., *Electrophoresis* 2021, *42*, 10–18.

[35] Hamm, M., Ha, S., Rustandi, R. R., *Anal. Biochem.* 2015, *478*, 33–39.

[36] Hamm, M., Wang, F., Rustandi, R. R., *Electrophoresis* 2015, *36*, 2687–2694.

[37] Lancaster, C., Pristatsky, P., Hoang, V. M., Casimiro, D. R., Schwartz, R. M., Rustandi, R., Ha, S., *J. Chromatogr. B: Anal. Technol. Biomed. Life Sci.* 2016, *1032*, 218–223.

[38] Rustandi, R. R., Anderson, C., Hamm, M., in: Beck, A. (Ed.), *Glycosylation Engineering of Biopharmaceuticals: Methods and Protocols*, Humana Press, Totowa, NJ 2013, pp. 181–197.

[39] Rustandi, R. R., Loughney, J. W., Hamm, M., Hamm, C., Lancaster, C., Mach, A., Ha, S., *Electrophoresis* 2012, *33*, 2790–2797.

[40] Rustandi, R. R., Wang, F., Hamm, C., Cuciniello, J. J., Marley, M. L., *Electrophoresis* 2014, *35*, 1072–1078.

[41] Zhou, W., Tomer, K. B., Khaledi, M. G., *Anal. Biochem.* 2000, *284*, 334–341.

[42] Guttman, M., Váradi, C., Lee, K. K., Guttman, A., *Electrophoresis* 2015, *36*, 1305–1313.

[43] Tran, N. T., Taverna, M., Chevalier, M., Ferrier, D., *J. Chromatogr. A* 2000, *866*, 121–135.

[44] Zhang, Z., Park, J., Barrett, H., Dooley, S., Davies, C., Verhagen, M. F., *Hum. Gene Ther.* 2021, *32*, 628–637.

[45] Loughney, J. W., Lancaster, C., Ha, S., Rustandi, R. R., *Anal. Biochem.* 2014, *461*, 49–56.

[46] Fabre, H., Blanchin, M. D., Bosc, N., *Anal. Chim. Acta* 1999, *381*, 29–37.

[47] Stålberg, O., Sander, K., Sänger–van de Griend, C., *J. Chromatogr. A* 2002, *977*, 265–275.

[48] Nickerson, B., *J. Pharm. Biomed. Anal.* 1997, *15*, 965–971.

[49] AB-Sciex, *IgG Purity and Heterogeneity Assay Kit: Application guide*, ID: RUO-IDV-05–6935-A, AB-Sciex, Framingham, MA 2018.

[50] FUJIFILM Wako Chemicals U.S.A. Corporation, *DNA Extractor Ⓡ Kit instructions*, *ID*: 1911KA2.

[51] AB-Sciex, *dsDNA 1000 Kit: Application guide*, ID: RUO-IDV-05–11136-A, AB-Sciex, Framingham, MA 2020.

[52] Bio-rad Laboratories, i., *ChemiDoc and ChemiDoc MP Imaging Systems with Image Lab Touch Software: User Guide*, ID: 10000062126 Ver E 2020.

[53] van Tricht, E., de Raadt, P., Verwilligen, A., Schenning, M., Backus, H., Germano, M., Somsen, G. W., Sänger–van de Griend, C. E., *J. Chromatogr. A* 2018, *1581–1582*, 25–32.

[54] Nowak, C., Cheung, J., Dellatore, S., Katiyar, A., Bhat, R., Sun, J., Ponniah, G., Neill, A., Mason, B., Beck, A., Liu, H., *mAbs* 2017, *9*, 1217–1230.

[55] European Medicines Agency (EMA), *Guideline on bioanalytical method validation*, ID: EMEA/CHMP/EWP/192217/2009 Rev. 1 Corr. 2, EMA, London 2011.

[56] Lechner, A., Giorgetti, J., Gahoual, R., Beck, A., Leize, E., François, Y., *J. Chromatogr. B: Anal. Technol. Biomed. Life Sci.* 2019, *1122–1123*, 1–17.

[57] Wang, X., An, Z., Luo, W., Xia, N., Zhao, Q., *Protein Cell* 2018, *9*, 74–85.

[58] Leach, M. N. E., Carpick, B., *CASSS* 2018, CEPharm 2018.

[59] Shala-Lawrence, A., Beheshti, S., Newman, E., Tang, M., Krylova, S.M., Leach, M., Carpick, B., Krylov, S.N., *Talanta* 2017, *175*, 273–279.

[60] Li, T., Malik, M., Yowanto, H., Mollah, S., *Purity Analysis of Adeno-Associated Virus (AAV) Capsid Proteins using CE-SDS Method*, ID: RUO-MKT-02–9761-A, AB-Sciex, Framingham, MA 2019.

[61] Zhang, C., Meagher, M.M., in: Phillips, T.M. (Ed.), *Clinical Applications of Capillary Electrophoresis: Methods and Protocols*, Springer, New York, New York, NY 2019, pp. 263–270.

[62] Coudeville, L., Bailleux, F., Riche, B., Megas, F., Andre, P., Ecochard, R., *BMC Med. Res. Methodol.* 2010, *10*, 18.

[63] Skehel, J., Wiley, D., *Annu. Rev. Biochem.* 2000, *69*, 531–569.

[64] Su, B., Wurtzer, S., Rameix-Welti, M.-A., Dwyer, D., van der Werf, S., Naffakh, N., Clavel, F., Labrosse, B., *PLoS One* 2010, *4*, e8495.

[65] Johansson, B. E., Bucher, D. J., Kilbourne, E. D., *J. Virol.* 1989, *63*, 1239–1246.

[66] Neirynck, S., Deroo, T., Saelens, X., Vanlandschoot, P., Jou, W. M., Fiers, W., *Nat. Med.* 1999, *5*, 1157–1163.

[67] Impagliazzo, A., Milder, F., Kuipers, H., Wagner, M. V., Zhu, X., Hoffman, R. M. B., van Meersbergen, R., Huizingh, J., Wanningen, P., Verspuij, J., de Man, M., Ding, Z., Apetri, A., Kükrer, B., Sneekes-Vriese, E., Tomkiewicz, D., Laursen, N. S., Lee, P. S., Zakrzewska, A., Dekking, L., Tolboom, J., Tettero, L., van Meerten, S., Yu, W., Koudstaal, W., Goudsmit, J., Ward, A. B., Meijberg, W., Wilson, I. A., Radošević, K., *Science* 2015, *349*, 1301–1306.

[68] van der Lubbe, J. E. M., Verspuij, J. W. A., Huizingh, J., Schmit-Tillemans, S. P. R., Tolboom, J. T. B. M., Dekking, L. E. H. A., Kwaks, T., Brandenburg, B., Meijberg, W., Zahn, R. C., Roozendaal, R., Kuipers, H., *Front. Immunol.* 2018, *9*, 2350–2350.

[69] Impagliazzo, A., Meijberg, J. W., Radosevic, K., Wagner, M., Ding, Z., US patent: US10117925B2 2015.

[70] Milder, F. J., Ritschel, T., Brandenburg, B., Jongeneelen, M. A. C., Truan, D., Langedijk, J. P. M., *European patent: EP18152991* 2019.

[71] Daniels, R., Kurowski, B., Johnson, A. E., Hebert, D. N., *Mol. Cell* 2003, *11*, 79–90.

[72] Hebert, D. N., Zhang, J. X., Chen, W., Foellmer, B., Helenius, A., *J. Cell Biol.* 1997, *139*, 613–623.

[73] Wang, A. L., Paciolla, M., Palmieri, M. J., Hao, G. G., *J. Pharm. Biomed. Anal.* 2020, *180*, 113006.

[74] Scheller, C., Krebs, F., Wiesner, R., Wätzig, H., Oltmann-Norden, I., *Electrophoresis* 2021, *42*, 1521–1531.

[75] Dotz, V., Haselberg, R., Shubhakar, A., Kozak, R. P., Falck, D., Rombouts, Y., Reusch, D., Somsen, G. W., Fernandes, D. L., Wuhrer, M., *TrAC Trends Anal. Chem.* 2015, *73*, 1–9.

[76] Cipollo, J. F., Parsons, L. M., *Mass Spectrom. Rev.* 2020, *39*, 371–409.

[77] AB-Sciex, *Fast Glycan Labeling and Analysis Kit: Application guide*, ID: RUO-IDV-05–4092-C, AB-Sciex, Framingham, MA 2020.

[78] Scientific, T. F., *GlycanAssure™ HyPerformance APTS Kit: User guide*, ID: MAN0016959 2018.

[79] AB-Sciex, *Beckman Coulter Capillary Isoelectric Focusing (cIEF) Analysis: Application guide*, ID: A78788AF, AB-Sciex, Framingham, MA 2014.

[80] ProteinSimple, *User Guide for Maurice, Maurice C. and Maurice S.*, ID: P/N 046–, 295, ProteinSimple, San Jose, CA 2020.

[81] Wu, J., Huang, T., *Electrophoresis* 2006, *27*, 3584–3590.

[82] Demirdirek, B., Lan, W., Qiu, D., Ding, W., Iyer, L. K., Bolgar, M. S., Valente, J. J., *J. Chromatogr. B: Anal. Technol. Biomed. Life Sci.* 2019, *1105*, 156–163.

[83] Chen, W., Kojtari, B., Satulovsky, J., Ostrowski, M. A., *Rapid and reproducible high-resolution charge variant analysis of adalimumab (mAb) using the IntaBio Imaged CIEF-MS System*, ID: RUO-MKT-02–13149, AB-Sciex, Framingham, MA 2021.

[84] Chen, W., Ostrowski, M. A., Gupta, D., Gentalen, E., *Rapid, comprehensive, high resolution charge variant characterization using the IntaBio iCIEF-MS System with SCIEX TripleTOF 6600+ and Protein Metrics Byos Software*, ID: RUO-MKT-02–13150, AB-Sciex, Framingham, MA 2020.

[85] Kouiavskaia, D., Puligedda, R. D., Dessain, S. K., Chumakov, K., *J. Virol. Methods* 2020, *276*, 113785.

[86] Crawt, L., Atkinson, E., Tedcastle, A., Pegg, E., sIPV StudyGroup, Minor, P., Cooper, G., Rigsby, P., Martin, J., *J. Infect. Dis.* 2019, *221*, 544–552.

[87] Minor, P. D., Ferguson, M., Evans, D. M. A., Almond, J. W., Icenogle, J. P., *J. Gen. Virol.* 1986, *67*, 1283–1291.

[88] Rezapkin, G., Neverov, A., Cherkasova, E., Vidor, E., Sarafanov, A., Kouiavskaia, D., Dragunsky, E., Chumakov, K., *J. Virol. Methods* 2010, *169*, 322–331.

[89] Mendonça, S. A., Lorincz, R., Boucher, P., Curiel, D. T., *NPJ Vaccines* 2021, *6*, 97.

[90] Pollard, A. J., Launay, O., Lelievre, J. D., Lacabaratz, C., Grande, S., Goldstein, N., Robinson, C., Gaddah, A., Bockstal, V., Wiedemann, A., Leyssen, M., Luhn, K., Richert, L., Bétard, C., Gibani, M. M., Clutterbuck, E. A., Snape, M. D., Levy, Y., Douoguih, M., Thiebaut, R., *Lancet Infect. Dis.* 2021, *21*, 493–506.

[91] Benevento, M., Di Palma, S., Snijder, J., Moyer, C. L., Reddy, V. S., Nemerow, G. R., Heck, A. J. R., *J. Biol. Chem.* 2014, *289*, 11421–11430.

[92] Luitjens, A., van Herk, H., US patent: US2012031.5696A1 2012.

[93] Berdichevsky, M., Gentile, M. P., Hughes, B., Meis, P., Peltier, J., Blumentals, I., Auniņs, J., Altaras, N. E., *Biotechnol. Prog.* 2008, *24*, 158–165.

[94] Cortin, V., Thibault, J., Jacob, D., Garnier, A., *Biotechnol. Prog.* 2004, *20*, 858–863.

[95] Goerke, A. R., To, B. C. S., Lee, A. L., Sagar, S. L., Konz, J. O., *Biotechnol. Bioeng.* 2005, *91*, 12–21.

[96] Luitjens, A., Lewis, J. A., US patent: US10041049B2 2018.

[97] Vogels, R., Bout, A., US patent: US7468181B2 2008.

[98] Vogels, R., Havenga, M., Mehtali, M., US patent: US6492169B1 2002.

[99] Weggeman, M., US patent: US6485958B2 2002.

[100] Graham, F. L., Smiley, J., Russell, W. C., Nairn, R., *J. Gen. Virol.* 1977, *36*, 59–72.

[101] Imler, J.-L., Mehtali, M., Pavirani, A., US patent: US6040174A 2000.

[102] Massie, B., US patent: US5891690A 1999.

[103] Kovesdi, I., Brough, D.E., McVey D.L., Bruder J.T., Lizonova, A., US patent: US5851806A 1998.

[104] Weggeman, M., US patent: US67006405P 2013.

[105] Weggeman, M., van Corven, E. J. J. M., US patent: US8124106B2 2012.

[106] Konz, J. O. Jr., Lee, A. L., To, C. S. B., Goerke, A. R., US patent: US7326555B2 2008.

[107] Carrión, M. E., Menger, M., Kovesdi, I., US patent: US6586226B2 2003.

[108] Shabram, P. W., Giroux, D. D., Goudreau, A. M., Gregory, R. J., Horn, M. T., Huyghe, B. G., Liu, X., Nunnally, M. H., Sugarman, B. J., Sutjipto, S., *Hum. Gene Ther.* 1997, *8*, 453–465.

[109] Tang, J. C.-T., Vellekamp, G., Bondoc, L. L. Jr., US patent: US6261823B1 2001.

[110] Evans, R. K., Nawrocki, D. K., Isopi, L. A., Williams, D. M., Casimiro, D. R., Chin, S., Chen, M., Zhu, D. M., Shiver, J. W., Volkin, D. B., *J. Pharm. Sci.* 2004, *93*, 2458–2475.

[111] Altaras, N. E., Aunins, J. G., Evans, R. K., Kamen, A., Konz, J. O., Wolf, J. J., *Adv. Biochem. Eng. Biotechnol.* 2005, *99*, 193–260.

[112] Evans, R. K. Volken, D. B., Isopi, L. A., US patent: US7456009B2 2008.

[113] Croyle, M. A., Cheng, X., Wilson, J. M., *Gene Ther.* 2001, *8*, 1281–1290.

[114] Adriaansen, J., US patent: US9974737B2 2018.

[115] Adriaansen, J., US patent: US20160199426A1 2016.

[116] Sosnowski, B., Hoganson, D. K., Ma, J., Asato, L., Ong, M., Printz, M., Huyghe, B., D'Andrea, M., *BioProcessing J.* 2002, *1*, 43–48.

[117] Mironov, G. G., Chechik, A. V., Ozer, R., Bell, J. C., Berezovski, M. V., *Anal. Chem.* 2011, *83*, 5431–5435.

[118] Azizi, A., Mironov, G. G., Muharemagic, D., Wehbe, M., Bell, J. C., Berezovski, M. V., *Anal. Chem.* 2012, *84*, 9585–9591.

[119] U.S. Food and Drug Administration (USFDA), *Characterization and Qualification of Cell Substrates and Other Biological Materials Used in the Production of Viral Vaccines for Infectious Disease Indications*, ID: FDA-2006-D-0223, USFDA, Silver Spring, MD 2010.

[120] European Directorate for the Quality of Medicines & HealthCare (EDQM), *European Pharmacopoeia, 5.2.3, ID: 01/2018:50203*, EDQM, Strasbourg 2020.

[121] European Directorate for the Quality of Medicines & HealthCare (EDQM), *European pharmacopoeia, 5.14, ID: 01/2018:50203*, EDQM, Strasbourg 2020.

[122] Fallaux, F. J., Bout, A., van der Velde, I., van den Wollenberg, D. J., Hehir, K. M., Keegan, J., Auger, C., Cramer, S. J., van Ormondt, H., van der Eb, A. J., Valerio, D., Hoeben, R. C., *Hum. Gene Ther.* 1998, *9*, 1909–1917.

[123] U.S. Food and Drug Administration (USFDA), NTIS Issue Number 201304 2012.

[124] Sheng-Fowler, L., Lewis, A. M., Jr., Peden, K., *Biologicals* 2009, *37*, 190–195.

[125] Sheng-Fowler, L., Lewis, A. M., Jr., Peden, K., *Biologicals* 2009, *37*, 259–269.

[126] Mast, T. C., Kierstead, L., Gupta, S. B., Nikas, A. A., Kallas, E. G., Novitsky, V., Mbewe, B., Pitisuttithum, P., Schechter, M., Vardas, E., Wolfe, N. D., Aste-Amezaga, M., Casimiro, D. R., Coplan, P., Straus, W. L., Shiver, J. W., *Vaccine* 2010, *28*, 950–957.

[127] Zhang, S., Huang, W., Zhou, X., Zhao, Q., Wang, Q., Jia, B., *J. Med Virol.* 2013, *85*, 1077–1084.

[128] Condezo, G. N., Marabini, R., Ayora, S., Carazo, J. M., Alba, R., Chillón, M., San Martín, C., *J. Virol.* 2015, *89*, 9653–9664.

[129] Daniell, E., *J. Virol.* 1976, *19*, 685–708.

[130] Burlingham, B. T., Brown, D. T., Doerfler, W., *Virology* 1974, *60*, 419–430.

[131] Yang, X., Agarwala, S., Ravindran, S., Vellekamp, G., *J. Pharm. Sci.* 2008, *97*, 746–763.

[132] Berkowitz, S. A., Philo, J. S., *Anal. Biochem.* 2007, *362*, 16–37.

[133] St George, J. A., *Gene Ther.* 2003, *10*, 1135–1141.

[134] Maizel, J. V., White, D. O., Scharff, M. D., *Virology* 1968, *36*, 115–125.

[135] Sweeney, J. A., Hennessey, J. P., Jr., *Virology* 2002, *295*, 284–288.

[136] Echavarria, M., Forman, M., van Tol, M. J., Vossen, J. M., Charache, P., Kroes, A. C., *Lancet* 2001, *358*, 384–385.

[137] Heim, A., Ebnet, C., Harste, G., Pring-Akerblom, P., *J. Med Virol.* 2003, *70*, 228–239.

[138] Lankester, A. C., van Tol, M. J., Claas, E. C., Vossen, J. M., Kroes, A. C., *Clin. Infect. Dis.* 2002, *34*, 864–867.

[139] Ma, L., Bluyssen, H. A. R., De Raeymaeker, M., Laurysens, V., van der Beek, N., Pavliska, H., van Zonneveld, A.-J., Tomme, P., van Es, H. H. G., *J. Virol. Methods* 2001, *93*, 181–188.

[140] Bettonville, V., Nicol, J. T. J., Furst, T., Thelen, N., Piel, G., Thiry, M., Fillet, M., Jacobs, N., Servais, A.-C., *Talanta* 2017, *175*, 325–330.

[141] Bettonville, V., Nicol, J. T. J., Thelen, N., Thiry, M., Fillet, M., Jacobs, N., Servais, A.-C., *Electrophoresis* 2016, *37*, 579–586.

[142] Römer, J., Montealegre, C., Schlecht, J., Kiessig, S., Moritz, B., Neusüß, C., *Anal. Bioanal. Chem.* 2019, *411*, 7197–7206.

[143] Sánchez-Hernández, L., Montealegre, C., Kiessig, S., Moritz, B., Neusüß, C., *Electrophoresis* 2017, *38*, 1044–1052.

[144] Römer, J., Kiessig, S., Moritz, B., Neusüß, C., *Electrophoresis* 2021, *42*, 374–380.

[145] Römer, J., Stolz, A., Kiessig, S., Moritz, B., Neusüß, C., *J. Pharm. Biomed. Anal.* 2021, *201*, 114089.

[146] Dai, J., Lamp, J., Xia, Q., *Anal. Chem.* 2018, *90*, 2246–2254.

[147] Mack, S., Arnold, D., Bogdan, G., Bousse, L., Danan, L., Dolnik, V., Ducusin, M., Gwerder, E., Herring, C., Jensen, M., Ji, J., Lacy, S., Richter, C., Walton, I., Gentalen, E., *Electrophoresis* 2019, *40*, 3084–3091.

[148] Kiesel, I., Paulus, M., Nase, J., Tiemeyer, S., Sternemann, C., Rüster, K., Wirkert, F. J., Mende, K., Büning, T., Tolan, M., *Langmuir* 2014, *30*, 2077–2083.

[149] Lucy, C. A., MacDonald, A. M., Gulcev, M. D., *J. Chromatogr. A* 2008, *1184*, 81–105.

[150] Verzola, B., Gelfi, C., Righetti, P. G., *J. Chromatogr. A* 2000, *868*, 85–99.

[151] American Type Culture Collection (ATTC), *Human adenovirus 5 VR-1516: product sheet*, ID: VR-1516, ATTC, Manassas, VA 2021.

Electrophoresis 2022, *43*, 143–166

Ramesh Kumar[1]
Andras Guttman[2,3]
Anurag S. Rathore[1]

[1]Department of Chemical Engineering, Indian Institute of Technology Delhi, Hauz Khas, New Delhi, India
[2]Horváth Csaba Memorial Laboratories of Bioseparation Sciences, Research Center for Molecular Medicine, Faculty of Medicine, University of Debrecen, Debrecen, Hungary
[3]Translational Glycomics Group, Research Institute of Biomolecular and Chemical Engineering, University of Pannonia, Veszprem, Hungary

Received June 16, 2021
Revised September 7, 2021
Accepted September 23, 2021

Review

Applications of capillary electrophoresis for biopharmaceutical product characterization

Capillary electrophoresis (CE), after being introduced several decades ago, has carved out a niche for itself in the field of analytical characterization of biopharmaceutical products. It does not only offer fast separation, high resolution in miniaturized format, but equally importantly represents an orthogonal separation mechanism to high-performance liquid chromatography. Therefore, it is not surprising that CE-based methods can be found in all major pharmacopoeias and are recommended for the analysis of biopharmaceutical products during process development, characterization, quality control, and release testing. Different separation formats of CE, such as capillary gel electrophoresis, capillary isoelectric focusing, and capillary zone electrophoresis are widely used for size and charge heterogeneity characterization as well as purity and stability testing of therapeutic proteins. Hyphenation of CE with MS is emerging as a promising bioanalytical tool to assess the primary structure of therapeutic proteins along with any impurities. In this review, we confer the latest developments in capillary electrophoresis, used for the characterization of critical quality attributes of biopharmaceutical products covering the past 6 years (2015–2021). Monoclonal antibodies, due to their significant share in the market, have been given prioritized coverage.

Keywords:
Biopharmaceuticals / Capillary electrophoresis / Critical quality attributes / Mass spectrometry / Monoclonal antibodies
DOI 10.1002/elps.202100182

1 Introduction

Capillary electrophoresis (CE) is an electric field mediated separation technique, first reported around 1970s, and increasingly popular in biopharmaceutical analysis [1–11]. It can be operated in various modes including capillary zone electrophoresis (CZE), capillary gel electrophoresis (CGE), capillary isoelectric focusing (cIEF), capillary electrochromatography (CEC), and micellar electrokinetic chromatography (MEKC), to facilitate characterization of different cations, anions, and even neutral molecules [12–15].

Biopharmaceuticals have been steadily gaining ground and currently overshadow their small molecule (pharmaceutical) counterparts with respect to growth in product sales. Biopharmaceuticals are protein or nucleic acid-based therapeutic products, primarily produced in living organisms [16]. Thus far, over 300 biotherapeutic products have been developed [17]. However, a primary concern with this category of products is heterogeneity due to their biological systems based production [18]. These heterogeneities come from cumulative contributions of the host cell line, culture media, and bioprocessing conditions. In addition, storage and transportation conditions may also have significant impacts. Since many of these heterogeneities are known to affect the safety and efficacy of the therapeutic products, their adequate characterization if often required by regulatory authorities [19,20]. Additionally, as the patents of many biologicals have expired or are on the verge of expiration, there has been a recent emergence of the biosimilar industry [17]. Biosimilars are biopharmaceuticals that have demonstrated similarity in their structure, function, quality, safety, and efficacy to the innovator product [21]. Since biosimilars are also produced by living organisms, extensive analytical characterization is necessary to prove their similarity to the reference product as minor alterations during manufacturing may lead to significant implications on the quality of the product. CE methods can be increasingly found in all major pharmacopoeias and are recommended for the analysis of biopharmaceutical products during process development, characterization, and quality control [12,22,23]. However, LC still remains one

Correspondence: Professor Anurag S. Rathore, Department of Chemical Engineering, Indian Institute of Technology Delhi, Hauz Khas, New Delhi, 110016, India
E-mail: asrathore@biotechcmz.com

Abbreviations: **AAV**, adeno-associated virus; **ADA**, antidrug antibody; **ADC**, antibody-drug conjugate; **AFM**, atomic force microscopy; **BsAb**, bispecific antibody; **CQA**, critical quality attribute; **DAR**, drug antibody ratio; **DoE**, design of experiment; **GU**, glucose unit; **HCP**, host cell protein; **icIEF**, imaged capillary isoelectric focusing; **LNP**, lipid nanoparticle; **NIST mAb**, National Institute of Standards and Technology monoclonal antibody; **QA**, quality attribute; **QC**, quality control; **SCX**, SPE-strong cation exchange–solid phase extraction; **UHPLC, ultra**, high-performance liquid chromatography; **UV**, ultraviolet

Color online: See article online to view Figs. 1–3 in color.

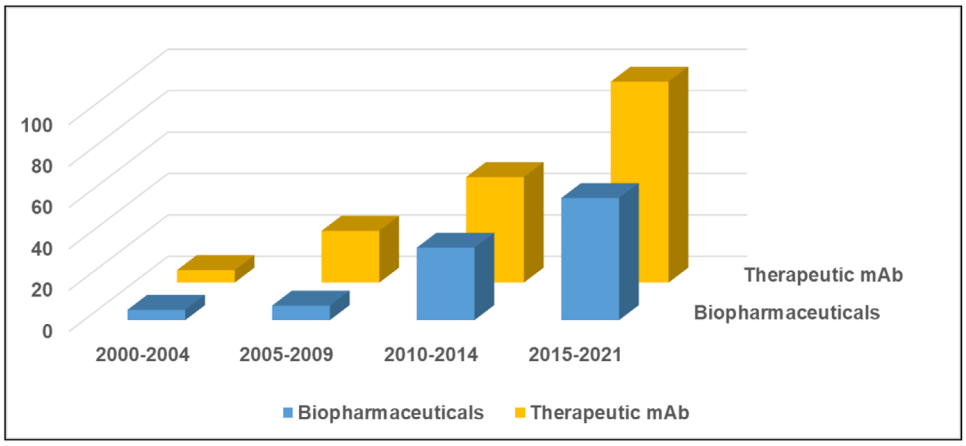

Figure 1. Number of publications reported on the use of capillary electrophoresis in biopharmaceutical analysis and therapeutic mAbs since 2000. Data were collected from "Scopus" using "capillary electrophoresis and biopharmaceuticals," and "capillary electrophoresis and therapeutic monoclonal antibody" in the "article title, abstract, and keywords" field.

of the most important technologies for characterizing biotherapeutics due to its robustness, high reproducibility, and easy coupling with the mass spectrometer. Also, the lack of well-trained CE scientists and the reluctance of learning new methodologies limits the use of CE. Enormous progress has, however, been made in CE to find its place in the standard analytical toolsets for biotherapeutic characterization. This impressive trend can also be seen from the published reports from the past two decades (Fig. 1).

In this review, we focus on CE applications towards characterizing the various quality attributes (QAs) of biopharmaceutical products. This product class is vast and includes diverse modalities such as monoclonal antibodies (mAbs), antibody-drug conjugates (ADCs), fusion proteins, growth factors, cytokines, nucleic acids, and viral vectors [17]. In this review, we focus more on the mAbs, in view of their present dominance in the biopharmaceutical pipelines [17]. Although many reviews have been published on advancements in CE in the past [9–11, 22-25], the present treatment focuses on CE applications published between 2015–2021 for the characterization of quality attributes of biopharmaceutical products (Fig. 2).

2 CE-based characterization of critical quality attributes (CQAs) of mAb products

One hundred mAb-based products have hit the market globally to treat more than thirty targets and diseases since the approval of the first one in 1986 [17,26–29]. Attributes such as primary sequence, charge and size heterogeneity, glycosylation pattern and other post-translational modifications (PTMs), and presence of host cell proteins (HCPs) are believed to potentially impact the quality, safety, and efficacy of the product and hence require monitoring [30,31]. Applying the right method has been identified as one of the most challenging steps when implementing quality by design approaches for the analysis of biotherapeutics and multiple, orthogonal tools typically part of the analytical toolbox that are used for their characterization [30,32–36]. In the following paragraphs, we review CE applications for the analysis of various attributes of mAb-based therapeutic products, also summarized in Table 1.

2.1 Charge heterogeneity analysis

Charge heterogeneity refers to the presence of product related species in the biopharmaceutical, which differ from the main product in terms of charge [37]. These species can arise due to PTMs, degradation reactions such as deamidation, C-terminal lysine processing, and glycation [38,32]. Their presence may result in altered product efficacy and pharmacokinetics or complete product inactivation, in the worst-case even immunogenicity [37].

Different separation modes of CE have been reported to effectively identify charge variants of which cIEF and imaged cIEF (icIEF) with ultraviolet (UV) detection have been implemented in quality control (QC) laboratories and have become reference methods for charge heterogeneity analysis [15]. A reproducible cIEF method has been proposed for mAb identification without the need of adding salt or urea to the sample [39]. The method was validated for mAbs with pIs between 7.0 and 9.0 according to Q2 (R1) guidelines of the International Council for Harmonisation of Technical Requirements for Pharmaceuticals for Human Use (ICH) and was reported to be suitable for transferring to QC laboratories. cIEF has also been coupled to MS for in-depth characterization of charge variants [40]. The results obtained correlated with standard icIEF-UV profiles. In addition, Mack et al. also showed charge variant analysis of mAbs by coupling microchip icIEF with MS [41]. In a comparison between cIEF and CZE, cIEF offered superior performance for pI analysis, while CZE was better for routine and rapid charge heterogeneity analysis [42]. CZE for charge variant analysis has been verified in an intra laboratory and international cross-company study for the analysis of mAbs involving eleven different sites [43]. More than one thousand separations were evaluated and the applicability of CZE for 23 mAbs with pI

Electrophoresis 2022, *43*, 143–166

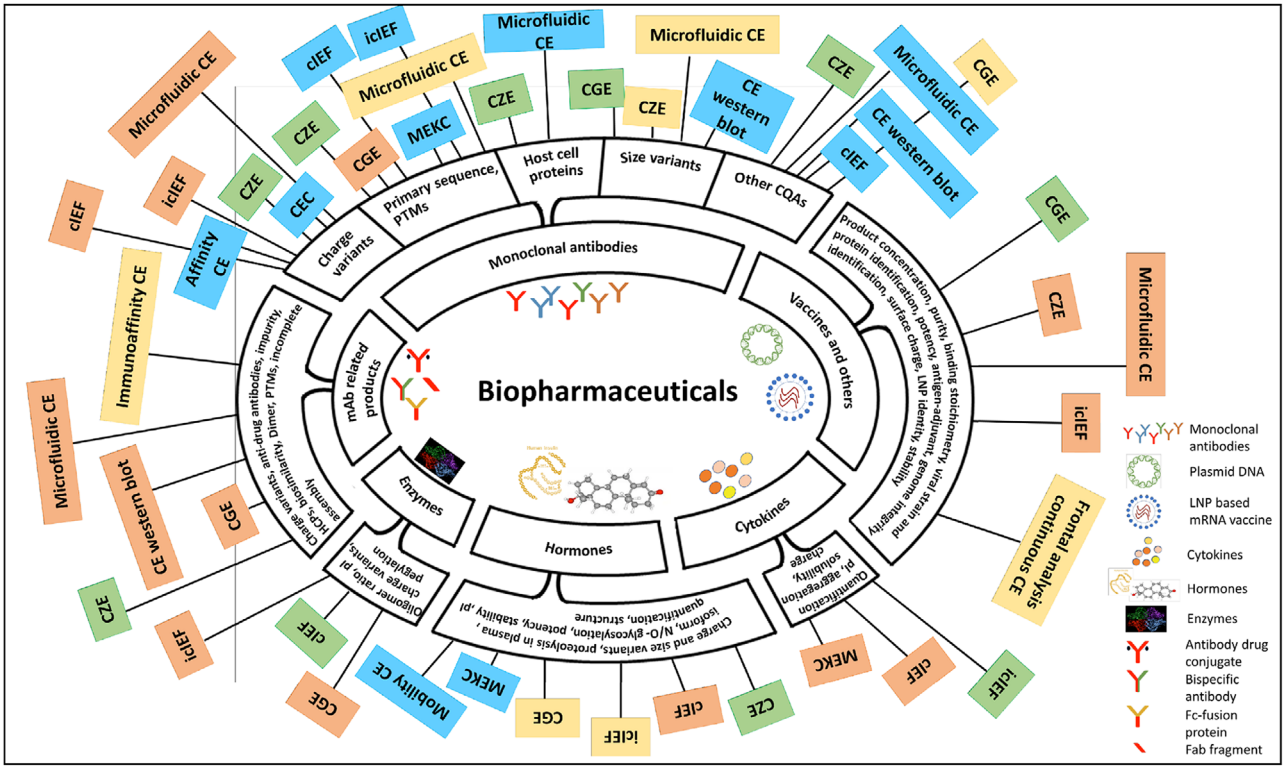

Figure 2. Schematic diagram representing capillary electrophoresis applications in characterizing critical quality attributes of biopharmaceuticals. The inner circle describes the types of biopharmaceuticals, while the outer circle depicts their critical quality attributes. The common CQAs and the respective CE modes used to characterize them and described in the article are illustrated. Different CE modes are highlighted in green, orange, yellow, and blue in the order of their usage for analyzing a given CQA, with green suggesting the maximally used methods.

between 7.4 and 9.5 was demonstrated with about 1% precision. Based on the results, CZE was proposed to be suitable for use in good manufacturing practice (GMP) environment. In another study, CEC was employed for charge heterogeneity analysis of mAbs [44]. BSA coated open tubular column was used to separate the up to seven charge variants of three mAbs. The method had good repeatability with <3.7% migration time RSD. The column was stable for 25 runs with no change in peak shape and resolution.

Microfluidic CE-based methods have also been reported for charge variant analysis of mAb products [41,45,46] Online ESI-MS was demonstrated for intact mAb charge heterogeneity analysis with major C-terminal lysine variants separated with an average resolution of 0.8 along with the minor acidic and basic species. The study also identified the glycosylation patterns of the 0-lysine, 1-lysine, and 2-lysine variants [45]. In another study, microfluidic CE was coupled with native MS has been used to retain and identify the original conformation of a mAb. The detected proteoforms were present at levels as low as 0.01% using just 1 ng of sample [46]. Besides the intact mAb analysis, CE-MS was helpful for charge variant profiling using the middle-up approach [47–49]. The proteolytic enzyme SpeB was combined with icIEF to analyze the domain-specific charge heterogeneity of the innovator and biosimilar forms of Rituximab [48].

Further characterization of charge variants has been reported using multidimensional approaches [50,51]. For example, a two-dimensional online CZE-CZE-MS platform was created for MS-based characterization of charge variants and deamidation products of a mAb [50]. Interestingly, precise mass data with deviations of less than 1 Da was obtained. In another study, cIEF-CZE-MS was used to separate model proteins and one peptide with pIs ranging from 5.1 to 10.3 in a single run and demonstrated to be applicate for mAbs analysis [51].

2.2 Primary sequence and PTM analysis

The primary structure of a protein refers to its amino acid sequence that is essential for maintaining its structure and function [31]. Primary structure analysis to identify sequence variants is also mentioned in the ICH guidelines [19]. Additional heterogeneity may be introduced in mAbs due to PTMs and biochemical changes, such as deamidation and oxidation [52–54], just to mention the most imported ones. CE is a robust and reproducible tool for primary structure and PTM analysis [55–57]. Peptide mapping of a mAb with identification of a wide variety of peptide lengths (3–65 amino acids), with a 100% sequence coverage was reported with mAb

Table 1. Recent applications of CE toward mAb characterization

Category	Sample(s)	Type(s)	Separation technique(s)	Detection	Specific application(s)	Reference(s)
Charge heterogeneity	Human IgG1	mAb	cIEF	UV	mAb identification testing	[39]
	Trastuzumab, infliximab, bevacizumab, cetuximab	mAb	cIEF, icIEF	MS, UV	Charge variant	[40]
	Trastuzumab biosimilar	mAb	Microchip icIEF	UV, MS	Quantitation of charge isoforms	[41]
	NIST mAb	mAb	cIEF, CZE	UV	*p*I, charge heterogeneity	[42]
	23 different mAbs	mAb	icIEF, CZE	UV	Charge heterogeneity	[43]
	Cetuximab, rituximab, trastuzumab	mAb	Open tubular CEC	UV	Charge variant	[44]
	Infliximab, IgG2, IgG1 ADC	mAb and ADC	Microfluidic CE	MS	Separation of intact mAb charge variants	[45]
	Rituximab, trastuzumab, bevacizumab	mAb	Microfluidic CE	Native MS	Charge variant profiling with limited sample amounts	[46]
	Cetuximab	mAb	CZE	UV, MS (CZE-UV was offline coupled to MS)	Charge variant	[47]
	Rituximab-innovator and biosimilar	mAb	icIEF	UV	Domain specific charge heterogeneities	[48]
	IgG1	mAb	CZE	MS	Charge variants (deamidated forms)	[49]
	Trastuzumab	mAb	CZE-CZE	UV, MS	Charge variants	[50]
	mAb X	mAb	cIEF-CZE	UV, MS	Charge variant	[51]
	Adalimumab, natalizumab, nivolumab, palivizumab, infliximab, rituximab and trastuzumab	mAb	CZE	MS	Charge variant	[62]
	Trastuzumab, rituximab and palivizumab	mAb	CZE	MS	Charge variants	[72]
	Unconjugated IgG2, ADC	mAb and ADC	Microfluidic CE	MS	Charge heterogeneity	[73]
	IgG1	mAb	IPG-IEF-icIEF	UV	Purity of fractionated charge variants	[93]
	IgG1, IgG2, ADC	mAb and ADC	Ultra-high voltage CE	UV	Charge variants, ADC separation	[101]
	Infliximab biosimilar	mAb	icIEF	UV	Charge heterogeneity	[178]
	mAbs, ADCs	mAb and ADC	CZE	UV	Charge variant	[179]
	mAb coformulation	mAb mixture	Flow through partial filling affinity capillary electrophoresis, CZE	UV	Antibody specific charge heterogeneity profiling	[180]
	Infliximab	mAb	cIEF	MS	Charge heterogeneity, pI of charge variants	[181]
	IgG1, IgG4	mAb	SEC-icIEF	UV	Quantitative charge variant analysis of individual light and heavy chains	[182]
	Omalizumab	mAb	CZE	UV	Charge variant	[183]
	mAbs	mAb	icIEF	UV	Charge variant, degradation rate	[184]
	NIST mAb	mAb	CZE	UV	Charge heterogeneity	[185]
	anti-tumor necrosis factorα	mAb	CZE	UV	Charge heterogeneity	[186]

(*Continued*)

Table 1. Continued

Category	Sample(s)	Type(s)	Separation technique(s)	Detection	Specific application(s)	Reference(s)
	Adalimumab, belimumab, atezolizumab, cetuximab, bevacizumab, denosumab, elotuzumab, ipilimumab, ixekizumab, nivolumab, obinituzumab, ofatumumab, palivizumab, pertuzumab, ramucirumab, rituximab and trastuzumab, mAb mixtures	mAb	CZE	UV	Charge variants	[187]
	Cetuximab	mAb	Microfluidic CE	MS	Charge variants	[188]
	Trastuzumab	mAb	icIEF, icIEF-CZE	UV, MS	Charge variant	[189]
	Cetuximab	mAb	cIEF, icIEF	MS, UV	Charge variant	[190]
	Commercial mAb	mAb	CZE	UV	Charge variant and deamidated forms	[191]
	Infliximab, adalimumab, NIST mAb	mAb	cIEF	MS	Charge variant, structural heterogeneity	[192]
	Cetuximab	mAb	CZE	UV, MS	Fc/2 variants and dimers	[193]
	IgG3	mAb	Microchip CE	Fluorescence	Charge variants	[194]
	Trastuzumab	mAb	icIEF	UV	Charge variant	[195]
	IgG1	mAb	Microfluidic CE	MS	Charge variants	[196]
	Bevacizumab	mAb	icIEF	UV	Charge variants	[197]
Primary structure and PTMs	IgG1	mAb	CZE	MS	PTM	[49]
	Adalimumab, natalizumab, nivolumab, palivizumab, infliximab, rituximab and trastuzumab	mAb	CZE	MS	PTM	[62]
	Trastuzumab	mAb	CE	MS	Primary sequence, PTM	[58]
	Infliximab, anti-CD-176	mAb	CE	MS	de novo sequencing	[59]
	IgG1, ADC	mAb, ADC	CZE	MS	Peptide mapping	[61]
	IgG1	mAb	RPLC-CZE	MS	Peptide mapping	[63]
	IgG1, bispecific single chain protein	mAbs, bispecific protein	Microfluidic CZE	MS	Sequence coverage and CQA identification	[198]
	Infliximab	mAb	cIEF	MS	PTMs on charge variants	[181]
	IgG1	mAb	CE	MS	Domain specific modification	[199]
	Trastuzumab biosimilar	mAb	Microchip icIEF	UV, MS	Glycan analysis of separated charge isoforms	[41]
	Infliximab, IgG2, IgG1 ADC	mAb and ADC	Microfluidic CE	MS	Glycoform analysis of charge variants	[45]
	Rituximab, trastuzumab and bevacizumab	mAb	Microfluidic CE	MS	Glycosylation analysis of charge variant	[46]
	Cetuximab	mAb	CZE	UV, MS (CZE-UV offline coupled to MS)	Separation of Fc/2 and F(ab')2 glycoforms	[47]
	IgG1	mAb	CZE	MS	Glycosylation	[49]
	Trastuzumab	mAb	CZE-CZE	UV, MS	Glycosylation variants	[50]

(*Continued*)

BACK TO CONTENTS

Table 1. Continued

Category	Sample(s)	Type(s)	Separation technique(s)	Detection	Specific application(s)	Reference(s)
	Adalimumab, natalizumab, nivolumab, palivizumab, infliximab, rituximab and trastuzumab	mAb	CZE	MS	Glycoform	[62]
	Rituximab, palivizumab, natalizumab, nivolumab, trastuzumab, panitumumab, adalimumab, infliximab, two infliximab biosimilars	mAb	CZE	MS	Relative quantification of glycans at glycopeptide level	[68]
	NIST mAb	mAb	CE	LIF, MS	Glycan analysis	[70]
	Adalimumab	mAb	CGE	LIF	Quantitative assessment of a specific glycan	[71]
	Trastuzumab, rituximab and palivizumab	mAb	CZE	MS	Glycoform analysis of charge variants	[72]
	Unconjugated IgG2, ADC	mAb and ADC	Microfluidic CE	MS	Glycoforms of charge variants	[73]
	Human IgG1, etanercept	Antibody, fusion protein	CE	LIF	N-glycan sequencing	[74]
	IgG	mAb	CE	LedIF	Under- or overloaded glycans	[75]
	Human IgG1	Commercial IgG	CE	LedIF	Glycan analysis	[76]
	Human IgG1	Commercial IgG	CE	Imaging LIF	Glycans	[77]
	Human IgG	Commercial IgG	CE	LIF	Virtual ladder for glycans	[78]
	Human IgG	Commercial IgG	CE	LIF	Calculate glucose unit for a given peak in the electropherogram, structure assignment to the glycan	[79]
	Human IgG	IgG	Capillary nanogel	LIF	Biantennary, bisected N-glycan	[81]
	Human IgG	Commercial IgG	CZE, CGE, MEKC	LIF	Parallel and orthogonal identification of glycans	[82]
	Adalimumab and etanercept	mAb and fusion protein	Multicapillary CGE	Fluorescence	N-glycan	[69]
	mAbs	mAb	CE	Fluorescence	Glycan	[184]
	NIST mAb	mAb	SDS-CGE	UV	Heavy chain glycan occupancy	[185]
	Cetuximab	mAb	cIEF, icIEF	MS, UV	Glycosylation analysis of charge variant	[190]
	IgG3	mAb	Microchip CE	Fluorescence	Glycans	[194]
	IgG1	mAb	CE	MS	Glycoforms of Fc/2	[199]
	Cetuximab	mAb	CE	MS	Site specific glycosylation, glycan distribution in charge variants	[200]
	NIST mAb	mAb	SDS-CGE	UV	Glycan occupancy of heavy chain	[201]

(*Continued*)

Table 1. Continued

Category	Sample(s)	Type(s)	Separation technique(s)	Detection	Specific application(s)	Reference(s)
	Trastuzumab	mAb	CZE	Native MS	Glycoforms	[202]
	Cetuximab	mAb	CZE	UV, MS	Glycofoms on $F_{c/2}$	[203]
	Omalizumab	mAb	SDS-CGE	UV	Separation of glycosylated and non-glycosylated mAb chains	[92]
	mAb and bispecific (bsAb) monoclonal antibody	mAb, BsAb	SDS-CGE	UV, LIF	Intact level, Subunit level, and N-glycan analysis	[97]
	Infliximab	Amino acid, peptides and mAb digest	CZE	MS	Qualitative analysis of amino acids, peptides and tryptic peptides of digested monoclonal antibodies	[204]
	NIST mAb, SigmaMAb	mAb	native cIEF-assisted CZE	MS	Glyco-proteoforms	[205]
HCP	Human mAb spiked with standard proteins	Synthetic HCP sample	CZE	MS	HCP	[86]
	mAb producing CHO cell culture supernatant (with and without mAb depletion)	cell culture supernatant	CZE, SCX-SPE-CZE	MS	HCP	[87]
	mAb producing CHO cell culture supernatant	cell culture supernatant	RPLC-CZE	MS	HCP	[88]
	Cathepsin D	Purified HCP	Microfluidic SDS-CGE	LIF	Identification and purity analysis of a specific HCP	[89]
Size variant	Trastuzumab biosimilar	mAb	Microchip icIEF	UV, MS	Mass isoforms of separated charge variants	[41]
	IgG1	mAb	CZE	MS	mAb dimer, free light chain, Lc dimer, mAb proteoforms	[49]
	IgG1, IgG4P	mAb	Microfluidic SDS-CE	LIF	Fragmentation	[89]
	IgG1	mAb	IPG-IEF-SDS-CGE	UV	Size variant analysis of acidic variant	[93]
	Cell culture harvest	Culture harvest	SDS-CGE	UV	Low molecular weight species quantification	[94]
	IgG1	mAb	SDS-CGE, RPLC-SDS-CGE	UV	Low and high molecular weight species, purity, SDS-CGE peak identification	[95]
	NIST mAb, other mAbs, bispecific mAb	mAb, bispecific mAb	SDS-CGE-CZE	UV, MS	Fragments, impurities, light chain separation for bispecific antibody	[96]
	IgG1, IgG4	mAb	Microfluidic CGE	Fluorescence	Purity, stability	[98]
	Infliximab biosimilar	mAb	SDS-CGE	UV	In-use stability	[178]
	NIST mAb	mAb	SDS-CGE	UV	Monomeric purity, thioether content, stability	[185]
	IgG3	mAb	Microchip CE	Fluorescence	Purity	[194]
	Trastuzumab	mAb	SDS-CGE	UV	Percent intact IgG	[195]

(*Continued*)

BACK TO CONTENTS

Table 1. Continued

Category	Sample(s)	Type(s)	Separation technique(s)	Detection	Specific application(s)	Reference(s)
	IgG1	mAb	CE	MS	intact mass analysis, degradation product	[199]
	IgG4	mAb	SDS-CGE	UV	Fragmentation, fragmentation rate	[206]
	NISTmAb	mAb	SDS-CGE	UV	Size heterogeneity	[201]
	IgG1, ADC	mAb, ADC	SDS-CGE	UV	Antibody fragmentation	[207]
	Roledumab	mAb	CGE-SDS	UV	Covalent and non-covalently bound high molecular weight species	[208]
	IgG1	mAb	SDS-CGE, CE western blot	UV, Chemiluminescence	Identification of mAb fragments	[209]
	Trastuzumab	mAb	CZE	Native MS	Degradation, Aggregation	[202]
	Rituximab	mAb	SDS-CGE	UV	In-use stability	[210]
	Cetuximab	mAb	CZE	UV, MS	Fc/2 homo and heterodimers, lysine truncated Fc/2	[203]
	Trastuzumab, mAb1, mAb2	mAb	SDS-CGE	LIF	Size variants	[211]
	IgG1	mAb	SC_XS-CGE	UV	aggregates, purity, stability testing	[212]
	mAb-1 and mAb-2	mAb	SHS-CGE	UV	Purity, aggregates, stability	[213]
	26 mAbs and 2 ADCs, NIST mAb	mAbs and ADCs	SDS-CGE	UV	Quantification of size variants	[214]
Other attributes	Rituximab	mAb	CGE	UV	Confirm cleavage after SpeB treatment	[48]
	CHO cell extract	Cell extract	CE	UV	Nucleotide and Nucleotide Sugar Analysis	[99]
	Cell culture harvest, purified drug substance	Culture harvest, purified drug	CE western blot	chemiluminescence	Product titer, isoform distribution	[100]
	IgG2	mAb	Ultra-high voltage CE	UV	Disulfide isomers	[101]
	Infliximab	mAb	CZE	MS (native)	Conformational states (native, unfolder monomer as well as dimer), cause of dimer formation	[102]
	Adalimumab	mAb	cIEF, SDS-CGE	UV	Biosimilarity	[103]
	Trastuzumab	mAb	CZE	Native MS	Molecular mass	[202]
	Spent media	Spent media	Microchip CE	MS	Quantification of media components	[215]
	IgG1, nanobodies	mAb, nanobody	cIEF	UV	characterization of ADA specificity	[216]
	Adalimumab, infliximab, tocilizumab, and belimumab, trastuzumab-emtansine	mAb, ADC	CZE	UV	Electrophoretic fingerprinting	[217]

Abbreviations, SHS, sodium hexadecyl sulfate; SC_XS, sodium sulfate head group, with "C_X" representing various tail lengths

Electrophoresis 2022, *43*, 143–166

digested with a single enzyme [58]. Various PTMs and low abundance glycoforms, with a relative abundance of glycans being as low as 0.29%, were identified successfully using only 100 fmol of the digested sample. In combination with LC-MS, CE-MS was also used to deliver the first proposed sequence of a novel anti-CD-176 antibody [59]. The study demonstrated the relevance of CE-MS in mAb sequencing. The authors claimed that a new mAb could potentially be sequenced using just 200 ng sample by the CE-MS-based approach.

Compared to conventional CZE-MS methods, a mixture of aqueous and organic solvent was proposed, significantly improving resolution with both sheath flow and sheathless CZE-MS interfaces [60]. The proposed methods offered higher sensitivity, excellent signal-to-noise ratio, and baseline resolution of peptides, comparable with RPLC-MS, and even allowing better recovery of small hydrophilic and large hydrophobic peptides. The methods have been reported to be useful for peptide mapping analysis of an ADC and its parent antibody, providing recovery of small, large, and conjugated peptides with 100% sequence coverage [61]. The authors also demonstrated the utility of this method for the quantitative analysis of common PTMs.

The applicability of CE-MS in PTM analysis was demonstrated with seven commercial therapeutic antibodies [62]. The method was used to identify glycoforms and other PTMs, especially low mass PTMs, using intact, middle-up, and bottom-up approaches. An offline coupling of RPLC and CE was reported to improve sequence coverage and PTM identification of a mAb, compared to traditional LC-MS- and CE-MS-based approaches [63]. The tryptic digest of the mAb was fractionated via RPLC in the first dimension. The fractions were pooled and analyzed via CZE-MS in the second dimension. Almost 150 peptide sequences and 280 PTMs were identified with this RPLC-CZE-MS approach, which were otherwise not detected by either LC-MS or CE-MS. The platform gave 99.6% and 98.6% sequence coverages for the mAb heavy and light chains, respectively, which was more than even the combined sequence coverage obtained with LC-MS and CE-MS.

Glycosylation, one of the major PTMs in mAbs, refers to the addition of sugar moieties (glycans) to the molecule [54]. The process of glycosylation is complex and usually results in protein molecules with varying glycosylation patterns in terms of glycosylation sites (macroheterogeneity), and glycan structures (microheterogeneity) [64,65]. Especially the N-glycosylation patterns are considered to be critical for receptor binding and mAb effector functions, and their alterations have been reported to affect the efficacy, *in vivo* half-life, and safety of mAbs [66,67].

The presence of major glycoforms, that is, 2x-glycosylated and 1x-glycosylated isoforms, in seven commercially available mAbs was recently analyzed in less than 12 min using CE-MS of intact and IdeS digested forms [62]. Glycosylation analysis has also been reported via relative quantification of N-glycans at the glycopeptide level [68]. The absolute profile variation of the method for different glycan structures was as low as 4%. Using ten different mAbs produced in different expression systems, the study established a CE-MS method for comprehensive mAb glycoprofiling. Recently, a new glucose unit (GU) database using multi-capillary CGE has been generated and utilized for N-glycosylation structure assignments to a mAb and a fusion protein [69]. Another study coupled fluorescence and MS detectors for simultaneous quantification and identification of N-glycans using an online CE-LIF-MS system and a high reactivity, novel Teal dye [70]. Identification and precise quantification of a specific target glycan have also been reported using a CGE based method [71]. By spiking an increasing amount of mannose-5 oligosaccharide in the N-glycan pool of a mAb, the authors demonstrated the presence and precise quantification of the concentration of a glycan of CQA interest in the investigated mAb sample.

Another area of mAb glycosylation analysis is the glycoform analysis of separated charge variants [45–47,50,72,73]. In one study, 1x, and 2x glycosylated mAb isoforms were identified from each of the charge variants and partially separated in less than 20 minutes using CZE-MS [72]. CE-MS has also been developed to separate $F(ab')_2$ glycoforms [47]. The method involved fractionation of an IdeS digested mAb with CZE-UV and offline MS analysis of the individual fractions, thereby, allowing the detection of both Fc/2 and $(Fab')_2$ variants as well as the glycoforms of each variant. The Fc/2 and the $F(ab')_2$ variants were separated with resolutions up to 2.10 and 1.05, respectively. Seven glycoforms of the Fc/2 fragments, and eight glycoforms of $F(ab')_2$ domain were detected. Quantitative glycoform analysis with intact mAbs has also been reported using microfluidic CE-MS, with results being largely similar to those observed with released glycan analysis [73]. Glycoforms, characteristic of mAbs expressed in Chinese hamster ovary cells, were obtained. Interestingly, the study also identified non-glycosylated mAb forms, information that cannot be obtained with the traditionally used released glycan analysis. By comparing data from glycosylated and non-glycosylated mAbs, precise mass analysis of glycosylation variants was reported using a two-dimensional CZE-CZE-MS system [50].

Method developments in mAb glycosylation analysis using CE were reported using commercial human IgG as the model sample [74–82]. For example, in one study, the hardware components of the CE instrument itself were used to develop semi and fully automated CE-LIF-based methods for carbohydrate sequencing of released glycans [74]. The instrument sample storage compartment was used for performing temperature-sensitive exoglycosidase reactions. The separation capillary, on the other hand, besides being used for resolving the released glycans, was also employed for sequential delivery of exoglycosidases into the reaction mixture for the consecutive digestion steps. CE analysis was performed after each enzyme addition step to enable glycan sequencing. High-resolution carbohydrate sequencing was achieved in 60 min with the semi-automated and in 128 min with the fully automated approach, which otherwise may take up to 4 days with the conventional methods. Besides human IgG, the platform was also useful for sequencing Etanercept, a fusion

protein-based biopharmaceutical. Researchers have recently reported a method for image processing of the fluorescent signal in real-time using LED-induced fluorescence detectors (LedIF) [75]. The system allowed retrospective correction of sample injection for under- and over-loaded labeled glycans. In other words, this novel approach enabled re-analysis of both either too low or highly saturating signals lying outside of the detection range of the system using the same set of data, that is, avoiding the need for reinjection/reanalysis. The approach expanded the dynamic range for CE-based separations and demonstrated the applicability of the method to generate evaluable and quantifiable signals for glycans derived from 0.2 mg/ml of IgG and up to 35 mg/ml maltooligosaccharide ladder samples. The sustainability of CE with LedIF detection for glycan analysis was also shown on a semi-automated home-built CE device with results comparable to a fully automated commercial CE system [76]. Both systems were capable to detect 13 glycans. A universal approach, independent of the ESI interface design, for simultaneous fluorescence-based quantitative and MS-based qualitative assessment of IgG released glycans was recently proposed [77]. With fluorophore labeled sugars, the authors used an imaging laser-induced fluorescence (iLIF) system at the Taylor cone of the electrospray interface to collect fluorescent signal. This allowed simultaneous optical and MS detection for quantitative and qualitative analyses, respectively. The system had high sensitivity and reproducibility with a limit of detection (LOD) of 40 attomole (inter-day peak area relative standard deviation RSD = 6.79%). The same group introduced a "coinjected triple-internal standard method" that generated a virtual ladder for GU calculation-based structural elucidation of glycans [78]. Three sugar standards, maltose, maltotriose, and maltopentadecaose were used to generate a virtual ladder. The method alleviated the need for an additional maltooligosaccharide ladder run for GU value calculations. The approach produced reliable results, independent of separation conditions including capillary length, coating, temperature, injection, and separation methods. With a maximum RSD of 1.07%, the method reduced the time required for glycan structural assignments. The authors also created a free online application called GUcal. The tool automatically calculates the respective GU values for all target analytes in an electropherogram and assigns structures based on a human IgG N-glycan database [79,80]. For rapid and automated identification of bisected N-glycans, a lectin-based capillary nanogel electrophoresis method was proposed [81]. A stationary zone of lectin was incorporated in self-assembled nanogels to identify specific glycans. The method was suitable to identify bisection, galactosylation, and sialylation in N-glycans. With this technique, baseline resolution of >1.5, and precision in migration time of 0.08% RSD could be obtained. The system had 70 and 300 pM detection limits with electrokinetic and hydrodynamic injections, respectively. A multiplexing CE method was recently reported for released glycan analysis from human IgG [82]. The study showed the utilization of CZE, CGE, and MEKC for parallel and orthogonal identification of glycans.

2.3 Host cell proteins analysis

Host cell proteins (HCPs) are other than the desired recombinant product produced by the host cell line during its normal life-cycle, and the accepted level is below 100 ppm in the final biotherapeutic product [83–85]. A higher level of HCPs may lead to unwanted immune responses in patients and may affect the stability and potency of the product. Due to its high resolving power, CE is gaining attention for its potential in HCP analysis and detection. By spiking twelve proteins at different concentrations in a mAb solution, researchers have demonstrated the ability of CZE-MS in detecting impurities present at 100 ppm in the sample [86]. One protein was even detected at ∼10 ppm level. The relevance of CE-MS for HCP analysis from cell culture samples with and without mAb depletion was also demonstrated [87]. CE was able to identify 220 and 185 protein groups with and without mAb depletion, respectively. To improve HCP identification without mAb depletion, the use of a strong cation exchange-solid phase extractor CZE-MS (SCX-SPE) was also reported in the same study. With successive pH stepwise elution from the SCX monolith, the number of protein groups identified increased to 230. Recently, Rathore and co-workers introduced a multidimensional RPLC-CZE-MS-based platform for HCP analysis in the culture supernatants of a mAb producing CHO cell line [88]. The platform identified 225 HCPs that were otherwise unidentified by either LC-MS or CE-MS alone. During cell growth in regular culture media and without serum starvation, the platform was used to identify more than 330 HCPs that may influence cell proliferation and other cellular processes. Fifty-seven proteins with catalytic activity on proteins and 22 peptidases were identified. With the identification of 146 secretory proteins, the study was also proposed to be useful for host cell secretome analysis from actual industrial samples. In another study, the authors used microfluidic SDS-CGE to confirm the identity and purity of a purified HCP [89].

2.4 Size variants

A biotherapeutic may contain multiple species of various sizes, ranging from few nanometers to micrometers. These species may arise due to the presence of protease impurities, incomplete assembly, or physical, chemical, and conformational stress processes that the product may experience during manufacturing, transport, or storage [90,91]. Characterization of size variants such as aggregates, which are considered critical quality attributes (CQA), is crucial as they may impact the potency and immunogenicity of the product. Sodium dodecyl sulfate capillary gel electrophoresis (SDS-CGE) by using borate cross-linked dextran gels is the most commonly used method for integrity, fragmentation, and purity assessments of mAbs [92]. For example, researchers have used reduced and non-reduced SDS-CGE for analyzing fractionated mAb acidic variants to identify their fragment composition [93]. Non-reduced SDS-CGE was also reported to

quantitate low molecular weight species in mAb producing cell harvest samples [94]. Microfluidic SDS-CGE was used as an orthogonal method to high-performance size exclusion chromatography (HP-SEC) for mAb fragmentation analysis and revealed more accurate molecular weight estimation than HP-SEC [89]. It should be noted, however, that for glycosylated species the estimated molecular weight can significantly differ than that of the actual one due to the bulky non-SDS binding glycan moiety [92].

Recently, an approach of identifying SDS-CGE determined size variants using RPLC-MS was reported [95]. The method allowed the identification of high and low molecular weight species observed with SDS-CGE. In combination with RPLC-MS, the method identified 58 unique product-related fragments, ranging from 10 to 130 kDa. By coupling RPLC with top-down MS analysis, identification of some unexpected PTMs, such as intact LC disulfide-linked with glutathione and half IgG containing thioether, present in these fragments and the precise clipping sites was also possible. In another study, an online two-dimensional SDS-CGE/CZE-MS system was reported where CZE-MS was used to analyze the peak of interest from the first-dimensional SDS-CGE separation [96]. The system was capable to resolve single SDS-CGE peaks into multiple proteoforms in the second dimension. The limit of detection of the system was estimated to be between 3 and 8 μg/ml, which would allow the characterization of similar mass impurities present at even as low as the 1% level. SDS-CGE was also suitable for separating the different light chains of a bispecific antibody [97].

Microfluidic CGE has also been developed for size heterogeneity analysis of mAbs. Critical parameters were optimized by the design of experiment (DoE) studies for purity and stability analysis of IgG1 type mAbs [98]. The optimized method was used with twelve other mAbs, including an IgG4 subtype. The platform was validated according to ICH Q2 (R1) guidelines and proposed to be useful for research and development for current GMP level applications.

2.5 Other critical quality attributes

Besides the aforementioned factors, heterogeneity may also be introduced in mAbs via various other sources that may directly or indirectly impact mAb quality. For instance, nucleotides and nucleotide sugars are known to directly affect mAb glycosylation. Estimation of their levels is thus essential to develop optimal cell culture processes. Researchers have developed a high-resolution CE-UV-based method for the separation and quantification of nucleotides and nucleotide sugars in CHO cell extracts [99]. The dynamic coating was used to obtain high reproducibility with RSD in migration time of 0.3%, and a limit of quantification (LOQ) of approximately 3 μM. Two other important factors to be looked at in cell culture harvests are the product titer and isoform distribution. Recently, researchers have reported a capillary western blot method for this purpose [100]. The process was fully automated and allowed high throughput analysis of these CQAs. Others developed an ultra-high voltage CE system capable of applying a potential of at least 120 kV resulting in electric field strengths of more than 2000 V/cm [101]. Besides using the system for monitoring charge variants of mAbs, the authors also used it for resolving mAb disulfide isomers, and an antibody-drug conjugate. Separation of disulfide isomers is challenging as having identical mass to charge ratios. Therefore, capillary electrophoresis that is rather based on charge to hydrodynamic volume, that is, shape-based separation, is a good choice. The system effectively detected additional 2–3 species otherwise not detected with conventional CE conditions.

In another report, CZE was coupled with native MS to identify the different conformational isomers of a mAb [102]. Interestingly, the conformational heterogeneity was preserved using non-denaturing conditions. Simultaneous detection of native and unfolded monomers as well as dimers were achieved in a single analysis, and the results were confirmed with atomic force microscopy (AFM). The same study also used a CZE-MS-based middle-up approach for stressed samples and identified Fab-Fab interactions as the major reason for dimer formation. Using cIEF and SDS-CGE for assaying different quality attributes, such as isoelectric points and size variants respectively, the technique was also used for biosimilarity assessments [103].

3 Analysis of new modality protein therapeutics

Apart from full-length canonical mAbs, new modalities of protein therapeutics include mAb-based products such as antibody-drug conjugates (ADCs), Fab fragments, fusion proteins, and nanobodies. CE has also been reported in the characterization of these products and a summary of some of these studies is given in Table 2. For example, sheathless CZE-ESI-MS has been useful for analyzing antibody-drug conjugates and the data generated showed the platform as a relevant alternative for comprehensive multilevel characterization [104]. The methodology involved intact, middle-up, and bottom-up approaches for mass measurements, primary structure characterization, average drug antibody ratio (DAR), drug loaded peptides, and analysis of light chain, Fc/2, and F(ab')2 subunits. Protocols for using CE for purity, charge heterogeneity, and primary structure analysis of ADCs have also been recently published [105,106]. CE and CE-MS has also been useful for intact and subunit-specific analysis of bispecific antibodies (BsAbs) [97,107]. The first report for the use of sheathless CE-MS for their characterization established the utility of CE in analyzing dimers, incomplete assemblies, and PTMs in this class of products [107]. Subunit-specific analysis of SpeB and IdeS digested BsAbs led to the identification of six different subunits (Lc1, Lc2, Fd'1, Fd'2, (Fc/2)1, and (Fc/2)2) with mass measurements at isotopic resolution. Proteoforms with modifications such as pyroglutamic acid and glycation were also determined. For Fab fragments,

Table 2. Recent applications of CE toward characterization of other biopharmaceuticals

Sample(s)	Type	Separation technique(s)	Detection	Specific application(s)	Reference(s)
ADC	ADC	Microfluidic CE	MS	Charge variants, drug load variants, conformational isoforms	[73]
Brentuximab vedotin	ADC	CZE	MS	Mass measurement, primary structure characterization, average drug antibody ratio, and analysis of light chain, Fc/2, and F(ab')2 subunits	[104]
Bispecific antibodies	Bispecific antibody	CE	MS	Dimer, incomplete assembly, PTM	[107]
Ranibizumab and its intended copy product	Fab fragment	SDS-CGE, CZE	Fluorescence (SDS-CGE), UV (CZE)	Biosimilarity	[108]
Fibroblast growth factor 21	Fc-fusion protein	Immunoaffinity capture-CE	MS	Fusion protein Stability and pharmacokinetics profiling	[109]
Purification process intermediates, fusion-fc protein	Process intermediates, fusion-fc protein	Capillary western blot	Chemiluminescence	Monitor purification process, impurity detection, HCP	[110]
Recombinant fusion protein X	Fusion protein	SDS-CGE	UV	Purity	[218]
Nanobodies	Nanobody	Capillary western	Chemiluminescence	Anti-drug antibodies, identification of immunogenic module	[111]
IFNβ-1b	Cytokine	MEKC	UV	Drug quantification	[112]
Recombinant human interferon-β	Cytokine	cIEF	UV	Quantitation of pI difference	[113]
Bone morphogenetic protein 2	Cytokine	icIEF	Fluorescence, UV	Aggregation/solubility, charge heterogeneity	[114]
Human insulin and its analog lispro	Hormone	CZE, CGE	UV (CZE, CGE), MS (CZE)	Charge and size variants	[115]
B-type natriuretic peptide	Hormone	CE	MS	Proteolysis in plasma	[116]
Human chorionic gonadotropin	Hormone	CGE, cIEF, CZE	UV (CGE, cIEF, CZE), MS (CZE)	Isoform, pI, differentiate drugs, glycan	[117]
Recombinant human parathyroid hormone (1-34)	Hormone	CZE	UV	Potency, stability	[118]
Insulin and its analogues	Hormone	MEKC	UV	Quantification, stability, excipients	[120]
Insulin	Hormone	CZE	UV, MS	Deamidation isoforms, degradation rate	[121]
Insulin	Hormone	Mobility CE	UV, MS	Hydrodynamic radius, structure prediction	[122]
Recombinant human erythropoietin	Hormone	CZE	UV	Isoforms	[123]
	Hormone	CZE	UV	Quantification of amino acids used as excipients	[124]
	Hormone	icIEF	UV	Charge variants, pI and quantification of isoforms	[125]
	Hormone	cIEF	UV	Isoforms, pI	[126]
	Hormone	CZE	UV	Isoform separation and quantification	[127]
	Hormone	CE	MS	N, O-glycopeptides	[119]
β-Glucuronidase	Enzyme	SDS-CGE, cIEF	UV	Monomer/dimer ratio, charge variants, pI	[128]
Erwinia chrysanthemi L-asparaginase	Enzyme	icIEF	UV	Extent of PEGylation	[219]
Cell free bioreactor broth harvest	Broth harvest	SDS-CGE	UV	Product concentration	[128]
Plasmid DNA	Plasmid DNA (cell, gene therapy)	CGE	LIF	Purity, degradation	[129]

(*Continued*)

Table 2. Continued

Sample(s)	Type	Separation technique(s)	Detection	Specific application(s)	Reference(s)
VP2 subviral particle, mAb production against VP2, vaccine-mAb complex	VP2 as subunit vaccine candidate	CZE	UV	Quantification, binding stoichiometry	[130]
Influenza vaccine (inactivated virus, virosome, upstream process sample)	Vaccine	CGE	UV	Identification and quantitation of viral proteins, identify viral strain	[131]
Western, Eastern, and Venezuelan equine encephalitis virus like particles (VLPs)	VLP based vaccine	Microchip SDS-CGE	Fluorescence	Purity, component protein size, component ratios	[132]
Influenza G1 mini-haemagglutinin protein vaccine (mini-HA) and inactivated polio vaccine (IPV)	Viral vaccine	SDS-CGE	UV	Purity, strain identification	[133]
Aprotinin	Polypeptide	CZE	UV	Potency (separation and detection of substrate and product)	[220]
AAV	Viral vector	SDS-CGE	UV, LIF	Full and empty ratio	[134]
AAV	Viral vector	SDS-CGE	UV	Capsid protein distribution	[135]
AAV	Viral vector	CGE	LIF	Genome integrity	[136]
AAV	Viral proteins	Microfluidic CE	MS	Serotype identification	[221]
AAV	Viral protein	SDS-CGE	LIF	Purity, quantification of viral protein	[222]
LNP based mRNA vaccine	mRNA vaccine	icIEF	UV	Surface charge, LNP identity, stability	[139]
Botulinum neurotoxin type A	Protein toxin	CE	LIF	Light chain activity	[223,224]
PrSA (peptidyl-prolyl *cis-trans* isomerase from *S. aureus*)	Vaccine antigen in development for the treatment of *S. aureus*	Frontal analysis continuous CE	UV	Antigen-adjuvant interaction	[225]

SDS-CGE and CZE methods were developed for analyzing size and charge variants, respectively [108]. Based on these analyses, the study assessed the similarity between the innovator product and its intended biosimilar. Similarly, for Fc fusion proteins, *in vivo* pharmacokinetics and purity assessments have been reported using immunoaffinity capture CE and capillary western-blot-based techniques [109,110]. Capillary western blot is another commercially available technique and was recently introduced for HCP analysis in harvest and purified samples of an Fc-fusion protein [110]. The results obtained with this setup were comparable to traditional western blot but it additionally offered improved throughput, good precision with RSD for molecular weight sizing, and relative quantity measurement of <2% and up to 15%, respectively. Also, it had acceptable linearity ranges for both products (24 μg/ml to 6 mg/ml) and target HCP (250 ng/ml to 1.25 μg/ml) quantitation with r^2 values greater than 0.99. Another application involved the monitoring of anti-drug antibodies (ADAs) against three experimental nanobodies with different modules [111]. The platform allowed rapid immunogenicity testing for up to 24 pure experimental nanobody preparations and was found to be suitable for detecting ADAs against cytokine fusions and recombinant growth factors as well.

Other modes of CE have also been useful for the characterization of cytokines and hormones. For example, MEKC has been reported for the quantification of interferon β-1b [112] with the LOQ of 20 μg/mL. Using the developed method, the potency of interferon beta-1b (IFN β-1b) was determined in 34 parenteral preparations from four brands. The method was proposed as a simple, rapid, and economical alternative to LC-based approaches. Additional methods were also developed for analyzing the charge heterogeneity and aggregation/solubility of cytokines [113,114].

Another study presented two CE methods for analyzing charge and mass variants of insulin and its analog, lispro [115]. A CZE based method for separation of deamidation products, and a CGE method for molecular weight transformation products were developed. Other hormones such as human chorionic gonadotropin, parathyroid hormone, and recombinant human erythropoietin were also characterized for their quality attributes like pI, isoforms, stability, plasma proteolysis, and potency using CE-based methods [115–127].

Enzymes, polypeptides, nucleic acids, vaccines, and viruses represent some other categories of biotherapeutics where CE has been applied for monitoring quality attributes. For example, SDS-CGE and cIEF were reported for investigating the monomer-dimer ratio, *p*I, charge variants of purified β-Glucuronidase, a therapeutic enzyme used for treating lysosomal storage diseases [128]. Analysis of β-Glucuronidase concentration in bioreactor harvest samples using SDS-CGE was also demonstrated in the same study.

Another category of biotherapeutics is nucleic acid-based drugs, which are used in vaccination, as well as in cell and gene therapies. For plasmid DNA, CGE-LIF was used for purity and degradation analysis [129] The method was fully automated and utilized to study plasmid topology and degradation under accelerated stability conditions as well.

Multiple reports have been published for vaccine products characterization [130–133]. For example, one study reported CZE-UV for quantification of a subunit vaccine [130]. Besides monitoring the purity and integrity of the viral particles, the method was also used to study its interaction and stoichiometry with the corresponding mAb. Other CE modes such as CGE, and SDS-CGE were reported for identification, quantification, and purity analysis of vaccine products [130–133].

Adeno-associated virus (AAV) is a frequently used gene therapy delivery vehicle with long-term transgene expression and good disease correction ability. Similar to other biotherapeutics, during production, several critical quality attributes should be monitored including full and empty ratio, capsid protein distribution, and transgene integrity. Partially filled or empty capsids decrease the efficacy and safety of the product. To address this issue, the full and empty ratio can be readily checked by capillary isoelectric focusing [134]. SDS-CGE is an excellent tool to assess the capsid protein distribution [135]. Capillary gel electrophoresis at the DNA level is a good approach for analyzing the genome integrity of AAV vectors, another important CQA for release testing [136]

Lipid nanoparticles (LNPs) are another important class of delivery vehicles for therapeutics and vaccines, especially during the current Covid 19 pandemic. However, due to their complexity, they are difficult to characterize [137,138]. An icIEF method was reported for measuring surface charge (pI) of a LNP based mRNA vaccine [139]. The method was specific to the cationic lipid composition of the LNP and was suitable for LNP identification and stability assessments.

4 Recent advances in commercial instrumentation for the characterization of biopharmaceuticals

In parallel to the enormous developments in CE methods and applications in academia for better, fast, and efficient characterization of biopharmaceuticals, instrument vendors have similarly attempted to simplify the worklist for CE scientists. In this regard, various new CE instruments have been launched in the market for high throughput, fast, or automated analysis of biotherapeutics in the past few years. A multicapillary electrophoresis system (C100HT) was recently developed by Sciex for high throughput analysis of complex carbohydrates, derived from glycoprotein biophamaceuticals (https,//www.sciex.com). Protein simple introduced the Maurice® system in 2016, a small instrument for rapid and automated cIEF and CE-SDS analysis (https,//www.proteinsimple.com/maurice.html). The system also offers high resolution and reproducibility for purity, identity, and heterogeneity analysis. Simple Western™ from the same company offers automated capillary western blotting option for up to 96 samples in a single run (https,//www.proteinsimple.com/simple_western_overview.html). Recently, CEInfinite established a new milestone in CE industry with the development of a preparative icIEF instrument, allowing simultaneous isolation and characterization of individual charge variants [140]. Additionally, the system can be coupled to a mass spectrometer for easy in-depth structural analysis of each variant [141]. To overcome the issues related to CE-MS coupling, 908 devices developed ZipChip® approach in which the chip inserts into the MS and automatically positions the optimal electrospray allowing the analysis of protein products at intact, reduced, and peptide levels. The commercial microfluidic CE-MS system also enables the analysis of amino acids and small molecules (https://908devices.com/products/zipchip/). BiOptic has also expanded its portfolio of single and multicapillary electrophoresis products for bioanalysis (https://www.bioptic.com.tw/).

5 Non-biotherapeutics based CE advancements

Despite the usual benefits of CE over other separation techniques, it has some limitations such as in loading capacity, low identification rates, and low detection sensitivity. Several advancements have been introduced using non-biotherapeutics in the last five years to overcome these limitations, which hold great potential to be applicable in the biopharmaceutical applications. For simplicity, these advancements may be categorized as methodological and technical as discussed below, and also summarized in Tables 3 and 4, respectively.

5.1 Methodological advancements

Methodological advancements include CE-based techniques that can be directly applied in the biopharmaceutical industry with existing instruments and accessories. For example, one of the significant limitations of CE is its limited sample loading capacity. At least two different new approaches have been introduced recently in this regard. First, methods were developed allowing analysis with minimum sample requirement, for example, N-glycan analysis from only 100 cells and nanoRPLC-CZE-MS/MS system for proteomics analysis

Table 3. Method advancements in CE

Category	Advancement(s)	Method(s)	Samples/Target analytes	Technique(s)	Reference(s)
Analysis with limited sample consumption	N-glycan analysis using only 100 cells	Combination of large-volume sample stacking and transient isotachophoresis for online sample preconcentration	Glucose ladder, N-glycans from human cell lines (HeLa, MCF7, HepG2)	CE-LIF	[142]
	Proteomics with sample consumption corresponding to about 1000 cells	Short capillary, high loading capacity, BSA treated sample vials, no lyophilization and redissolution of RPLC eluates, single-spot solid phase sample preparation (SP3) method, first report on CZE-MS based proteomics with small number of human cells	HEK293T cells	Nano-RPLC-CZE-MS	[143]
	Multidimensional analysis with only 5μg proteome digest	Micro RPLC based prefractionation, dynamic pH junction to boost capillary loading volume	MCF7 cell proteome digest	Micro RPLC-CZE-MS	[226]
Separation window, loading capacity, peak capacity, large scale proteomics	Loading capacity of 1 μl, separation window of 90 minutes, peak capacity of 280	Dynamic pH junction	*Escherichia coli* proteome (intact proteins)	CZE-MS	[144]
	Separation window of 180 min, sample loading, 2μl, proteoforms identification using 25ng sample as well	1.5m long capillary, high sample loading	Standard protein mixture, *Escherichia coli*, zebrafish brain (cerebellum and optic tectum regions)	CZE-MS	[145]
	Loading capacity of microlitre scale, separation window of over 2 hrs, peak capacity of approx. 380	Dynamic pH junction sample stacking	Standard protein digest, mouse liver digest, mouse brain digest	CZE-MS, RPLC-CZE-MS	[146]
	Largest dataset for bacterial top-down proteomics, peak capacity (∼4000), loading capacity of 500 nL	High sample loading, high peak capacity with multidimensional set up	*Escherichia coli* lysate (intact proteins)	SEC-RPLC-CZE-MS	[147]
Peptide identification rate	Doubling of identification rate	Multisegment injections	Yeast proteome digest	CZE-MS	[148]
	Better peptide identification rate	Sequential sample injection	Protein digest from Human lymphoblastic T cell line	RPLC-CE-MS	[149]

(*Continued*)

BACK TO CONTENTS

Table 3. Continued

Category	Advancement(s)	Method(s)	Samples/Target analytes	Technique(s)	Reference(s)
Glycosylation analysis	Single CE method for analysis of glycopeptides, released glycans, and monosaccharides	Aminoxy TMT labeling, linkage specific derivatization	Glycoprotein standard, monosaccharide standard	Microfluidics based CE-MS	[150]
	~35% and 70% more N-glycopeptide identification than UHPLC-MS and CZE-MS, respectively	Multidimensional set up	Alpha-1-acid glycoprotein	HILIC-UHPLC-CZE-MS	[151]
	Lectin based glycoprotein enrichment protocol	Combination of microchip CGE with magnetic beads-based lectin affinity enrichment of glycoproteins	Model glycoproteins, human serum, fungal glycoproteins	Microchip CGE	[227]
in vitro stability, *in vivo* pharmacokinetics	Simple assay without the need for enrichment or specific mAb	Capillary western	Recombinant therapeutic protein under development	Capillary western blot (Chemilumines-cence)	[152]
Protein-protein interactions	Analysis without the need to maintain non-covalent interaction during electrophoresis	Protein cross linking CE	Lysozyme-antibody, Hsp70-Bag3, Hsp70-Bag3- inhibitors	CE-LIF	[153]
Complex stability, antibody peptide interactions	In-flow assay for detection, and stability analysis of antigen-antibody interactions	Sequential injection of antibody and peptide	Monoclonal anti-FLAG M2 antibody and 5,6-carboxyfluorescein-labeled FLAG tag	CE-fluorescence	[228]
Conformation	Assignment of protein isoforms that differ by 1 Da only	Sheath liquid CE-ESI-SQ MS and CE- ESI-TOF MS Sheathless CE-nanoESI-Q-TOF MS	$Beta_2$-microglobulin	CE-MS	[229]
CZE coupling with MS	First study that coupled CZE with ETD and AI-ETD, more than double protein sequence coverage, higher quality tandem mass spectra, identification of more proteins	Coupling of CZE with ETD, AI-ETD	Standard protein mixture, secretome of *Mycobacterium marinum*	CZE-MS	[230]

Abbreviations. AI-ETD, activated ion electron transfer dissociation; ETD, electron transfer dissociation; SQ, single quadrupole; Q-TOF, quadrupole time of flight.

BACK TO CONTENTS

Table 4. Technological advancements in CE

Challenge	Solution	Samples/Target analytes	Reference(s)
Difficult interfacing with MS	Low sheath flow interface	Drugs, neural cells	[156,157]
	Gold foil covered capillary tip as ESI electrode	Alkaloids, trypsin digest of cytochrome C, organic anions	[158]
	Microfabricated liquid junction hybrid ESI interface	Proteins, peptides, oligosaccharides	[160]
	For cIEF-MS, Sequential injection with ampholytes in narrow pH range	Standard protein mixture	[231]
Similar CE and ESI flow rate	Induced ESI based sheathless interface	Tripropylamine, atenolol	[159]
Non compatibility of CE with MS	2D CE-MS with a mechanical valve	BSA tryptic digest	[232]
Carrier ampholytes in cIEF results in reduced UV detection sensitivity and difficult hyphenation with MS	cIEF in porous layer open-tubular capillary column with immobilized pH gradient (PLOT-IPG) column	Protein standards, human serum, amino acids	[163]
Difficult temperature control across capillary effects thermally unstable compounds and detectors.	3D printed cartridge	Monoethyl carbonate	[164]
Detection methods (low sensitivity)	C^4D-MS dual detection	Phenolic compounds	[165]
	C^4D-MS dual detection	Ions, biomolecules, vitamin B food supplement	[166]
	Dual C^4D-ESI based detection	Sugars, biogenic amines, carboxylic acids	[167]
Glycan analysis	Double layer PVA coating	N-glycans from human serum, maltooligosaccharide standards	[162]
Resolution	Multi-snapshot imaging	DNA fragments, ladders	[233]
Diffusion coefficient measurement by cIEF	Fourier analysis with cIEF and imaging plug flow	Standard model proteins	[234]

consuming small peptide amounts roughly corresponding to 1000 cells [142,143]. Second, improvements in loading capacity were recently reported with up to 2 μl injections for bottom-up analysis of complex protein samples [144–146]. The latter group also improved the peak capacity of CE using an SEC-RPLC-CE-MS approach. Along with high sample loading of about 500 nL, the system featured a high peak capacity of ∼4000, and a large bacterial top-down proteomics dataset with the identification of 5700 proteoforms [147]. Another limitation of CE over LC, is its lower peptide identification rate. In this regard, researchers have introduced a multisegment injection approach to double the peptide identification rate without compromising peak width and separation efficiency [148]. The injections were timed in a way that each was done before the previous sample left the capillary. With such well-timed injections, dead time between runs was significantly reduced, and the peptide identification rate was significantly enhanced. The authors demonstrated their method with a bottom-up proteomic analysis of the yeast proteome. Another study employed sequential injection of RPLC based pre-fractionated peptides to improve peptide identification rate in CE-MS [149].

One recent study reported a single CE method for analyzing glycopeptides, monosaccharides, and released glycans of glycoprotein standards using a commercial microfluidic CE-ESI system [150]. Since glycosylation is characterized at different levels, this single CE method dramatically simplified the task. In another study, hydrophilic interaction liquid chromatography (HILIC) and ultra-high-performance liquid chromatography (UHPLC) were coupled to CZE-MS for selective enrichment and analysis of glycopeptides [151]. The method detected a total of 268 site-specific N-glycopeptides from eight glycosylation sites from two isomers of the glycoprotein. The number of N-glycopeptides identified were approximately 35%, and 70% more than those obtained with conventional UHPLC-MS and CE-MS analyses, respectively.

A capillary western blot-based immunoassay was developed for *in vitro* stability and *in vivo* pharmacokinetics of a recombinant protein in development for therapeutic use [152]. The method was used to study the profile of a 55 kDa epitope-tagged recombinant protein in mouse plasma. With the ability to test up to a hundred samples per day, the authors presented a fully automated and economical assay for *in vitro* and *in vivo* analysis of biologics to support early development stages. Another interesting development aimed to analyze protein–protein interactions by CE. For example, a protein cross-linking workflow was reported that circumvented the need to maintain noncovalent interactions during separation and promoted method development for quantitative analysis of protein–protein interactions [153].

5.2 Advancements in CE instrumentation

One of the critical aspects of CE-based analysis of biomolecules is its coupling with mass spectrometry

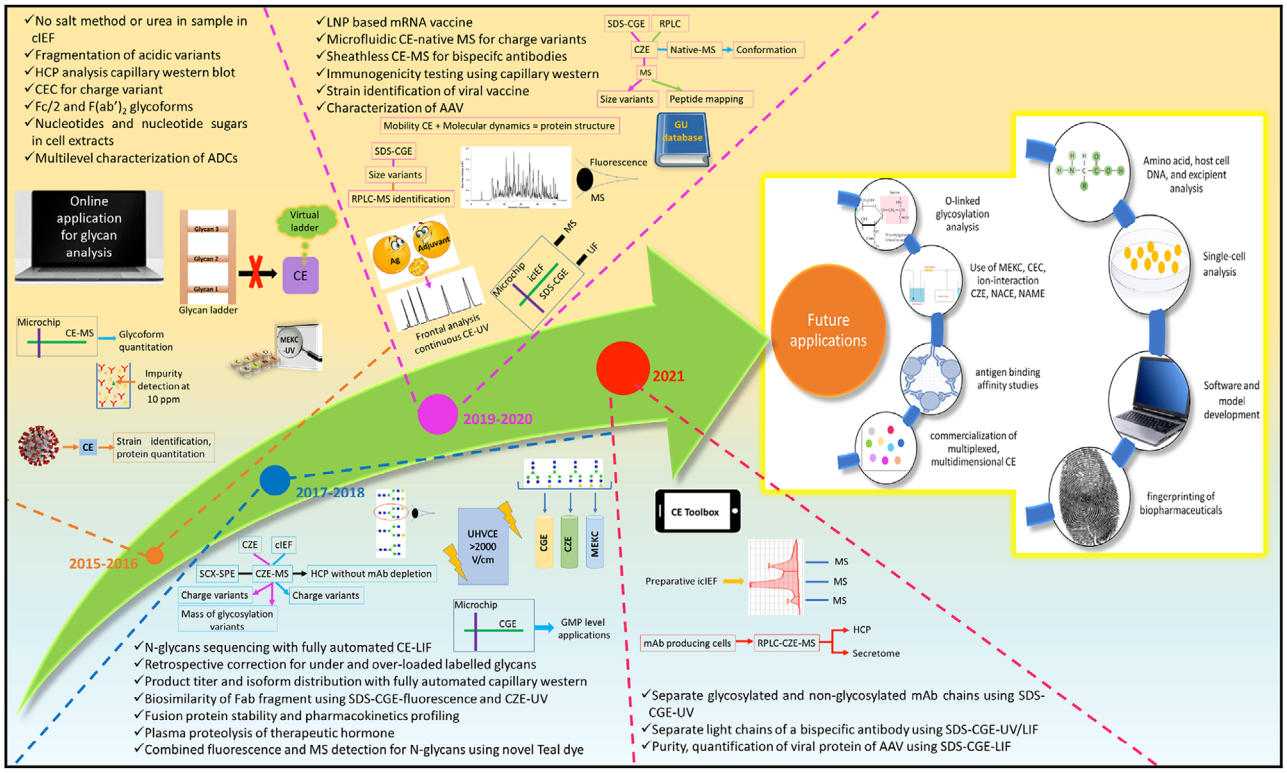

Figure 3. Recent and future advancements of capillary electrophoresis for biopharmaceutical analysis. Some major year-wise advancements in CE since 2015 are summarized. Future perspectives are also illustrated.

[154,155]. Although quite a few commercial interfaces have been introduced in the past, practical difficulties in coupling CE with MS still remains an issue. Several improvements in sheath flow, liquid junction, and sheathless interfaces have been reported offering improved stability and sensitivity [156–160]. Advances in capillary coatings were also reported with demonstrated applications of analyzing protein samples with UV and MS, for example, the use of double-layer polyvinyl alcohol (PVA) coated capillaries for better detection of glycans in a human serum sample [161,162].

cIEF in a partially filled porous layer open-tubular capillary column with immobilized pH gradient, low back pressure, high phase ratio, reduced non-specific adsorption and protein precipitation was demonstrated to separate model proteins from their isomers and impurities [163]. The method was also used to separate five amino acids having *p*Is between 5.05 and 5.98. Leucine and Tryptophan with pIs of 5.98 and 5.89 were adequately separated, while Methionine, Phenylalanine, and Cysteine were baseline resolved. This can be useful for developing multidimensional separation-based platforms for proteome and biomarker-based studies. In another interesting attempt, a 3D printed cartridge allowed the use two C^4D detectors and featured improved heat dissipation [164]. By improving the temperature control, the cartridge enabled better CE-MS interfacing and generated almost five times greater peak area for thermally unstable monoethyl carbonate.

To enhance sensitivity and selectivity, capillary electrophoresis was coupled with two different detectors, namely capacitively coupled contactless conductivity detection (C^4D) and electrospray ionization time-of-flight mass spectrometry (ESI-TOF-MS) [165–167]. Measurements of counter-electroosmotic species in less than 60 s demonstrated the excellent separation efficiency attained. The authors also showed that detector-induced band broadening can be neglected in the CE-C^4D/MS system. Besides providing continuous monitoring of the sample to detect any unexpected species, the use of C^4D detector also allowed to foresee peak shape and position.

6 Future perspectives

Despite the substantial advancements in CE methodologies and instrumentation witnessed in the last few decades, still substantial room remains for future innovation (Fig. 3). (1) One of the important ones on the methodology side is the development of CE-based techniques for the analysis of O-glycopeptides/ O-linked glycans, which latter is mainly dependent on the availability of specific releasing enzymes to avoid chemical reaction mediated peeling. The next generation of mAbs may be IgAs that are alternative or better than currently used IgG-based therapeutics but have additional heterogeneity due to O-linked glycans, thus, they are difficult

to characterize with currently available tools [168,169]. (2) Another one is the use of non-aqueous CE (NACE) for the analysis of biotherapeutics. In a recent example, the stability of an mRNA drug substance was investigated using CGE under non-aqueous conditions [170]. Interestingly, only 1% of published reports on CE have used NACE in biopharmaceuticals since 1994 [23]. Non-aqueous microchip electrophoresis is another emerging tool, which is yet to enter the mAb analysis field [171]. (3) Applications of less commonly used CE modes in the industry include MEKC, capillary electrochromatography (CEC), and the relatively new ion-interaction CZE [172]. (4) Antigen-binding affinity studies using CE as an economical alternative to surface plasmon resonance and ELISA are preferable since CE uses minimal amounts of samples and reagents and has been reported as an appropriate tool to study protein–protein interactions with limited samples, hence may be a good alternative for therapeutic protein-target interaction studies. (5) Commercialization of multicapillary CE for high throughput analysis. Some CE-based separations are still time-consuming, thus, not always amenable for the analysis of a large number of samples. (6) The use of CE for the analysis of other quality attributes of biotherapeutics such as amino acid analysis, host cell DNA, and excipient analysis. (7) CE for single-cell analysis that may be particularly helpful in developing process analytical technologies, or for deciphering the effect of the manufacturing process on the product, such as culture conditions on cellular metabolic heterogeneity using transcriptomics and proteomics [173]. (8) More CE-based multidimensional methods for the analysis of therapeutic proteins including new modalities and commercial LC-CE and CE-CE systems may be introduced in the future. For example, 3D/4D-based analysis such as coupling of 2D LC with CE or protein A-digestion-LC-CE methods for better characterization. (9) Advancement in software and model development for the prediction of migration behavior of proteins and peptides might be useful for better method optimization, similar to existing LC programs such as DryLab. For example, the peptide retention time prediction tools of LC, android application–CE Toolbox–for calculating CE injection parameters, and the Peak Master software for calculating CE system parameters and predicting electropherograms for analytes [174–177]. (10) CE-based fingerprinting of biopharmaceuticals may be developed for the model generation to predict the product quality attributes.

7 Concluding remarks

CE has found numerous applications toward the characterization of biotherapeutics. Analysis of charge, size, and glycosylation heterogeneities of mAbs have been a frequent target of CE applications. Besides mAbs, there are a plethora of CE methods for the analysis of new modality biopharmaceuticals as well. Given the high resolving power, sensitivity, fast separations, and the availability of different separation modes, CE can be used for addressing multiple separation challenges. As mentioned in this review, there is plenty of room for future innovation both in methods and instrumentation. For instance, improved loading capacity may provide greater proteomic coverage in HCP and host cell secretome studies. Better, easy-to-use CE-MS interfaces will improve system stability, sensitivity, resolution, and data quality. The availability of the simultaneous use of multiple detectors would enable the analysis of even trace amounts of heterogeneities and impurities present in the product. Better capillary coatings will reduce sample adsorption onto capillary walls, and the use of NACE may increase resolution in CE in cases not viable with aqueous background electrolytes. Some developments in these directions have already been reported with non-biopharma products. Considering its increased use in the past few years, CE has carved a niche for itself in biopharmaceutical analysis.

This work was funded by the Department of Biotechnology, Ministry of Science and Technology (BT/COE/34/SP15097/2015). This work was also supported by the TKP2020-IKA-07 project financed under the 2020–4.1.1-TKP2020 Thematic Excellence Programme by the National Research, Development and Innovation Fund of Hungary. This is contribution #193 of the Horváth Csaba Memorial Laboratory of Bioseparation Sciences.

The authors have declared no conflict of interest.

Data availability statement

Data sharing not applicable to this article as no datasets were generated or analysed during the current study.

8 References

[1] Hjerten, S., *Chromatogr. Rev.* 1967, *9*, 122–219.

[2] Mikkers, F. E. P., Everaerts, F. M., Verheggen, T. P. E. M., *J. Chromatogr.* 1979, *169*, 11–20.

[3] Jorgenson, J. W., Lukacs, K. D., *Anal. Chem.* 1981, *53*, 1298–1302.

[4] Jorgenson, J. W., Lukacs, K. D., *Clin. Chem.* 1981, *27*, 1551–1553.

[5] Jorgenson, J. W., Lukacs, K. D., *Science* 1983, *222*, 266–272.

[6] Cohen, A. S., Paulus, A., Karger, B. L., *Chromatographia* 1987, *24*, 15–24.

[7] Karger, B. L., *Nature* 1989, *339*, 641–642.

[8] Karger, B. L., Cohen, A. S., Guttman, A., *J. Chromatogr. B: Biomed. Sci. Appl.* 1989, *492*, 585–614.

[9] Gahoual, R., Beck, A., Leize-Wagner, E., François, Y. N., *J. Chromatogr. B: Anal. Technol. Biomed. Life Sci.* 2016, *1032*, 61–78.

[10] Gahoual, R., Giorgetti, J., Beck, A., Giorgetti, E., François, Y. N., *Capill. Electromigr. Sep. Methods* 2018, 453–480.

[11] Lechner, A., Giorgetti, J., Gahoual, R., Beck, A., Leize-wagner, E., François, Y., *J. Chromatogr. B: Anal. Technol. Biomed. Life Sci.* 2019, *1122–1123*, 1–17.

[12] Suntornsuk, L., *J. Chromatogr. Sci.* 2007, *45*, 559–577.

[13] Gummadi, S., Kandula, N., *Int. J. Pharm. Sci. Res.* 2020, *11*, 6038–6056.

[14] Voeten, R. L. C., Ventouri, I. K., Haselberg, R., Somsen, G. W., *Anal. Chem.* 2018, *90*, 1464–1481.

[15] Toraño, J. S., Ramautar, R., Jong, G. De, *J. Chromatogr. B: Anal. Technol. Biomed. Life Sci.* 2019, *1118–1119*, 116–136.

[16] Lill, J. R., *Analytical Characterization of Biotherapeutics*, John Wiley & Sons, 2017, pp. 1–14.

[17] Walsh, G., *Nat. Biotechnol.* 2018, *36*, 1136–1145.

[18] DiPaolo, B., Pennetti, A., Nugent, L. D., Venkat, K., *Pharm. Sci. Technol. Today* 1999, *2*, 70–82.

[19] International Council for Harmonisation of Technical Requirements for Pharmaceuticals for Human Use (ICH), *ICH Harmonised Tripartite Guideline*, ICH, Geneva 1999, pp. 1–16.

[20] European Medicines Agency (EMA), *Guideline on Development, Production, Characterisation and Specification for Monoclonal Antibodies and Related Products*, EMA, Amsterdam 2016.

[21] Rathore, A. S., Chhabra, H., Bhargava, A., *Expert Opin. Biol. Ther.* 2021, *21*, 19–28.

[22] Zhao, S. S., Chen, D. D. Y., *Electrophoresis* 2014, *35*, 96–108.

[23] Tamizi, E., Jouyban, A., *Electrophoresis* 2015, *36*, 831–858.

[24] Creamer, J. S., Oborny, N. J., Lunte, S. M., *Anal. Methods* 2014, *6*, 5427–5449.

[25] Dadouch, M., Ladner, Y., Perrin, C., *Separations* 2021, *8*, 1–30.

[26] Ecker, D. M., Jones, S. D., Levine, H. L., *mAbs* 2015, *7*, 9–14.

[27] Singh, S., Tank, N. K., Dwiwedi, P., Charan, J., Kaur, R., Sidhu, P., Chugh, V. K., *Curr. Clin. Pharmacol.* 2018, *13*, 85–99.

[28] Shepard, H. M., Phillips, G. L., Thanos, C. D., Feldmann, M., *Clin. Med.* 2017, *17*, 220–232.

[29] Mullard, A., *Nat. Rev. Drug Discovery* 2021, *20*, 491–495.

[30] Reason, A. J., Weiskopf, A., Rathore, A. S., *BioPharm Int.* 2014, *27*, 34–43.

[31] Rathore, A. S., Krull, I. S., Joshi, S., *LCGC North Am.* 2018, *36*, 376–384.

[32] Singh, S. K., Narula, G., Rathore, A. S., *Electrophoresis* 2016, *37*, 2338–2346.

[33] Singh, S. K., Kumar, D., Rathore, A. S., *AAPS J.* 2017, *19*, 1826–1841.

[34] Rathore, A. S., *Trends Biotechnol.* 2009, *27*, 546–553.

[35] Rathore, A. S., Winkle, H., *Nat. Biotechnol.* 2009, *27*, 26–34.

[36] Rathore, A. S., Krull, I. S., Joshi, S., *LCGC North Am.* 2018, *36*, 814–822.

[37] Chung, S., Tian, J., Tan, Z., Chen, J., Lee, J., Borys, M., Li, Z. J., *Biotechnol. Bioeng.* 2018, *115*, 1646–1665.

[38] Khawli, L. A., Goswami, S., Hutchinson, R., Kwong, Z. W., Yang, J., Wang, X., Yao, Z., Sreedhara, A., Cano, T., Tesar, D., Nijem, I., Allison, D. E., Wong, P. Y., Kao, Y. H., Quan, C., Joshi, A., Harris, R. J., Motchnik, P., *mAbs* 2010, *2*, 613–624.

[39] Suba, D., Urbányi, Z., Salgó, A., *J. Pharm. Biomed. Anal.* 2015, *114*, 53–61.

[40] Dai, J., Lamp, J., Xia, Q., Zhang, Y., *Anal. Chem.* 2018, *90*, 2246–2254.

[41] Mack, S., Arnold, D., Bogdan, G., Bousse, L., Danan, L., Dolnik, V., Ducusin, M. A., Gwerder, E., Herring, C., Jensen, M., Ji, J., Lacy, S., Richter, C., Walton, I., Gentalen, E., *Electrophoresis* 2019, *40*, 3084–3091.

[42] Turner, A., Schiel, J. E., *Anal. Bioanal. Chem.* 2018, *410*, 2079–2093.

[43] Moritz, B., Schnaible, V., Kiessig, S., Heyne, A., Wild, M., Finkler, C., Christians, S., Mueller, K., Zhang, L., Furuya, K., Hassel, M., Hamm, M., Rustandi, R., He, Y., Solano, O. S., Whitmore, C., Park, S. A., Hansen, D., Santos, M., Lies, M., *J. Chromatogr. B: Anal. Technol. Biomed. Life Sci.* 2015, *983–984*, 101–110.

[44] Zhang, Y., Wang, W., Xiao, X., Jia, L., *J. Chromatogr. A* 2016, *1466*, 180–188.

[45] Redman, E. A., Batz, N. G., Mellors, J. S., Ramsey, J. M., *Anal. Chem.* 2015, *87*, 2264–2272.

[46] Carillo, S., Jakes, C., Bones, J., *J. Pharm. Biomed. Anal.* 2020, *185*, 113218.

[47] Biacchi, M., Gahoual, R., Said, N., Beck, A., Leize-Wagner, E., François, Y. N., *Anal. Chem.* 2015, *87*, 6240–6250.

[48] Zhang, Z., Perrault, R., Zhao, Y., Ding, J., *J. Chromatogr. B: Anal. Technol. Biomed. Life Sci.* 2016, *1020*, 148–157.

[49] Belov, A. M., Zang, L., Sebastiano, R., Santos, M. R., Bush, D. R., Karger, B. L., Ivanov, A. R., *Electrophoresis* 2018, *39*, 2069–2082.

[50] Jooß, K., Hühner, J., Kiessig, S., Moritz, B., Neusüß, C., *Anal. Bioanal. Chem.* 2017, *409*, 6057–6067.

[51] Hühner, J., Jooß, K., Neusüß, C., *Electrophoresis* 2017, *38*, 914–921.

[52] Uversky, V. N., in: Maloy, S., Hughes, K. (Eds.), *Brenner's Encyclopedia of Genetics*, Elsevier Inc., London 2013, pp. 425–430.

[53] Walsh, C. T., Garneau-Tsodikova, S., Gatto, G. J., *Angew. Chem., Int. Ed.* 2005, *44*, 7342–7372.

[54] Li, W., Kerwin, J. L., Schiel, J., Formolo, T., Davis, D., Mahan, A., Benchaar, S. A., in: Schiel, J. E., Davis, D. L., Borisov, O. V (Eds.), State-of-the-Art and Emerging Technologies for Therapeutic Monoclonal Antibody Characterization, Vol. 2: Biopharmaceutical Characterization: The NISTmAb Case Study, American Chemical Society, Washington DC 2015, pp. 119–183.

[55] Wang, W., in: Xia, J. Q., Zhang, L. (Eds.), *Capillary Electrophoresis–Mass Spectrometry: Therapeutic Protein Characterization*, Springer, Cham 2016, pp. 43–51.

[56] Whitmore, C. D., Gennaro, L. A., *Electrophoresis* 2012, *33*, 1550–1556.

[57] Gahoual, R., Leize-Wagner, E., Houzé, P., François, Y. N., *Rapid Commun. Mass Spectrom.* 2019, *33*, 11–19.

[58] Lew, C., Gallegos-Perez, J.-L., Fonslow, B., Lies, M., Guttman, A., *J. Chromatogr. Sci.* 2015, *53*, 443–449.

[59] Cheng, J., Wang, L., Rive, C. M., Holt, R. A., Morin, G. B., Chen, D. D. Y., *J. Proteome Res.* 2020, *19*, 2700–2707.

[60] Dada, O. O., Zhao, Y., Jaya, N., Salas-Solano, O., *Anal. Chem.* 2017, *89*, 11227–11235.

[61] Dada, O. O., Zhao, Y., Jaya, N., Salas-Solano, O., *Anal. Chem.* 2017, *89*, 11236–11242.

[62] Giorgetti, J., Beck, A., Leize-Wagner, E., François, Y. N., *J. Pharm. Biomed. Anal.* 2020, *182*, 113107.

[63] Kumar, R., Shah, R. L., Rathore, A. S., *J. Chromatogr. A* 2020, *1620*, 460954.

[64] Zhang, L., Luo, S., Zhang, B., *mAbs* 2016, *8*, 205–215.

[65] Schjoldager, K. T., Narimatsu, Y., Joshi, H. J., Clausen, H., *Nat. Rev. Mol. Cell Biol.* 2020, *21*, 729–749.

[66] Wang, Z., Zhu, J., Lu, H., *Appl. Microbiol. Biotechnol.* 2020, *104*, 1905–1914.

[67] Reusch, D., Tejada, M. L., *Glycobiology* 2015, *25*, 1325–1334.

[68] Giorgetti, J., D'atri, V., Canonge, J., Lechner, A., Guillarme, D., Colas, O., Wagner-Rousset, E., Beck, A., Leize-Wagner, E., François, Y.-N., *Talanta* 2018, *178*, 530–537.

[69] Filep, C., Borza, B., Jarvas, G., Guttman, A., *J. Pharm. Biomed. Anal.* 2020, *178*, 112892.

[70] Khan, S., Liu, J., Szabo, Z., Kunnummal, B., Han, X., Ouyang, Y., Linhardt, R. J., Xia, Q., *Rapid Commun. Mass Spectrom.* 2018, *32*, 882–888.

[71] Szigeti, M., Chapman, J., Borza, B., Guttman, A., *Electrophoresis* 2018, *39*, 2340–2343.

[72] Giorgetti, J., Lechner, A., Del Nero, E., Beck, A., François, Y. N., Leize-Wagner, E., *Eur. J. Mass Spectrom.* 2019, *25*, 324–332.

[73] Redman, E. A., Mellors, J. S., Starkey, J. A., Ramsey, J. M., *Anal. Chem.* 2016, *88*, 2220–2226.

[74] Szigeti, M., Guttman, A., *Sci. Rep.* 2017, *7*, 11663.

[75] Szarka, M., Guttman, A., *Anal. Chem.* 2017, *89*, 10673–10678.

[76] Szarka, M., *DRC Sustain. Futur. J. Environ. Agric. Energy* 2020, *1*, 60–65.

[77] Szarka, M., Szigeti, M., Guttman, A., *Anal. Chem.* 2019, *91*, 7738–7743.

[78] Jarvas, G., Szigeti, M., Chapman, J., Guttman, A., *Anal. Chem.* 2016, *88*, 11364–11367.

[79] Jarvas, G., Szigeti, M., Guttman, A., *Electrophoresis* 2015, *36*, 3094–3096.

[80] Jarvas, G., Szigeti, M., Guttman, A., *J. Proteomics* 2018, *171*, 107–115.

[81] Lu, G., Holland, L. A., *Anal. Chem.* 2019, *91*, 1375–1383.

[82] Feng, Hua-Tao., Su, M., Rifai, F. N., Li, P., Li, S. F. Y., *Anal. Chim. Acta* 2017, *953*, 79–86.

[83] Wang, X., Hunter, A. K., Mozier, N. M., *Biotechnol. Bioeng.* 2009, *103*, 446–458.

[84] Prakash, K., Chen, W., in: Schiel, J. E., Davis, D. L., Borisov, O. V. (Eds.), *State-of-the-Art and Emerging Technologies for Therapeutic Monoclonal Antibody Characterization, Vol. 2: Biopharmaceutical Characterization: The NISTmAb Case Study*, American Chemical Society, Washington DC 2015, pp. 387–404.

[85] Wang, F., Richardson, D., Shameem, M., *BioPharm Int.* 2015, *28*, 32–38.

[86] Zhu, G., Sun, L., Heidbrink-Thompson, J., Kuntumalla, S., Lin, H., Larkin, C. J., McGivney, J. B., IV, Dovichi, N. J., *Electrophoresis* 2016, *37*, 616–622.

[87] Zhang, Z., Albanetti, T., Linkous, T., Larkin, C. J., Schoner, R., McGivney, J. B., IV, Dovichi, N. J., *Electrophoresis* 2017, *38*, 401–407.

[88] Kumar, R., Shah, R. L., Ahmad, S., Rathore, A. S., *Electrophoresis* 2021, *42*, 735–741.

[89] Cui, T., Chi, B., Heidbrink Thompson, J., Kasali, T., Sellick, C., Turner, R., *J. Biotechnol.* 2019, *305*, 51–60.

[90] Torkashvand, F., Vaziri, B., *Iran. Biomed. J.* 2017, *21*, 131–141.

[91] Joubert, M. K., Luo, Q., Nashed-Samuel, Y., Wypych, J., Narhi, L. O., *J. Biol. Chem.* 2011, *286*, 25118–25133.

[92] Filep, C., Guttman, A., *Anal. Chem.* 2021, *93*, 3535–3541.

[93] Dada, O. O., Jaya, N., Valliere-Douglass, J., Salas-Solano, O., *Electrophoresis* 2015, *36*, 2695–2702.

[94] Yu, D., Mayani, M., Song, Y., Xing, Z., Ghose, S., Li, Z. J., *Biotechnol. Bioeng.* 2019, *116*, 2610–2620.

[95] Wang, W. H., Cheung-Lau, J., Chen, Y., Lewis, M., Tang, Q. M., *mAbs* 2019, *11*, 1233–1244.

[96] Römer, J., Montealegre, C., Schlecht, J., Kiessig, S., Moritz, B., Neusüß, C., *Anal. Bioanal. Chem.* 2019, *411*, 7197–7206.

[97] Filep, C., Szigeti, M., Farsang, R., Haberger, M., Reusch, D., Guttman, A., *Anal. Chim. Acta* 2021, *1166*, 338492.

[98] Smith, M. T., Zhang, S., Adams, T., DiPaolo, B., Dally, J., *Electrophoresis* 2017, *38*, 1353–1365.

[99] Bucsella, B., Fornage, A., Denmat, C. Le, Kálmán, F., *Chimia (Aarau).* 2016, *70*, 732–735.

[100] Xu, D., Marchionni, K., Hu, Y., Zhang, W., Sosic, Z., *J. Pharm. Biomed. Anal.* 2017, *145*, 10–15.

[101] Henley, W. H., He, Y., Mellors, J. S., Batz, N. G., Ramsey, J. M., Jorgenson, J. W., *J. Chromatogr. A* 2017, *1523*, 72–79.

[102] Le-Minh, V., Tran, N. T., Makky, A., Rosilio, V., Taverna, M., Smadja, C., *J. Chromatogr. A* 2019, *1601*, 375–384.

[103] Liu, J., Eris, T., Li, C., Cao, S., Kuhns, S., *BioDrugs* 2016, *30*, 321–338.

[104] Said, N., Gahoual, R., Kuhn, L., Beck, A., François, Y. N., Leize-Wagner, E., *Anal. Chim. Acta* 2016, *918*, 50–59.

[105] Ning, W., Zhao, Y., *Methods Mol. Biol.* 2020, *2078*, 251–262.

[106] Saadé, J., Gahoual, R., Beck, A., Leize-Wagner, E., François, Y.-N., *Methods Mol. Biol.* 2020, *2078*, 263–272.

[107] Gstöttner, C., Nicolardi, S., Haberger, M., Reusch, D., Wuhrer, M., Domínguez-Vega, E., *Anal. Chim. Acta* 2020, *1134*, 18–27.

[108] Griaud, F., Winter, A., Denefeld, B., Lang, M., Hensinger, H., Straube, F., Sackewitz, M., Berg, M., *mAbs* 2017, *9*, 1337–1348.

[109] Han, M., Pearson, J. T., Wang, Y., Winters, D., Soto, M., Rock, D. A., Rock, B. M., *Anal. Biochem.* 2017, *539*, 118–126.

[110] Xu, D., Mane, S., Sosic, Z., *Electrophoresis* 2015, *36*, 363–370.

[111] Wiswell, D., Neupane, D., Chen, M., Bowman, E. P., Linn, D., Sawant, A., Chackerian, A., Zhang, S., Escandón, E., *J. Pharmacol. Toxicol. Methods* 2020, *103*, 106872.

[112] Dadgarnejad, M., Rastegar, H., Ilka, H., Shekarchi, M., Adib, N., Alebouyeh, M., Keypour, N., Shoeibi, S., Kobarfard, F., Fazeli, M. R., *Iran. J. Pharm. Res.* 2015, *14*, 747–755.

[113] Song, K., Moon, D. B., Kim, N. Y., Shin, Y. K., *ACS Omega* 2020, *5*, 6619–6627.

[114] Sundermann, J., Zagst, H., Kuntsche, J., Wätzig, H., Bunjes, H., *Pharmaceutics* 2020, *12*, 1–20.

[115] Pajaziti, B., Petkovska, R., Andrási, M., Nebija, D., *Pharmazie* 2020, *75*, 167–171.

[116] Zhang, S., Raedschelders, K., Santos, M., Van Eyk, J. E., *J. Proteome Res.* 2017, *16*, 4515–4522.

[117] Camperi, J., De Cock, B., Pichon, V., Combes, A., Guibourdenche, J., Fournier, T., Vander Heyden, Y., Mangelings, D., Delaunay, N., *Talanta* 2019, *193*, 77–86.

[118] Maldaner, F. P. S., Perobelli, R. F., Xavier, B., Remuzzi, G. L., Walter, M. E., Dalmora, S. L., *Talanta* 2017, *162*, 567–573.

[119] Mancera-Arteu, M., Giménez, E., Benavente, F., Barbosa, J., Sanz-Nebot, V., *J. Proteome Res.* 2017, *16*, 4166–4176.

[120] Lamalle, C., Servais, A. C., Radermecker, R. P., Crommen, J., Fillet, M., *J. Pharm. Biomed. Anal.* 2015, *111*, 344–350.

[121] Andrasi, M., Pajaziti, B., Sipos, B., Nagy, C., Hamidli, N., Gaspar, A., *J. Chromatogr. A* 2020, *1626*, 4–11.

[122] Zhang, R., Wu, H., He, M., Zhang, W., Xu, W., *J. Phys. Chem. B* 2019, *123*, 2335–2341.

[123] Santos, M. R., *Separation of Recombinant Human Erythropoietin (rhEPO) using the European Pharmacopoeia Method on the PA 800 plus Pharmaceutical Analysis System*, Sciex, Framingham, MA 2016.

[124] de Souza Crespo, I. C., de Resende, M. T., Pereira Netto, A. D., de Carvalho Marques, F. F., *Electrophoresis* 2015, *36*, 1179–1185.

[125] Li, X., Shi, X., Qin, X., Yu, L., Zhou, Y., Rao, C., *Anal. Methods* 2020, *12*, 3836–3843.

[126] Ren, T., Zhang, X., Li, X., Chen, H., *Electrophoresis* 2020, *41*, 2055–2061.

[127] Gao, T., Li, X., Jia, Z., Hendrickx, F., Falmagne, J.-B., Chen, H.-X., *Electrophoresis* 2020, *53*, 2596–2606.

[128] Parhiz, H., Ketcham, S. A., Zou, G., Ghosh, B., Fratz-Berilla, E. J., Ashraf, M., Ju, T., Madhavarao, C. N., *Appl. Microbiol. Biotechnol.* 2019, *103*, 6081–6095.

[129] Cook, K. S., Luo, J., Guttman, A., Thompson, L., *Curr. Mol. Med.* 2020, *20*, 798–805.

[130] Hsieh, M. K., Sung, C. H., Hsieh, P. F., Hsiao, P. F., Wu, B. Y., Chou, C. C., *Poult. Sci.* 2019, *98*, 1658–1663.

[131] Van Tricht, E., Geurink, L., Pajic, B., Nijenhuis, J., Backus, H., Germano, M., Somsen, G. W., Sänger-Van De Griend, C. E., *Talanta* 2015, *144*, 1030–1035.

[132] Gollapudi, D., Wycuff, D. L., Schwartz, R. M., Cooper, J. W., Cheng, K. C., *Electrophoresis* 2017, *38*, 2610–2621.

[133] Geurink, L., van Tricht, E., Dudink, J., Pajic, B., Sänger – van de Griend, C. E., *Electrophoresis* 2020, *42*, 10–18.

[134] Li, T., Santos, M., Guttman, A., *Chromatogr. Today* 2020, 2–4.

[135] Li, T., Gao, T., Chen, H., Pekker, P., Menyhart, A., Guttman, A., *Curr. Mol. Med.* 2020, *20*, 814–820.

[136] Luo, J., Guttman, A., *LCGC Eur.* 2020, *33*, 33–38.

[137] Scioli Montoto, S., Muraca, G., Ruiz, M. E., *Front. Mol. Biosci.* 2020, *7*, 587997.

[138] Fan, Y., Marioli, M., Zhang, K., *J. Pharm. Biomed. Anal.* 2021, *192*, 113642.

[139] Loughney, J. W., Minsker, K., Ha, S., Rustandi, R. R., *Electrophoresis* 2019, *40*, 2602–2609.

[140] Advanced Electrophoresis Solutions Ltd., *Appl. Notebook* 2016, *5*, 541–542.

[141] Chen, T., Kwok, T., Esmin, A. R., Li, V., Rozing, G., Huang, T., *Chromatogr. Today* 2021.

[142] Kawai, T., Ota, N., Imasato, A., Shirasaki, Y., Otsuka, K., Tanaka, Y., *J. Chromatogr. A* 2018, *1565*, 138–144.

[143] Yang, Z., Shen, X., Chen, D., Sun, L., *J. Proteome Res.* 2019, *18*, 4046–4054.

[144] Lubeckyj, R. A., Mccool, E. N., Shen, X., Kou, Q., Liu, X., Sun, L., *Anal. Chem.* 2017, *89*, 12059–12067.

[145] Lubeckyj, R. A., Basharat, A. R., Shen, X., Liu, X., Sun, L., *J. Am. Soc. Mass Spectrom.* 2019, *30*, 1435–1445.

[146] Chen, D., Shen, X., Sun, L., *Analyst* 2017, *142*, 2118–2127.

[147] McCool, E. N., Lubeckyj, R. A., Shen, X., Chen, D., Kou, Q., Liu, X., Sun, L., *Anal. Chem.* 2018, *90*, 5529–5533.

[148] Boley, D. A., Zhang, Z., Dovichi, N. J., *J. Chromatogr. A* 2017, *1523*, 123–126.

[149] Faserl, K., Sarg, B., Sola, L., Lindner, H. H., *Proteomics* 2017, *17*, 1700310.

[150] Khatri, K., Klein, J. A., Haserick, J. R., Leon, D. R., Costello, C. E., McComb, M. E., Zaia, J., *Anal. Chem.* 2017, *89*, 6645–6655.

[151] Qu, Y., Sun, L., Zhang, Z., Dovichi, N. J., *Anal. Chem.* 2018, *90*, 1223–1233.

[152] Li, Y., Duah, E., Long, N., Persaud, A., Vangundy, Z., Magliery, T., Poi, M. J., *Bioanalysis* 2019, *11*, 471–483.

[153] Ouimet, C. M., Shao, H., Rauch, J. N., Dawod, M., Nordhues, B., Dickey, C. A., Gestwicki, J. E., Kennedy, R. T., *Anal. Chem.* 2016, *88*, 8272–8278.

[154] Risley, J. M., Jong, C. A. G. De, Chen, D. D. Y., *Capillary Electrophoresis Mass Spectrometry: Principles and Applications*, John Wiley & Sons, Hoboken 2016, pp. 7–39.

[155] Rathore, A. S., Kumar, R., Krull, I. S., *LCGC North Am.* 2019, *37*, 386–391.

[156] González-Ruiz, V., Codesido, S., Far, J., Rudaz, S., Schappler, J., *Electrophoresis* 2016, *37*, 936–946.

[157] González-Ruiz, V., Codesido, S., Rudaz, S., Schappler, J., *Electrophoresis* 2018, *39*, 853–861.

[158] Zhang, H., Lou, C., Li, J., Kang, J., *J. Chromatogr. A* 2020, *1624*, 461215.

[159] Yin, Y., Li, G., Guan, Y., Huang, G., *Rapid Commun. Mass Spectrom.* 2016, *30*, 68–72.

[160] Krenkova, J., Kleparnik, K., Luksch, J., Foret, F., *Electrophoresis* 2019, *40*, 2263–2270.

[161] Hajba, L., Guttman, A., *TrAC Trends Anal. Chem.* 2017, *90*, 38–44.

[162] Zhang, Y. W., Zhao, M. Z., Liu, J. X., Zhou, Y. L., Zhang, X. X., *J. Sep. Sci.* 2015, *38*, 475–482.

[163] Liu, R., Cheddah, S., Liu, S., Liu, Y., Wang, Y., Yan, C., *Anal. Chim. Acta* 2019, *1048*, 204–211.

[164] Francisco, K. J. M., do Lago, C. L., *Talanta* 2018, *185*, 37–41.

[165] Beutner, A., Cunha, R. R., Richter, E. M., Matysik, F. M., *Electrophoresis* 2016, *37*, 931–935.

[166] Beutner, A., Scherer, B., Matysik, F. M., *Talanta* 2018, *183*, 33–38.

[167] Francisco, K. J. M., do Lago, C. L., *Electrophoresis* 2016, *37*, 1718–1724.

[168] Sterlin, D., Gorochov, G., *Pharmacology* 2021, *106*, 9–19.

[169] Leusen, J. H. W., *Mol. Immunol.* 2015, *68*, 35–39.

[170] Lu, T., Klein, L. J., Ha, S., Rustandi, R. R., *J. Chromatogr. A* 2020, *1618*, 460875.

[171] Duarte, L. M., Moreira, R. C., Coltro, W. K. T., *Electrophoresis* 2020, *41*, 434–448.

[172] Popa, T. V., Mant, C. T., Hodges, R. S., *J. Chromatogr. A* 2006, *1111*, 192–199.

[173] Dickinson, A. J., Armistead, P. M., Allbritton, N. L., *Anal. Chem.* 2013, *85*, 4797–4804.

[174] Moruz, L., Käll, L., *Mass Spectrom. Rev.* 2017, *36*, 615–623.

[175] François, Y. N., Biacchi, M., Gahoual, R., Vezin, A., Pansanel, J., *Electrophoresis* 2021, *42*, 1431–1435.

[176] Malý, M., Dovhunová, M., Dvořák, M., Gerlero, G. S., Kler, P. A., Hruška, V., Dubský, P., *Electrophoresis* 2019, *40*, 683–692.

[177] Jaroš, M., Hruška, V., Štědrý, M., Zusková, I., Gaš, B., *Electrophoresis* 2004, *25*, 3080–3085.

[178] Vimpolsek, M., Gottar-Guillier, M., Rossy, E., *Drugs Res. Dev.* 2019, *19*, 127–140.

[179] Kubota, K., Kobayashi, N., Yabuta, M., Ohara, M., Naito, T., Kubo, T., Otsuka, K., *Chromatography* 2016, *37*, 117–124.

[180] Hutanu, A., Kiessig, S., Bathke, A., Ketterer, R., Riner, S., Olaf Stracke, J., Wild, M., Moritz, B., *Electrophoresis* 2019, *40*, 3014–3022.

[181] Wang, L., Bo, T., Zhang, Z., Wang, G., Tong, W., Da Yong Chen, D., *Anal. Chem.* 2018, *90*, 9495–9503.

[182] Vanam, R. P., Schneider, M. A., Marlow, M. S., *mAbs* 2015, *7*, 1118–1127.

[183] Gómez, I. A., Hernández, V., Palomares, L. A., Ramírez, O. T., *Biochem. Eng. J.* 2018, *132*, 244–254.

[184] Hu, Z., Hsu, W., Pynn, A., Ng, D., Quicho, D., Adem, Y., Kwong, Z., Mauger, B., Joly, J., Snedecor, B., Laird, M. W., Andersen, D. C., Shen, A., *Biotechnol. Prog.* 2017, *33*, 1449–1455.

[185] Schiel, J. E., Turner, A., Mouchahoir, T., Yandrofski, K., Telikepalli, S., King, J., DeRose, P., Ripple, D., Phinney, K., *Anal. Bioanal. Chem.* 2018, *410*, 2127–2139.

[186] E-De La Garza, C. E., Salazar-Flores, R. D., Pérez, N. O., Flores-Ortiz, L. F., Medina-Rivero, E., *J. Vis. Exp.* 2017, *119*, e55082.

[187] Goyon, A., Francois, Y. N., Colas, O., Beck, A., Veuthey, J. L., Guillarme, D., *Electrophoresis* 2018, *39*, 2083–2090.

[188] Fussl, F., Trappe, A., Carillo, S., Jakes, C., Bones, J., *Anal. Chem.* 2020, *92*, 5431–5438.

[189] Montealegre, C., Neusüß, C., *Electrophoresis* 2018, *39*, 1151–1154.

[190] Dai, J., Zhang, Y., *Anal. Chem.* 2018, *90*, 14527–14534.

[191] Suba, D., Urbányi, Z., Salgó, A., *J. Chromatogr. B: Anal. Technol. Biomed. Life Sci.* 2016, *1032*, 224–229.

[192] Wang, L., Chen, D. D. Y., *Electrophoresis* 2019, *40*, 2899–2907.

[193] Biacchi, M., Said, N., Beck, A., Leize-Wagner, E., François, Y. N., *J. Chromatogr. A* 2017, *1498*, 120–127.

[194] Agarabi, C. D., Chavez, B. K., Lute, S. C., Read, E. K., Rogstad, S., Awotwe-Otoo, D., Brown, M. R., Boyne, M. T., 2nd, Brorson, K. A., *Biotechnol. Prog.* 2017, *33*, 163–170.

[195] Kim, S., Song, J., Park, S., Ham, S., Paek, K., Kang, M., Chae, Y., Seo, H., Kim, H. C., Flores, M., *mAbs* 2017, *9*, 704–714.

[196] Sun, Q., Wang, L., Li, N., Shi, L., *Anal. Biochem.* 2021, *625*, 114214.

[197] Cousteils, K., Hu, J., Li, V., Huang, T., *Chromatogr. Today* 2019, 16–19.

[198] Dykstra, A. B., Flick, T. G., Lee, B., Blue, L. E., Angell, N., *J. Am. Soc. Mass Spectrom.* 2021, *32*, 1952–1963.

[199] Han, M., Rock, B. M., Pearson, J. T., Rock, D. A., *J. Chromatogr. B: Anal. Technol. Biomed. Life Sci.* 2016, *1011*, 24–32.

[200] Váradi, C., Jakes, C., Bones, J., *J. Pharm. Biomed. Anal.* 2020, *180*, 113035.

[201] Turner, A., Yandrofski, K., Telikepalli, S., King, J., Heckert, A., Filliben, J., Ripple, D., Schiel, J. E., *Anal. Bioanal. Chem.* 2018, *410*, 2095–2110.

[202] Belov, A. M., Viner, R., Santos, M. R., Horn, D. M., Bern, M., Karger, B. L., Ivanov, A. R., *J. Am. Soc. Mass Spectrom.* 2017, *28*, 2614–2634.

[203] François, Y.-N., Biacchi, M., Said, N., Renard, C., Beck, A., Gahoual, R., Leize-Wagner, E., *Anal. Chim. Acta* 2016, *908*, 168–176.

[204] Wang, L., Cheng, J., McNutt, J. E., Morin, G. B., Chen, D. D. Y., *Electrophoresis* 2020, *41*, 1832–1842.

[205] Shen, X., Liang, Z., Xu, T., Yang, Z., Wang, Q., Chen, D., Pham, L., Du, W., Sun, L., *Int. J. Mass Spectrom.* 2021, *462*, 116541.

[206] Yang, B., Li, W., Zhao, H., Wang, A., Lei, Y., Xie, Q., Xiong, S., *J. Chromatogr. B: Anal. Technol. Biomed. Life Sci.* 2019, *1112*, 1–10.

[207] Liu, R., Chen, X., Dushime, J., Bogalhas, M., Lazar, A. C., Ryll, T., Wang, L., *mAbs* 2017, *9*, 490–497.

[208] Rouby, G., Tran, N. T., Leblanc, Y., Taverna, M., Bihoreau, N., *mAbs* 2020, *12*, e1781743.

[209] Zhu, Y., Ahluwalia, D., Chen, Y., Belakavadi, M., Katiyar, A., Das, T. K., *Electrophoresis* 2019, *40*, 2888–2898.

[210] Lamanna, W. C., Heller, K., Schneider, D., Guerrasio, R., Hampl, V., Fritsch, C., Schiestl, M., *J. Oncol. Pharm. Pract.* 2019, *25*, 269–278.

[211] Molina, P., Schick, A. J., Welch, L., Niedringhaus, T., del Hierro, G., Deperalta, G., Hieb, A., *Anal. Biochem.* 2020, *609*, 113948.

[212] Guan, Q., Atsma, J., Tulsan, R., Voronov, S., Ding, J., Beckman, J., Li, Z. J., *Electrophoresis* 2020, *41*, 1245–1252.

[213] Guan, Q., Knihtila, R., Atsma, J., Tulsan, R., Singh, S., Kar, S., Beckman, J., Ding, J., Li, Z. J., *J. Chromatogr. B: Anal. Technol. Biomed. Life Sci.* 2020, *1152*, 122230.

[214] Wagner, E., Colas, O., Chenu, S., Goyon, A., Murisier, A., Cianferani, S., François, Y., Fekete, S., Guillarme, D., D'Atri, V., Beck, A., *J. Pharm. Biomed. Anal.* 2020, *184*, 113166.

[215] Elliott, K., Anderson, J. Y. L., Gavin, C. M., Blakeman, K. H., Harcum, S. W., Harris, G. A., *Bioprocess. J.* 2020, *19*, https://doi.org/10.12665/J19OA.Elliott.

[216] Zhang, S., Chen, M., Zhou, S., Raoufi, F., Wiswell, D., Hsieh, S. C., Seghezzi, W., *J. Immunol. Methods* 2021, *494*, 113047.

[217] Dadouch, M., Ladner, Y., Bich, C., Montels, J., Morel, J., Perrin, C., *Electrophoresis* 2021, *42*, 1229–1237.

[218] Shen, B. B, Zhang, Z., Yuan, J. J., Zheng, A., Zeng, S., Gao, J. Q., Bao, W., Barnard, J., Wang, H., Fang, W. J., *Pharm. Res.* 2020, *37*, 228.

[219] Minshull, T. C., Wood, A., Roberts, D., Hallam, C., Lewis, J., Orekoya, A., Gervais, D., *Anal. Biochem.* 2020, *611*, 113953.

[220] He, S., Zhang, J., Dong, Y., Duan, X., Yang, F., Luo, T., Wang, Z., Dong, Y., *Electrophoresis* 2020, *41*, 168–174.

[221] Zhang, Y., Wang, Y., Sosic, Z., Zang, L., Bergelson, S., Zhang, W., *Anal. Biochem.* 2018, *555*, 22–25.

[222] Zhang, Z., Park, J., Barrett, H., Dooley, S., Davies, C., Verhagen, M. F., *Hum. Gene Ther.* 2021, *32*, 628–637.

[223] Field, M., Splevins, A., Picaut, P., van der Schans, M., Langenberg, J., Noort, D., Foster, K., *Toxins* 2018, *10*, 535.

[224] van Uhm, J. I. M., Visser, G. W. M., van der Schans, M. J., Geldof, A. A., Meuleman, E. J. H., Nieuwenhuijzen, J. A., *EJNMMI Res.* 2015, *5*, 1–9.

[225] Malburet, C., Leclercq, L., Cotte, J. F., Thiebaud, J., Cottet, H., *Biomacromolecules* 2020, *21*, 3364–3373.

[226] Yang, Z., Shen, X., Chen, D., Sun, L., *Anal. Chem.* 2018, *90*, 10479–10486.

[227] Engel, N. Y., Weiss, V. U., Wenz, C., Glück, S., Rüfer, A., Kratzmeier, M., Marchetti-Deschmann, M., Allmaier, G., *Anal. Bioanal. Chem.* 2017, *409*, 6625–6634.

[228] Wang, J., Qiu, L., You, Y., Ma, L., Zhu, Z., Yang, L., Wang, J., Wang, X., Liu, L., Liu, X., Chang, Y., Li, J., Gao, L., Li, Y. Q., *J. Sep. Sci.* 2018, *41*, 4544–4550.

[229] Bertoletti, L., Schappler, J., Colombo, R., Rudaz, S., Haselberg, R., Domínguez-Vega, E., Raimondi, S., Somsen, G. W., De Lorenzi, E., *Anal. Chim. Acta* 2016, *945*, 102–109.

[230] Zhao, Y., Riley, N. M., Sun, L., Hebert, A. S., Yan, X., Westphall, M. S., Rush, M. J. P., Zhu, G., Champion, M. M., Medie, F. M., Champion, P. A. D., Coon, J. J., Dovichi, N. J., *Anal. Chem.* 2015, *87*, 5422–5429.

[231] Páger, C., Biherczová, N., Ligetvári, R., Berkics, B. V., Pongrácz, T., Sándor, V., Bufa, A., Poór, V., Vojs Staňová, A., Kilár, F., *J. Sep. Sci.* 2017, *40*, 4825–4834.

[232] Kohl, F. J., Montealegre, C., Neusüß, C., *Electrophoresis* 2016, *37*, 954–958.

[233] Hopgood, J. R., Connelly, M., McHoull, B., Troy, D., *IEEE Trans. Biomed. Eng.* 2019, *66*, 119–129.

[234] Zarabadi, A. S., Pawliszyn, J., *Anal. Chem.* 2015, *87*, 2100–2106.